Master's thesis

NTNU
Norwegian University of Science and Technology
Faculty of Natural Sciences
Department of Materials Science and Engineering

Sigmund A. K. Forberg

Reduction of SilicoManganese Slags

Comparing Coke and Charcoal as Reductants

Master's thesis in Material Science and Engineering
Supervisor: Merete Tangstad
June 2023

NTNU
Norwegian University of
Science and Technology

Sigmund A. K. Forberg

Reduction of SilicoManganese Slags

Comparing Coke and Charcoal as Reductants

Master's thesis in Material Science and Engineering
Supervisor: Merete Tangstad
June 2023

Norwegian University of Science and Technology
Faculty of Natural Sciences
Department of Materials Science and Engineering

NTNU
Norwegian University of
Science and Technology

Acknowledgements

This Master thesis with its experimental work are submitted to the Norwegian University of Science and Technology (NTNU), Department of Materials Science and Engineering spring 2023.

First and foremost, I would like to express my deepest gratitude to my supervisor, Professor Merete Tangstad. Her careful guidance and wealth of experience have been instrumental to the completion of this project. I am grateful for all the opportunities, knowledge and insights I have gained under her supervision.

I am truly thankful for her patience and understanding, as she provided valuable support throughout my master period.

I would also like to extend my thanks to Senior Engineer Morten Peder Raanes for conducting the EPMA analysis, and to Senior Engineer Yingda Yu for always being helpful and for his assistance with the SEM operation.

I would like to acknowledge Arman Hoseinpur Kermani, who, during his time at the Department of Material Science, provided valuable assistance with the TG furnace. His support and technical expertise were crucial in the execution of the experimental work.

Lastly, I would like to express my heartfelt appreciation to Tichaona Mukono, who is now working for Eramet in their ferromanganese plant in Sauda. As a PhD candidate, he provided me with invaluable guidance and support during the initial stages of this project. His insights and willingness to assist were invaluable.

Abstract

Silicomanganese (SiMn) production, a carbothermic reduction process, traditionally relies on coke as the primary carbonaceous reducing agent. However, growing environmental concerns have prompted interest in exploring alternative carbon sources that are renewable. Charcoal, derived from biomass, holds promise as a sustainable carbon material that could reduce CO_2 emissions associated with SiMn production. This study aims to investigate and compare coke and charcoal as reducing agents in the SiMn process, with a particular focus on the reduction rate of SiMn slag. Furthermore, the study examines the influence of sulfur in slags reduced with charcoal. Additionally, the effect of varying particle sizes were investigated.

The experiments were conducted in a thermogravimetric (TGA) furnace, utilizing a CO gas environment and heating temperatures of approximately 1635-1645°C. Equilibrium experiments and experiments targeting specific weight losses, were performed using three different raw material charges: one with coke as the reducing agent, and two with charcoal—one with sulfur added and one without. These charges consisted of Comilog manganese ore, limestone, and quartz, with particle sizes of 1-2 mm and 3.15-4 mm. Weight loss measurements were recorded during furnace experiments, and slag and alloy samples were analyzed using electron probe microanalysis (EPMA).

The obtained weight loss curves revealed a higher reduction rate for charges utilising coke compared to charcoal. The reduction pathway of charges with coke exhibited two distinct stages: an initial slow and stable stage followed by a rapid rate increase during the second stage. Charges with charcoal exhibited a consistently slow reduction rate throughout the isothermal heating process. However, the introduction of sulfur in the charcoal charges significantly enhanced the reduction rate. Particle size variations had minimal impact on reduction, but when differences were observed, charges with larger particle sizes tended to initiate reduction earlier than charges of smaller size.

Sammendrag

Produksjonen av silisiummangan (SiMn) er en karbotermisk reduksjonsprosess. Prosessen benytter seg hovedsakelig av det fossile karbonmaterialet koks som reduksjonsmiddel. Økende miljøbekymringer har ført til større intensiver til å utforske alternative fornybare karbonkilder. Trekull, utvunnet fra biomasse, er et potensielt bærekraftig karbonmateriale som dermed kan redusere CO_2-utslippene knyttet til SiMn-produksjonen. Denne studien har som mål å undersøke og sammenligne koks og trekull som reduksjonsmidler i SiMn-prosessen med fokus på reduksjonshastigheten til SiMn-slagg. Studien tar også for seg effekten av tilsatt svovel i slagg redusert med trekull. I tillegg er effekten av varierende partikkelstørrelser for råmaterialene gitt et fokus.

Eksperimentene ble utført i en termogravimetrisk (TGA) ovn med CO gassatmosfære og temperaturer opp mot omtrent 1635-1645°C. Det ble utført forsøk opp mot likevektkomposisjon og mot spesifikke vekttap ved hjelp av tre forskjellige blandinger av råmaterial (kalt en charge): én med koks som reduksjonsmiddel og to med trekull; én tilsatt svovel og én uten. Chargene bestod i tillegg av Comilog-manganmalm, kalkstein og kvarts, med partikkelstørrelser på henholdsvis 1-2 mm og 3.15-4 mm. Vekttapet ble målt underveis i ovnseksperimentene, og slagg- og metallprøver ble analysert ved hjelp av elektronsonde-mikroanalyse (EPMA).

Vekttapskurver fra ovnsforsøkene viste en høyere reduksjonshastighet for charger som brukte koks som reduksjonsmiddel sammenlignet med trekull. Reduksjonsprosessen for charger med koks hadde to tydelige faser: en innledende langsom og stabil fase, som ble etterfulgt av en rask hastighetsøkning under den påfølgende fasen. Charger med trekull viste derimot en jevn og langsom reduksjonshastighet gjennom hele den isoterme oppvarmingsprosessen. Tilsetningen av svovel til trekull-charger førte imidlertid til en betydelig økning i reduksjonshastigheten og graden av reduksjon. Variasjoner i partikkelstørrelse hadde liten innvirkning på reduksjonen. Når forskjeller ble observert, hadde charger med større partikkelstørrelser en tendens til å starte reduksjonen tidligere enn de med mindre partikler.

Contents

List of Figures

List of Tables

1 Introduction

The pressing need to mitigate human impact on the world's climate and the growing attention towards its harmful consequences have become an important drivers for countries and industries to reduce their greenhouse gas emissions. This global awareness is most notably solidified by the Paris Agreement, a UN led initiative where the majority of nations worldwide have committed to work towards limiting the rise in temperature by the year 2030 [1]. As a signatory to the agreement, Norway has set a target of reducing its emissions by 55% compared to 1990 levels [2].

The metal industry in Norway constitutes a significant portion of the country‘s total emissions, with the production of manganese ferroalloys being a prominent contributor. Greenhouse gas emissions from metal-producing industries are primarily attributed to the burning of fossil fuel for energy generation and specific chemical reactions related to the choice of raw materials. In Norway, the ferroalloy industry relies predominantly on hydropower to supply the energy to operate the furnaces, thus minimizing carbon dioxide emissions from energy production. However, the smelting process still contributes significantly to CO_2-emissions, mainly due to the use of carbon-based materials [2].

Carbon is an essential raw material in ferroalloy production as it functions as a reducing agent in the process. The prevalent carbon material used is coal-based coke, a fossil source. In order for the ferroalloy industry is to reduce its emission, alternative carbon sources must be considered and explored. Charcoal, or biocarbon, derived from wood, can be seen as a renewable resource if utilized in a well-balanced manner, and are a promising alternative for a greener carbon source [3].

While charcoal has been extensively used in the ferroalloy production in Brazil, the world's largest charcoal supplier, Norwegian producers have limited experience with its use. To promote a wider adoption of charcoal as a viable substitute for coke in the industry, extensive research on charcoal is required. A particular focus should be placed on the interaction between slag and charcoal, as the slag-carbon relation plays a significant role in the overall process.

This thesis aims to study the the reduction of silicomanganese (SiMn) slag produced in a thermogravimetrical (TGA) furnace, by comparing coke and charcoal as reductants in the process. A secondary objective is to investigate the effect of sulfur addition to the slags reduced by charcoal.

2 Theory

2.1 Manganese and manganese ferroalloys

Manganese (Mn) is a hard and brittle transition element, widely distributed as the 12th most abundant element in the earth's crust. Due to its properties, manganese is an important component in the steel-alloy industry. Steelmakers incorporate manganese as an alloying element for various reasons, with the primary objective being the enhancement of the steel's strength, toughness and hardness. Additionally, manganese serves as a deoxidizer and sulphur stabilizer in the steel production process [4].

Silicomanganese (SiMn) and ferromanganese (FeMn) are the two main branches of the manganese ferroalloys, consisting mainly of manganese, silicon (Si), iron (Fe) and carbon (C). The silicon content as serves a distinguishing factor between SiMn and FeMn. While various grades of these two alloys exists, standard SiMn typically contains 18-20% silicon and 70% manganese, while FeMn usually has a lower silicon content of 1-2%. To further differentiate the two branches, the amount of saturated carbon in the alloy is of interest, see Figure 2.1. Standard SiMn genreally contains 1.5-2% carbon, in addition to iron and some trace elements [4]. Table 2.1 exemplifies some typical manganese alloy specifications.

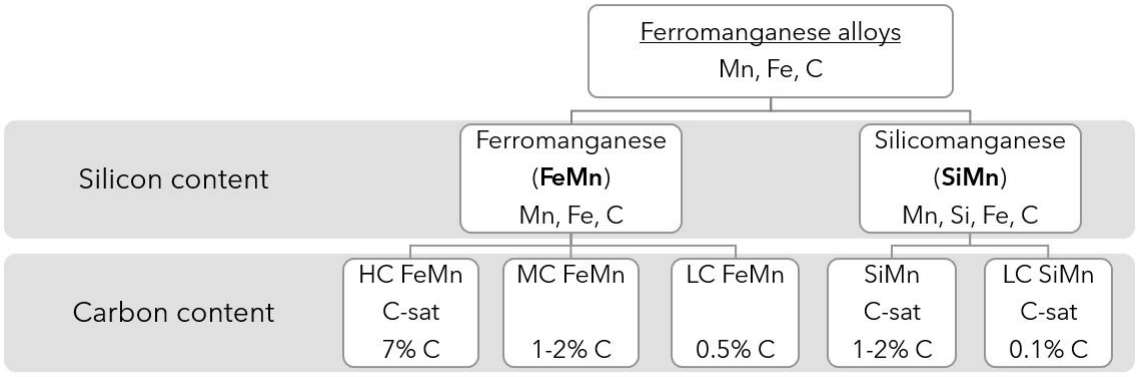

Figure 2.1: Overview of the major manganese ferroalloys. HC, MC and LC are abbreviations of high, medium and low carbon content. Further division is given by trace elements specifications. (After [5])

Table 2.1: Typical manganese alloy specifications in weight percent [wt%] [4].

Manganese ferroalloy	Mn	Si	C
HC FeMn	78	0.3	7.5
SiMn	67-68	17-20	1.5-2.0

2.2 Production of silicomanganese

The production processes for FeMn and SiMn are very similar, both utilizing the same type of furnaces and many of the same raw materials. However, there are some significant distinctions in terms of the raw materials used. The FeMn process does not require a silicon source (such as quartz), resulting in a different slag composition, final product, and lower operating temperatures compared to the SiMn process. Given the focus of this thesis on the reduction of SiMn slags, the subsequent chapters primarily describes the SiMn process.

2.2.1 Raw materials

In the silicomanganese production process, the combination of raw materials is referred to as the charge. While the composition of a charge may vary to obtain a wanted composition of the alloy, its primary components are manganese ore, quartz, and a carbon material. Quartz, a crystalline mineral containing SiO_2 (silica), provides the process with the necessary amount of silicon. Additionally, other sources of manganese, such as MnO-rich slag derived from FeMn production, and silicon, such as Si-rich metallic remelt, are often introduced into the charge [4]. In order to influence the various slag properties, flux materials can be added in small quantities. Dolomite or limestone ($CaCO_3$) are the most commonly used basic fluxes and consists of oxides which will end up in the slag phase and ensures a high manganese yield [5].

In its natural state, manganese occurs in the form of minerals and is always bound with oxygen as manganese oxides. Among the manganese oxides, higher Mn-oxides like MnO_2, Mn_2O_3, Mn_3O_4 are the most prevalent. However, these oxides become thermally unstable at elevated temperatures, as MnO is the only stable manganese oxide under such conditions. Manganese ores also contain iron oxides and various other oxides, such as Al_2O_3, CaO, MgO. Ferroalloy producers utilize several different commercial manganese ores based on their specific criteria and requirements. One notable example is Comilog, a high-oxygen ore with a significant Mn-content. Comilog ore is primarily

composed ofMnO_2-oxides. It is considered an acidic ore, with a higher concentration of acidic oxides (SiO_2, Al_2O_3) compared to basic oxides (CaO, MgO).

Carbon materials acts as a reducing agent to produce SiMn alloy, removing oxygen from the specific oxides in the slag. A dedicated chapter will follow, providing a more detailed description of the significant role of carbon materials in the SiMn process, see section 2.3

2.2.2 SiMn production process

Silicomanganese is produced using submerged arc furnaces (SAF) equipped with carbon electrodes (Søderberg), where electricity serves as the energy source for the process. The electrodes are submerged into the charge, with the electrode tip positioned in a region containing carbon materials in the lower section of the furnace. This particular area is commonly known as the coke bed due to the predominant use of coke as carbon source. The resistivity within the coke bed generates heat, which is essential for the melting of the materials and the subsequent oxide reduction into liquid metal during the production process [4–6].

SiMn is produced through carbothermic reduction of the oxidic raw materials present in the charge, where heat and a carbon material reduces the Mn-containing ore and quartz. The process results in the yield of SiMn alloy, a discard oxide slag and the release of off-gas, most notably CO and CO_2. Figure 2.2 shows a sketch of SAF with a simplified overview of the input and output of the process. The figure shows the coke bed around the electrodes and the tapping of liquid alloy from the bottom of the furnace.

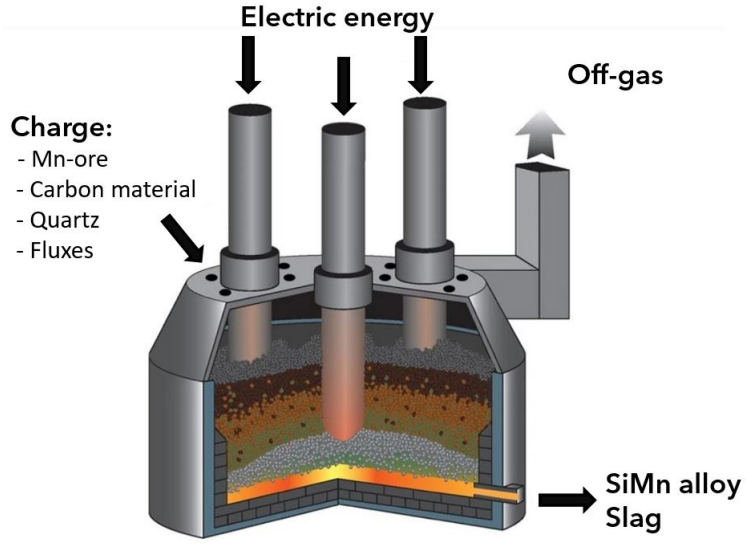

Figure 2.2: Sketch of a submerged arc furnace used in SiMn production [7].

The charge is initially introduced at the top of the SAF in a solid state. The specific temperature at the top of the charge can vary depending of the furnace, typically ranging between 200°C to 600°C in closed furnaces [5]. As the charge descends further down in the furnace, the temperature continues to increase, and temperature depending reactions occurs throughout the process. Near the bottom of the furnace, at the tapping hole, the operating temperature is in the range of 1600°C-1650°C [4].

During the SiMn process, the furnace can be divided into two distinct regions. The pre-reduction zone, also known as the low temperature zone, extends from the top of the furnace down to the melt. In this zone, the raw materials in the charge are primarily in solid form, and there is no significant presence of a liquid phase. The high temperature (coke bed) zone starts from the melt and extends to the bottom of the furnace. Each zone is characterised by a specific temperature range and the chemical reactions taking place. In Figure 2.3, these two zones and their associated reactions are depicted. The green line in the figure separates the pre-reduction reactions from the coke bed reactions.

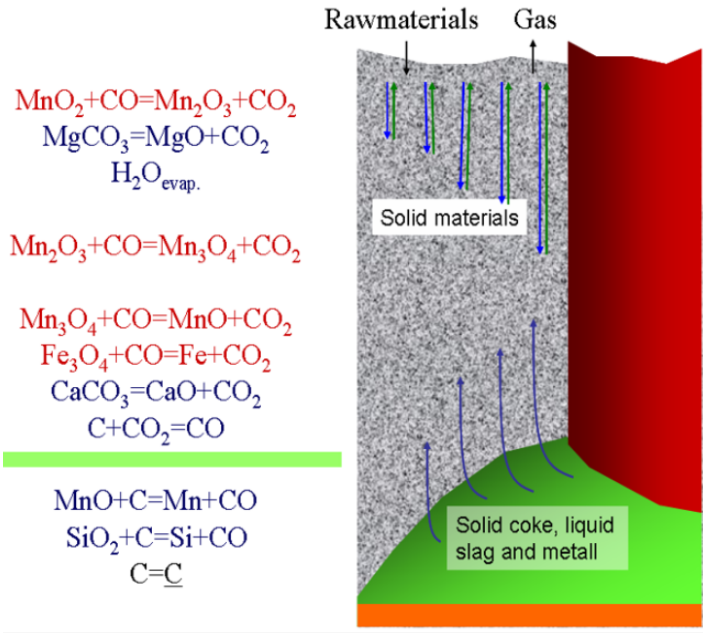

Figure 2.3: Illustration of chemical reactions inside a furnace during SiMn production. The exothermic reactions are highlighted in red while the endothermic reactions are denoted in blue. The green area represents the coke bed, a mixture of solid coke and liquid slag and metal. The metal alloy, in molten form, is depicted as the orange bottom line. At the right side of the figure, the electrode is marked red [4].

Pre-reduction zone

As seen in Figure 2.3, the pre-reduction zone encompasses a number of reactions. In this zone, the fluxes and higher manganese oxides present in the charge are heated and reduced by the off-gases rising from the coke bed zone, mainly carbon monoxide (CO) gas. Furthermore, with temperatures at the top of the furnaces above 100°C, water evaporation of moisture in the harge mixture occurs.

$$H_2O_{(l)} \rightleftharpoons H_2O_{(g)} \qquad \Delta H^{\circ}_{298} = 44.0kJ \tag{2.1}$$

The thermal decomposition of the different flux materials refers to the breakdown of carbonates, forming basic oxides (e.g MgO and CaO) and CO_2-gas. Limestone decompose at around 900°C.

$$CaCO3 \rightleftharpoons CaO + CO_2 \qquad \Delta H^{\circ}_{298} = 178.3kJ \tag{2.2}$$

Equation 2.1-Equation 2.2 are endothermic reactions ($\Delta H^{\circ}_{298} > 0$), contributing to the total power consumption [5].

The higher manganese oxides present in the manganese ore, as mentioned in subsection 2.2.1 regarding raw materials, are thermodynamically relatively unstable and readily undergo reduction in the solid state at low temperatures. In the presence of CO gas, a series of reactions occur, resulting in the gas reduction of these oxides to MnO. As Equation 2.3-Equation 2.5 are exothermic reactions ($\Delta H^{\circ}_{298} < 0$), heat is produced and contributes to the pre-heating of the charge materials [5].

$$\mathrm{MnO_2} + \tfrac{1}{2}\,\mathrm{CO} \rightleftharpoons \tfrac{1}{2}\,\mathrm{Mn_2O_3} + \tfrac{1}{2}\,\mathrm{CO_2} \qquad \Delta H^{\circ}_{298} = -99.9kJ \tag{2.3}$$

$$\tfrac{1}{2}\mathrm{Mn_2O_3} + \tfrac{1}{6}\,\mathrm{CO} \rightleftharpoons \tfrac{1}{3}\,\mathrm{Mn_3O_4} + \tfrac{1}{6}\mathrm{CO_2} \qquad \Delta H^{\circ}_{298} = -31.3kJ \tag{2.4}$$

$$\tfrac{1}{3}\mathrm{Mn_3O_4} + \tfrac{1}{3}\,\mathrm{CO} \rightleftharpoons \mathrm{MnO} + \tfrac{1}{3}\,\mathrm{CO_2} \qquad \Delta H^{\circ}_{298} = -16.9kJ \tag{2.5}$$

Furthermore, iron oxides present in the charge are reduced to metallic iron at around 1150 °C, going completely into the metallic phase. This is represented by Equation 2.6

$$\tfrac{1}{2}\,\mathrm{Fe_2O_3} + \tfrac{3}{2}\,\mathrm{CO} \rightleftharpoons \mathrm{Fe} + \tfrac{3}{2}\,\mathrm{CO_2} \qquad \Delta H^{\circ}_{298} = -12.9kJ \tag{2.6}$$

Coke bed zone

The coke bed zone is situated below the electrode tip and extends downwards. It is characterised by the reduction of metal oxides to pure metal, particularly in the lower regions where temperatures are highest. In addition to its role as a reducing agent, the coke bed can also be considered a heating element. Heat is generated in the coke bed due to the resistivity of the carbon materials as electric current flows trough from the electrodes. The resistance encountered by the electric current results in the conversion of electrical energy into heat energy. Consequently, both energy and temperature distribution in the furnace are determined by the coke bed [4].

Upon entering the coke bed zone, typically around 1250°C, the remaining oxide blend starts to melt, forming a partially liquid slag phase. This slag flows downward into the coke layer, where the temperature continues to rise, initiating the the two main metal-producing reactions of the SiMn process. The reduction mechanics of MnO and SiO_2 are given by Equation 2.7 and Equation 2.8, showing the two oxides reacting with solid carbon in the coke bed.

$$\mathrm{MnO_{(l)}} + \mathrm{C} \rightleftharpoons \mathrm{Mn_{(l)}} + \mathrm{CO_{(g)}} \qquad \Delta H^{\circ}_{298} = 252.3kJ \tag{2.7}$$

$$\mathrm{SiO_{2(l)}} + 2\,\mathrm{C} \rightleftharpoons \mathrm{Si_{(l)}} + 2\,\mathrm{CO_{(g)}} \qquad \Delta H^{\circ}_{298} = 754.9kJ \tag{2.8}$$

Typically, MnO starts to reduce to liquid manganese ($\mathrm{Mn_{(l)}}$) at a around 1350-1400°C. Higher process temperatures are needed to reduce $\mathrm{SiO_2}$ and it must be above 1600°C to obtain the necessary amount of silicon ($\mathrm{Si_{(l)}}$). CO-gas is formed in these metal-forming reactions and will flow upwards in the furnace, contributing to the reduction of oxides in the pre-reduction zone.

The resulting metal phase is a Fe-Si-Mn-$\mathrm{C_{sat}}$ system, as some carbon is dissolved in the metal up to carbon saturation, $\mathrm{C_{sat}}$. Irreducible oxides such as $\mathrm{Al_2O_3}$, CaO and MgO, and the remaining unreduced MnO and $\mathrm{SiO_2}$, ends up in the end slag phase. The distribution between manganese and silicon between the metal and slag phase is dependent on the slag composition and temperature. For the SiMn-process to produce an alloy with sufficient silicon content and discard slag with a low amount of MnO, temperatures in range of 1600 to 1650 °C are needed [4].

2.3 Carbon materials

In the highly complex SiMn process, carbon plays an important role as the reducing agent, enabling the removal of oxygen from the oxides, either through the presence of solid carbon particles or the gaseous form of CO. The choice of carbon material has a significant impact on various process parameters. In general, carbonaceous materials exhibit a wide range of chemical and physical properties, further adding to the complexity of the process. While coal-based coke is commonly used as the carbon source, there are alternative options available, such as biomass-based carbon like charcoal. Producers in Brazil, in particular, have extensively utilized charcoal as a cost-effective alternative to importing coke [8].

The difference in some properties between coke and charcoal is highlighted in Table 2.2. Typically, charcoal exhibits some less desirable characteristics, such as lower fixed carbon content and a higher volatile matter content compared to coke. However, charcoal possesses a favorable lower ash content, although the composition of the ash can vary considerably depending on the type of tree used in the charcoal production. Further-

more, compressive strength and electrical resistance are important properties given the carbon material's position in the bottom of the furnace. These properties influences the temperature distribution and stability of furnace operation [8].

Table 2.2: Typical properties for metallurgical coke and charcoal [8]

	Coke	**Charcoal**
Fixed carbon [%]	86-88	65-85
Volatile matter [%]	10-12	15-35
Ashes [%]	10-12	0.4-4
Ash composition [%]		
SiO_2	25-55	5-25
Fe_2O_3	5-45	1-13
Al_2O_3	13-30	2-12
P_2O_5	0.4-0.8	4-12
CaO	3-6	20-60
MgO	5-12	5-12
K_2O	7-35	1-4
Compressive strength $[kg/cm2]$	130-160	10-80
Volume weight $[kg/m3]$	500-550	180-350
Electrical resistance [ohm m]	Low	High
CO_2-reactivity (AC-method)	0.1	3-4
CO_2-reactivity (NTNU/SINTEF)	Low-Medium	Medium-High

Metallurgical coke has long been the preferred carbon source for the SiMn process due to its many suitable properties. Producers place great emphasis on the amount of carbon available for the reduction of Mno and SiO_2 in the coke bed zone, referred to as fix C. A fix C content exceeding 85% is recommended, but ideally, it should be as high as possible. Furthermore, a low ash content is desired as it represents impurities and contribute to higher slag volumes. Each additional percentage of ash in the carbon would results in an increase of approximately 10-15 kg slag per ton of ferroalloy, thereby requiring more energy. The presence of impurities, particularly sulfur and phosphorous, is of significance. Typically, the sulfur content in coke is in the range 0.6 to 0.8%. Phosphorus, being the most undesirable impurity in the carbon, would mix with the alloy and create issues for steelmakers in subsequent processes [9].

Jayakumari (2019) listed some additional properties of importance for the carbon reductant during the furnace operation [10]:

- Rectivity towards reaction with CO_2, see Equation 2.9.
- Reactivity of solid carbon with components in the liquid slag, see section 2.5

The reactivity of carbon materials with CO_2 can be evaluated through the Boudouard reaction, as shown in Equation 2.9. In this reaction, solid carbon reacts with CO_2 gas to form CO gas. A high CO_2-reactivity would result in increased carbon consumption and energy usage in the process. Hence, a low CO_2-reactivity is considered a desirable property, as it allows for more efficient utilization of carbon and reduces energy requirements [4].

$$CO_2\,g + C\,(s) \rightleftharpoons 2\,CO\,(g) \tag{2.9}$$

In a study on the use of charcoal as a reduction agent in the SiMn process, **Monsen et al.** (2004) conducted experiments using pilot-scale furnaces. As part of their investigation, measurements of the CO_2-reactivity of different carbon materials were performed. Tree different reducing agents were tested, including coke and various types of charcoal. The results of these experiments, shown in Figure 2.4a, revealed significant differences in CO_2-reactivity among the carbon materials. Coke exhibited a low CO_2-reactivity, while charcoal displayed a higher reactivity, with notable variations observed among the different types of charcoal. Additionally, when charcoal was impregnated with potassium (K), its CO_2-reactivity was found to increase significantly [8].

Another study by **Monsen et al.** (2007) investigated the CO_2-reactivity using Brazilian coke, charcoal from preserved wood and some different metallurgical cokes. The results are presented in Figure 2.4b, and demonstrates that charcoal exhibited significantly higher CO_2-reactivity compared to the cokes. Furthermore, charcoal from preserved wood had a higher CO_2-reactivity than Brazilian charcoal [11].

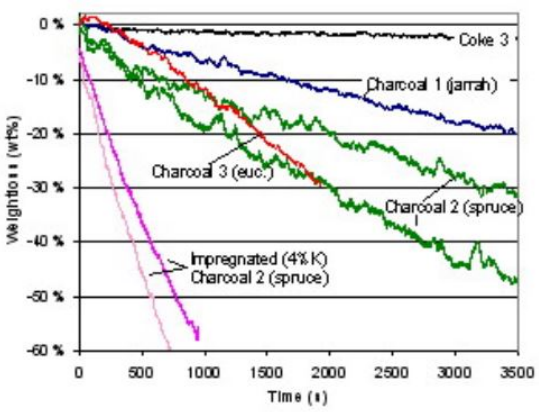

(a) Coke, charcoal and K-impregnated charcoal [8].

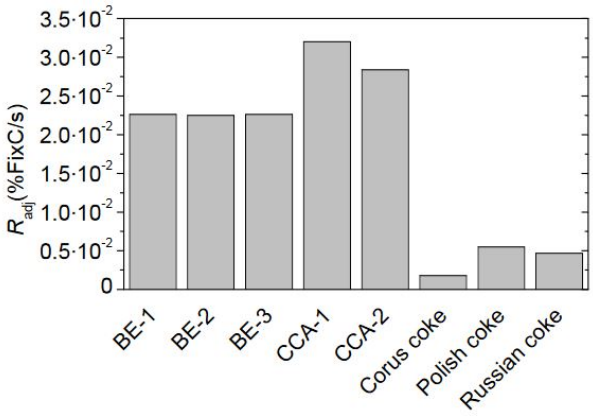

(b) Brazilian charcoal from eucalyptus (BE), charcoal from preserved wood (CCA) and metallurgical cokes [11].

Figure 2.4: CO_2-reactivity of different carbonaceous materials, measured by **Monsen et al.** [8] [11]

.

Studies have investigated the effect of particle size and quantity of the carbon material on the SiMn process, as these parameters are relevant for ferroalloy producers to optimize furnace operation. In a study by **Jayakumari and Tangstad** (2019), the reduction and melting of a silicomanganese charge on top of a coke bed was examined using various types of carbon materials with different particle sizes. The aim was to understand how these factors influenced the reduction temperature and the behavior of MnO-containing slags. The experiments were conducted using an open induction furnace and crucibles with a height of 40 cm an inner diameter of 11 cm. These crucibles allowed for the use of particles close to industrial size, with a maximum size of 20 mm. Three different types of coke and one type of anthracite were utilized in the study, with particle sizes ranging from 3 to 20 mm [10].

The findings, some illustrated in Figure 2.5, revealed a trend where larger carbon particles had slower reduction rates compared to smaller particles, resulting in higher reduction temperatures. The smaller coke particles gave a higher flow of slag into the coke bed, facilitating a higher reduction rate. It should be noted that a slower reduction rate, or the slag flow into the coke bed at a slow rate, would increase the temperature in the slag, hence leading to a higher silicon content in the metal and a lower MnO content in the slag [10].

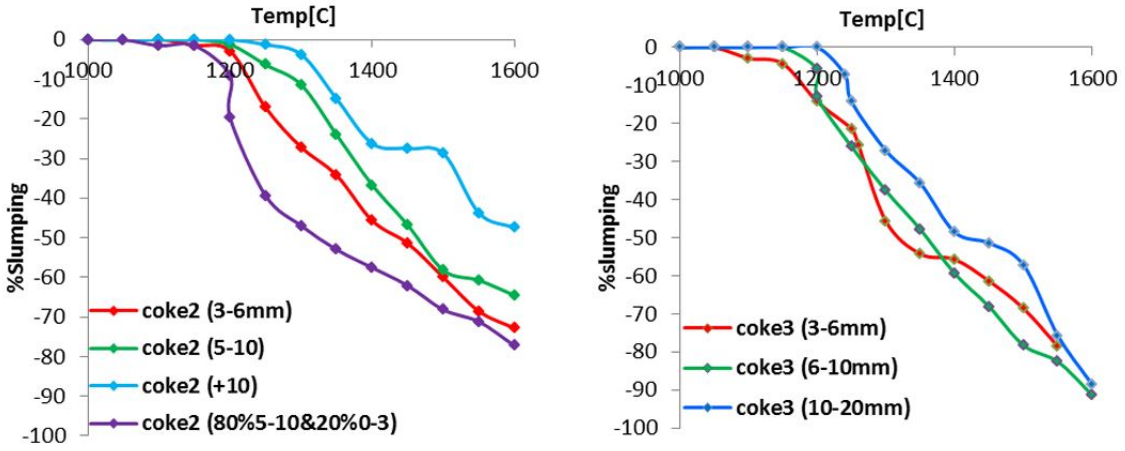

Figure 2.5: Reduction behavior of Mn raw materials using two of the coke types with various particle sizes employed in the experiments [10].

These findings are consistent with the research conducted by **Dijs and Smith** (1980), who emphasized that the reduction rate tends to increase with a decrease in the particle size of the carbonaceous reducing agent. This observation can be attributed to the larger surface area available for reaction with the slag [12].

Some research has been conducted on the influence of carbon quantity in the charge. Notably, **Ringdalen et al.** (2010) highlighted that the amount of carbon in the charge was the main factor affecting the silicon content of SiMn. When an excess of carbon was present, the reduction products at equilibrium consisted of Mn-Fe-Si-C alloy, graphite and silicon carbide. Conversely, a carbon "deficit" led to an increased Si content in SiMn, as it prevented the formation of graphite in the reduction products [13].

In their review, **Surup et. al** (2020). discuss the potential of charcoal as an alternative reductant in the production of ferroalloy. The review highlights the environmental benefits of using charcoal, as it is a renewable carbon source when sustainable extracted and produced. However, there are several challenges that need to be addressed for ferroalloy producers to successfully replace coke with charcoal. Extensive research is being conducted to improve charcoal production and overcome some of the disadvantages associated with its use in the industry[14].

2.4 Thermodynamics

The production of SiMn is a complex process, and an insight into its kinetics is important for a comprehensive understanding of the overall process. The kinetics of the reactions is connected to the distance from chemical equilibrium for reactions, emphasizing the importance of comprehending the underlying thermodynamics. This chapter aims to describe the thermodynamics of the SiMn process, providing an overview of the SiMn metal and slag systems, as well as the equilibrium distribution of manganese and silicon.

Manganese alloys, similar to iron, forms several stable oxides and carbides. Understanding the stability of manganese oxides in relation to carbon, which serves as the reducing agent for MnO, is of importance. Figure 2.6 illustrates the calculated equilibrium relations in the Mn-O-C system. The diagram shows that the lowest temperature required to produce carbon-saturated liquid manganese metal is close to 1370°C, with an oxygen partial pressure of $p_{O_2} \approx 10^{-16} atm$. Additionally, as the temperature rises, it becomes evident that higher manganese oxides are reduced by CO gas.

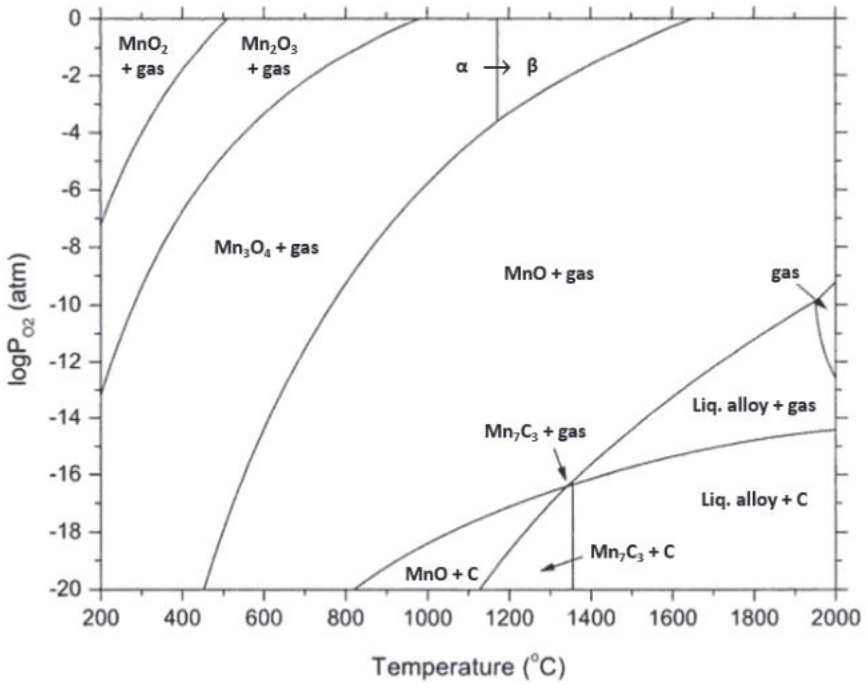

Figure 2.6: Calculated equilibrium relations in the Mn-O-C system. [4]

The SiMn slag systems

As mentioned in Equation 2.2.2, oxides from the raw materials will end up in the SiMn slag system. However, FeO is a notable exception as it is assumed to reduce to metallic iron during the pre-reduction stage (see Equation 2.6). The main components of the slag include MnO, SiO_2, Al_2O_3, CaO and MgO.

The MnO-SiO_2 binary system is given in Figure 2.7, where the approximate MnO/SiO_2 ratio in SiMn slags (blue) and FeMn slags (red) is shown. According to this binary system, the melting of of pre-reduced manganese ore to form liquid slag initiates at approximately 1250°C while the complete formation of liquid SiMn slag occurs above 1350°C. Exact temperature would depend on the amount of SiO_2 in the slag.

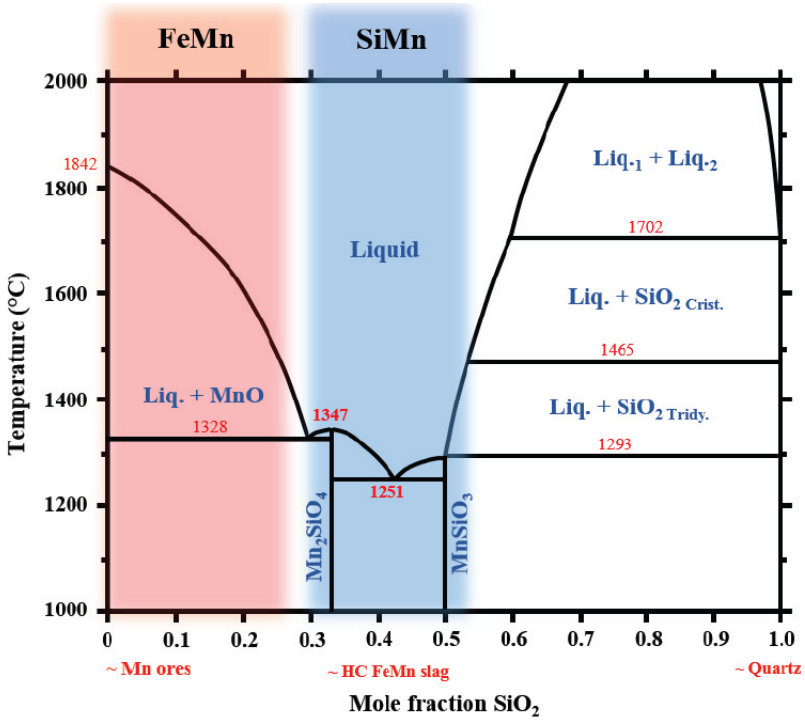

Figure 2.7: Calculated phase diagram for the MnO-SiO_2 binary system [4] (re-illustrated [15]). MnO/SiO_2 ratio for SiMn slag is highlighted in blue.

Manganese and silicon distribution

The composition of the final product in the silicomanganese process is determined by the the distribution of manganese and silicon in the SiMn slag. Since the end slag is considered a waste product, it is undesirable to have a high concentration of manganese as in the slag phase as MnO. A loss of valuable manganese through the end slag has

negative implications for the economic feasibility of the process. Consequently, one of the primary objectives in SiMn production is to minimize the presence of manganese in the slag, thereby ensuring a high yield of manganese in the desired metal product. As previously mentioned and seen in Equation 2.7-Equation 2.8, MnO and SiO_2 is key slag elements and directly relates to the production of Mn and Si metals. This relationship is further highlighted by simplifying the two metal-producing reactions, with parentheses representing liquid slag phase and underscore symbolizing the liquid metal phase.

$$(\mathrm{MnO}) + \mathrm{C} \rightleftharpoons \underline{\mathrm{Mn}} + \mathrm{CO_{(g)}} \tag{2.10}$$

$$(\mathrm{SiO_2}) + 2\,\mathrm{C} \rightleftharpoons \underline{\mathrm{Si}} + 2\,\mathrm{CO_{(g)}} \tag{2.11}$$

With Equation 2.10 and Equation 2.11 at complete chemical equilibrium, the relation of Mn and Si in slag and metal phases can be described by the equilibrium constants. These equilibrium constants are expressed in terms of the activities of the reactants and products involved in the reactions. The activity of a compound is the effective concentration of this compound in the phase [4].

$$\mathrm{K_{MnO}} = \frac{\mathrm{a_{Mn}} \cdot \mathrm{p_{CO}}}{\mathrm{a_{MnO}} \cdot \mathrm{p_C}} \tag{2.12}$$

$$\mathrm{K_{SiO_2}} = \frac{\mathrm{a_{Si}} \cdot \mathrm{p_{CO}}^2}{\mathrm{a_{SiO_2}} \cdot \mathrm{p_C}^2} \tag{2.13}$$

K_{MnO} represents the equilibrium constant for the reaction, a denotes the activity of the component, and p represents the partial pressure of gases involved in the reaction. These two equations can be simplified into Equation 2.14 and Equation 2.15, assuming that the activity of carbon and the partial pressure of CO gas both equals 1. These assumptions are based on the understanding that the reduction occurs on top of the coke bed with solid coke particles and CO gas. In this high-temperature region of the furnace, the partial pressure of CO is approximately equal to the total pressure ($p_{CO} \approx p_{tot} \approx 1atm$) as there would be no presence of CO_2 in this area [4].

$$a_{Mn} = K_{MnO} \cdot a_{MnO} \tag{2.14}$$

$$a_{Si} = K_{SiO_2} \cdot a_{SiO_2} \tag{2.15}$$

This implies that the equilibrium concentration of Mn and Si in the metal primarily depend on the temperature, as the equilibrium constant is highly temperature dependent, and the slag composition influencing the activity of MnO an SiO_2. The activities of the species are dependent on the other compounds in the same phase, and the activity of a compound represents its effective concentration within that phase.

The distribution of silicon has an additional condition to consider, which occurs when carbon is stable as silicon carbide (SiC) at higher silicon content in the metal. Autoref bile SiC-carbon sat indicates that carbon transform from graphite to SiC above 17 wt% silicon at a temperature of 1650°C. Consequently, this implies that the SiO_2-reduction does not occur as described in Equation 2.11, where graphite is the reductant, but rather with SiC as expressed in Equation 2.16 and Equation 2.17 [4] [15].

$$SiO_{2(l)} + 2\,SiC_{(s)} \rightleftharpoons 3\,Si_{(l)} + 2\,CO_{(g)} \tag{2.16}$$

$$K_{II,SiO_2} = \frac{a_{Si}{}^3 \cdot p_{CO}{}^2}{a_{SiO_2} \cdot a_{SiC}{}^2} \tag{2.17}$$

Under the assumptions of CO atmospheric pressure and solid silicon carbide ($a_SiC \approx 1$), the equilibrium expression can be simplified as shown in Equation 2.18.

$$a_{Si} = \sqrt[3]{K_{II,SiO_2} \cdot a_{SiO2}} \tag{2.18}$$

This also indicates that distribution of silicon in metal phase is dependent on temperature and slag composition, but to a different extent compared to the reaction in Equation 2.11.

In summary, the distribution of silicon in the alloy and metal phases can be described as follows: SiO_2-reduction can occur with either graphite or silicon carbide as the reductant. If the silicon content is below 17 wt%, graphite is stable according to reaction in Equation 2.11. However, if the silicon content exceeds above 17 wt% Si, silicon carbide becomes stable according to the reaction in Equation 2.16. For both

reactions, the Si-content will be dependent on temperature and the activity of SiO_2 (which again is affected by the slag composition). Since there are two forms of carbon coexisting with the slag and metal phases, both mentioned reactions must be taken into consideration when calculating the silicon distribution. The maximum achievable Si content in an ordinary SiMn process will be about 20-22 %Si [4] [15].

The silicon distribution in a Mn7Fe-Si-C_{sat} alloy (weight ratio Mn/Fe=7) has been calculated for various activities of SiO_2, slag/metal compositions and temperatures. In both Figure 2.8 and Figure 2.9, it is evident that the silicon content in the metal phase increases with temperature, and Figure 2.9 shows that the Si content is higher when using slags saturated with SiO_2. The ratio between manganese and iron also has an impact on the Si distribution. As shown in Figure 2.10, an increased Mn/Fe ratio leads to a higher amount of Si in the alloy. Moreover, if the pressure of CO gas is reduced, the Si concentration will increase [4] [16].

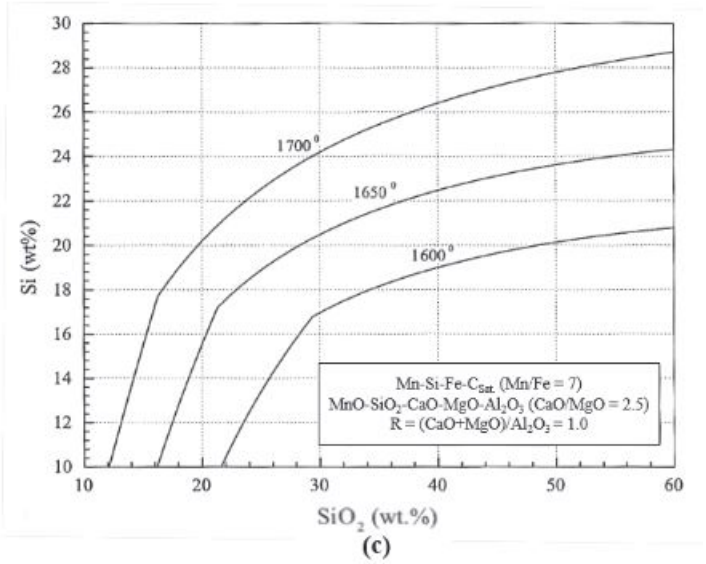

Figure 2.8: The effect of temperature on silicon distribution showing an increased Si content in the metal phase with higher temperatures [4].

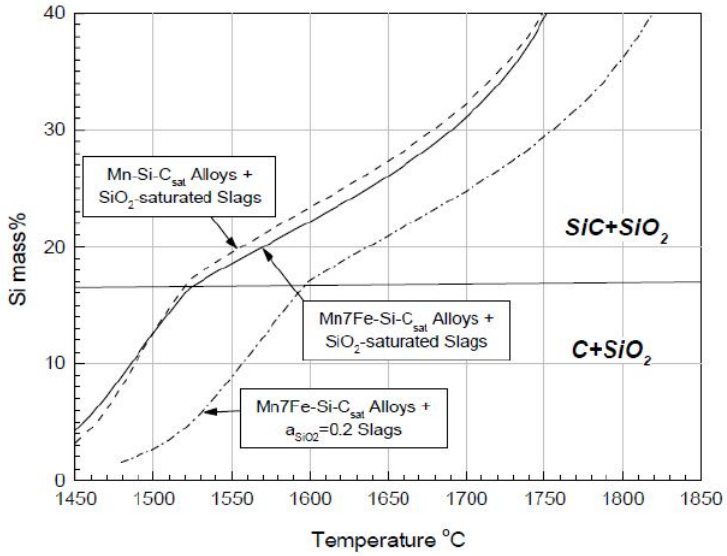

Figure 2.9: Calculated Si content as a function of temperature for Mn-Si-C_{sat} and Mn7Fe-Si-C_{sat} alloys in equilibrium with slags having different SiO_2 activities at atmospheric pressure [16]

From Figure 2.9 it can be observed that in order to achieve a Si concentration of 20 wt% in the metal, slags with an SiO_2-activity of 0.2 require an approximate temperature of 1640°C.

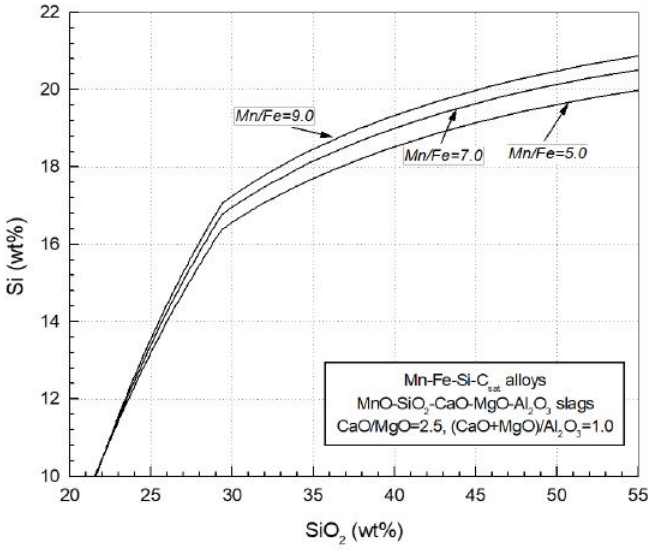

Figure 2.10: Silicon distribution in the slag and alloys, depending on the Mn/Fe ratio [4].

The graphs depicted in Figure 2.8, Figure 2.9 and Figure 2.10 exhibit a distinct inflection point around the silicon concentration range of 16-18 wt% Si. This characteristic feature strongly indicates that the Si-distribution is considered with both (Equation 2.15 and Equation 2.18.

As indicated by the activity equations, the amount of Si in the metal and the MnO content in the slag rely on the slag composition. Hence, to have control over the composition of the slag is crucial, as it directly influences the composition of the alloy. The R-ratio is a slag parameter which describes the ratio between the acidic and basic oxides that are considered irreducible in the slag, and is given by Equation 2.19. The consistent ratio between these oxides throughout the reduction process makes the R-ratio a valuable tool for controlling the slag composition. CaO an Al_2O_3 are typically the primary contributors to the ratio.

$$\mathrm{R} = \frac{\%\mathrm{CaO} + \%\mathrm{MgO}}{\%\mathrm{Al_2O_3}} \tag{2.19}$$

As depicted in Figure 2.11, the equilibrium concentration of MnO in the slag is expected to be below 10 wt% when having an R-ratio of 1.5. In industrial slags, the MnO content typically falls within the range of 6% to 10% for an R-ratio of 1.5, suggesting that process temperatures slightly higher than 1600°C are employed [16] [4].

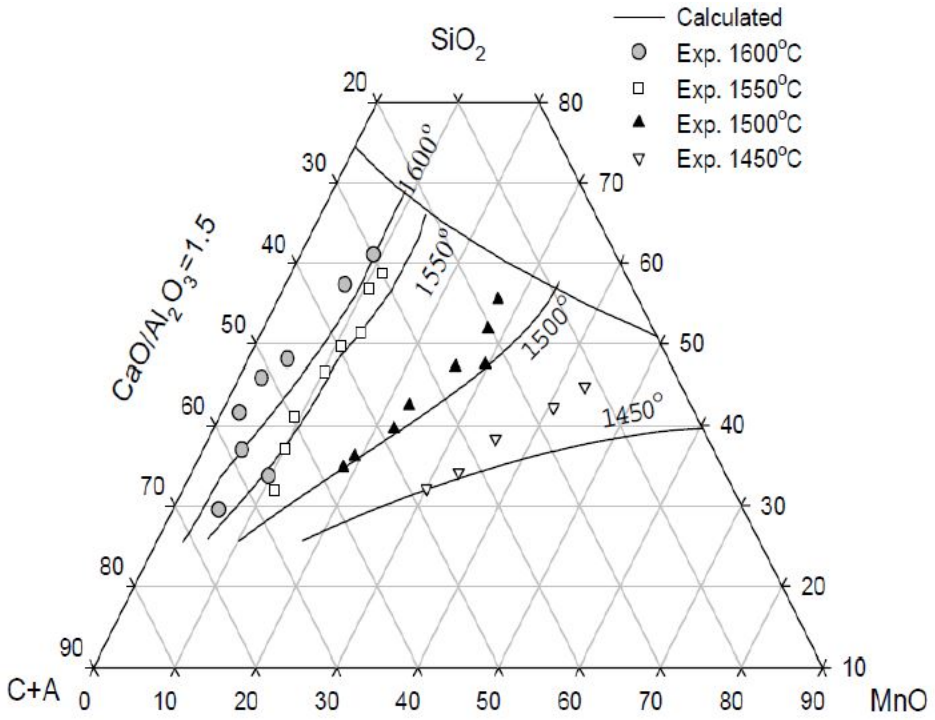

Figure 2.11: Equilibrium composition of SiMn slag at 1450°C, 1500°C, 1550°C and 1600°C. Fixed CaO/Al_2O_3 ratio of 1.5 [16].

In Figure 2.12, the significance of the R-ratio on silicon distribution is illustrated. With a constant value of R, an increase in SiO_2 content in the slag leads to an increase in the Si content in the metal. As the R-ratio increases, there is a notable rise in the concentration of SiO_2 in the slag. This indicates that, without considering kinetics, an increasing amount of CaO or MgO becomes unfavorable for achieving higher Si content in the metal phase. Consequently, the equilibrium silicon content in the metal can vary significantly depending on the slag composition [15].

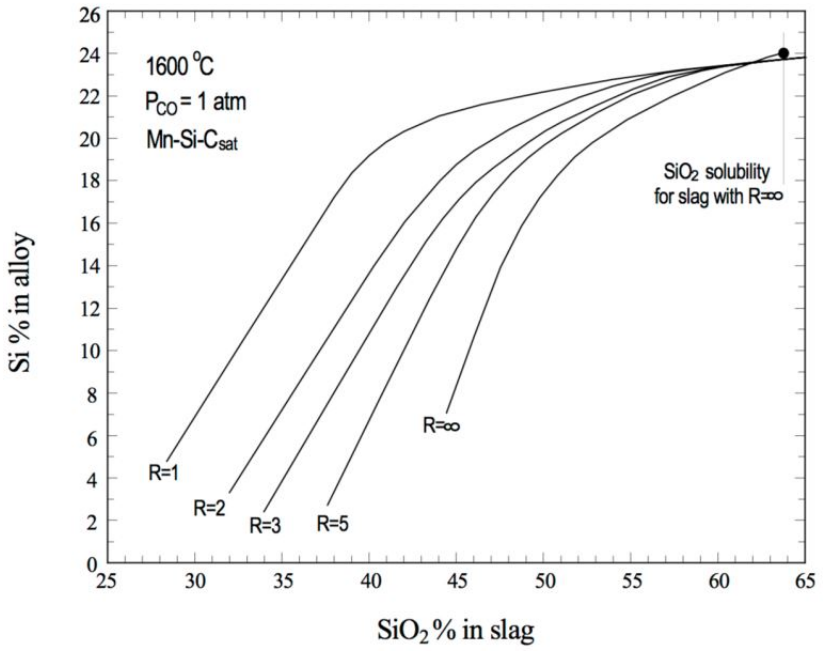

Figure 2.12: Silicon distribution as a function of the R-ratio. T = 1600° [4].

Ding and Olsen (2000) conducted a comprehensively study on the equilibrium distribution of SiMn metal and slag. The diagram presented in Figure 2.13 depicts the complete equilibrium relations between a MnO-SiO_2-CaO-Al_2O_3-MgO slag and Mn-Fe(10%)-Si-C_{sat} alloy. The diagram demonstrates the strong influence of temperature on the equilibrium distribution. Higher temperatures, as well as slag basicities, results in a lower MnO content in the slag [17].

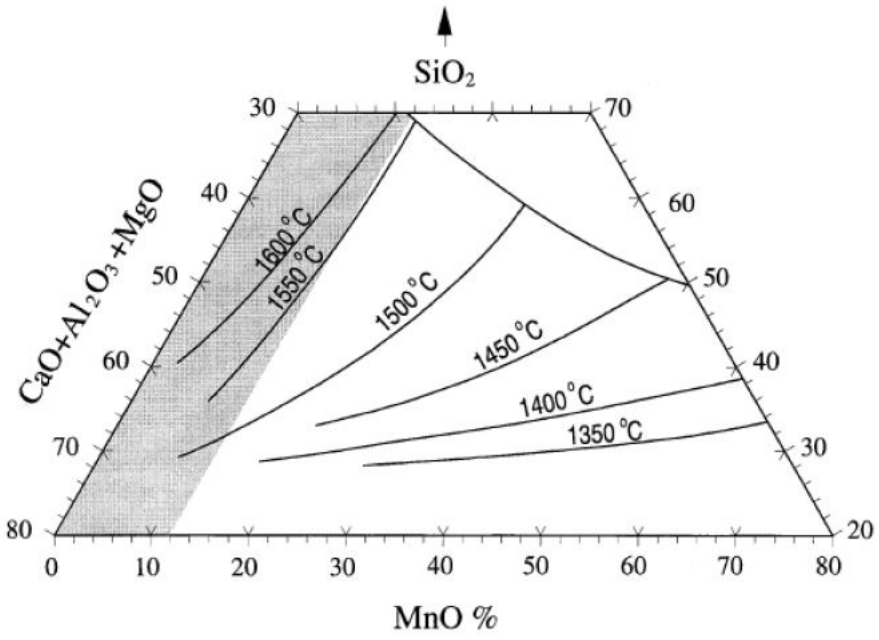

Figure 2.13: Equilibrium composition diagram for MnO-SiO_2-CaO-Al_2O_3-MgO slag and Mn-Fe(10%)-Si-C_{sat} alloy at several temperatures. $Ca/Al_2O_3 = 1.5$ and $MgO/Al_2O_3 = 0.8$. $p_{CO} = 1$ atm. The grey area is of interest for the study [17].

A typical result of complete slag/metal/gas equilibrium at a temperature of 1600°C is presented in Figure 2.14. The experiments were conducted with MnO-SiO_2-CaO-Al_2O_3 slags with a mass ratio of $CaO/Al_2O_3 = 4$. Notably, the equilibrium content of MnO in the slag reaches a minimum when the SiO2 content is approximately 44%. Furthermore, Figure 2.15 illustrates that the equilibrium curves changes with the R-ratio. The R-ratio, in addition to the temperature, has a significant effect on the distribution of Mn and Si in the metal and slag, thus on the equilibrium minimum of MnO and SiO_2 [17].

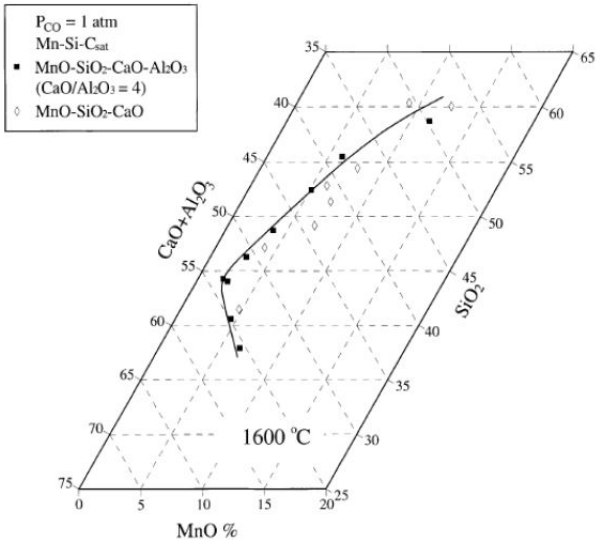

Figure 2.14: Equilibrium compositions of MnO-SiO_2-CaO-Al_2O_3 slag. CaO/Al_2O_3 = 4 at T = 1600°C [17]

.

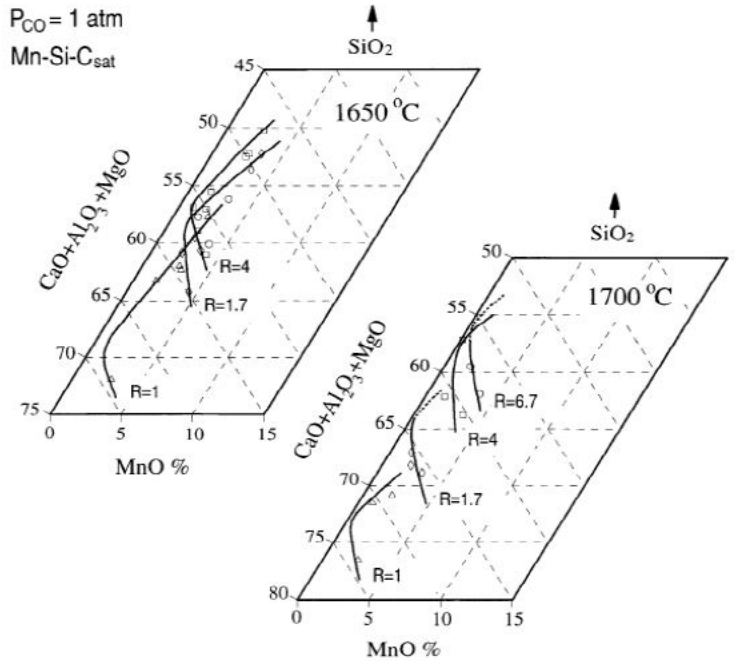

Figure 2.15: Equilibrium compositions for MnO-SiO_2-CaO-MgO-Al_2O_3 slags with different R-ratios at higher temperatures of 1640°C and 1700°C [17].

The distribution of Si between saturated Mn-Si-C alloys and MnO-SiO2-CaO-Al2O3

slags is further illustrated in Figure 2.16. The figure shows the equilibrium distribution at temperatures of 1600°C, 1650°C, and 1700°C. It can be observed that as the temperature increases, the MnO content in the slag decreases. This indicates that at higher temperatures, more MnO is reduced and transferred to the metal phase. Furthermore, an increase in temperature results in a higher Si content in the alloy phase.

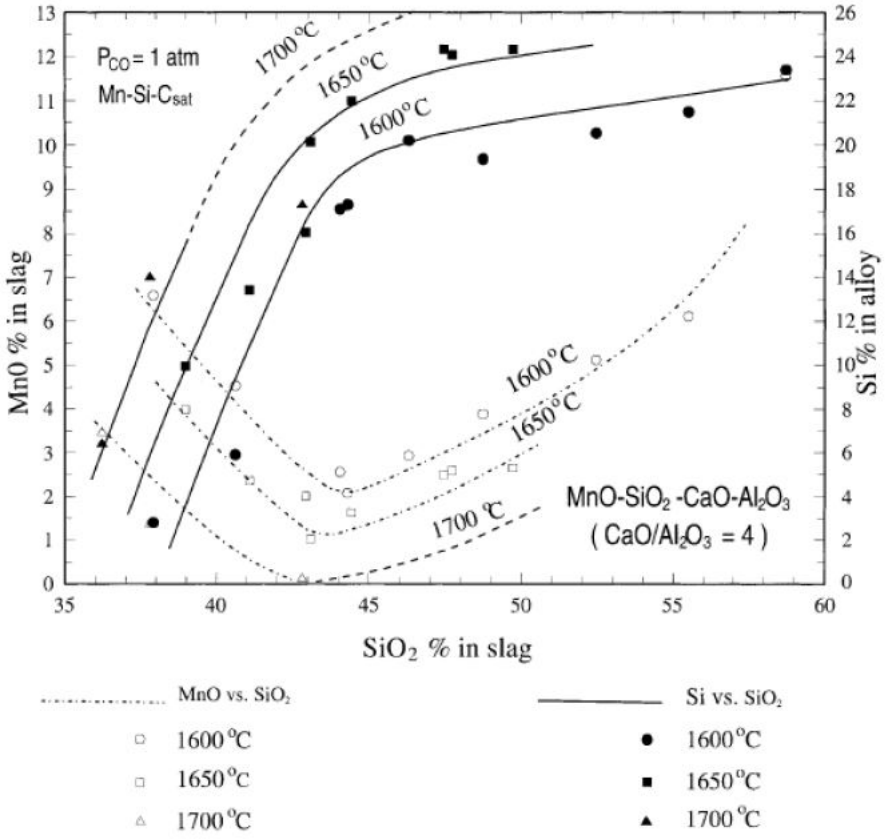

Figure 2.16: Equilibrium compositions for MnO-SiO_2-CaO-MgO-Al_2O_3 slags. CaO/Al_2O_3-ratio = 4, and temperatures of 1600°C, 1650°C and 1700°C [17].

Olsen and Tangstad (2004) emphasized that the distribution of Si between the SiMn alloy and the MnO-SiO_2-CaO-Al_2O_3-MgO slags is primarily determined by three key factors: the process temperature, the silica content in the slag, and the R-ratio [18].

2.5 Kinetics

In the following section, the kinetics of the SiMn process will be described, and previous studies on the reduction kinetics of SiMn will be discussed. While thermodynamics can describe the final equilibrium state of a reaction at a given temperature and provide insights into the composition and distribution of components in the slag and metal phases, it does not provide information about the rate at which this equilibrium state is achieved. Therefore, in order to assess the performance of metal production, it is necessary to consider the reduction rates of MnO and SiO_2. These rates provide information on the speed at which the reduction process occurs towards reaching the equilibrium state.

The reduction of MnO is highly influenced by temperature, and it has been assumed that the reduction rate is primarily limited by the chemical reaction. The reduction of MnO to liquid Mn-metal is given in Equation 2.7. Studying the MnO reduction in FeMn slags, **Ostrovski et. al** (2002) described the reduction rate of MnO by Equation 2.20 and Equation 2.21 [4] [19]:

$$r_{MnO} = \frac{-dm_{MnO}}{dt} = k_{MnO} \cdot A \cdot (a_{MnO} - a_{MnO,eq}) = k_{MnO} \cdot A \cdot (a_{MnO} - \frac{a_{Mn} \cdot p_{CO}}{K_{T,MnO}}) \quad (2.20)$$

$$k_{MnO} = k_{0,MnO} \cdot e^{-\frac{E_{MnO}}{RT}} \quad (2.21)$$

where r_{MnO} [g/min] represents the rate of MnO reduction, k_{MnO} denotes the rate and rate constant of MnO reduction. The reduction interface area is represented by A, and a_{MnO} refers to the activity of MnO, while $a_{MnO,eq}$ is the activity of MnO at equilibrium. At equilibrium, as seen from Equation 2.14, a_{MnO} can be expressed in terms of the activity of Mn (aMn), the partial pressure of CO gas (p_{CO}, and the equilibrium constant at temperature T for the reaction ($K_{T,MnO}$). CO_g partial pressure is often assumed to be equal to 1. Equation 2.21 is an Arrhenius equation where $k_{0,MnO}$ represents the pre-exponential constant of MnO reduction, E_{MnO} denotes the activation energy of MnO reduction, R is the gas constant and T is the temperature.

From Equation 2.20, the driving force for the MnO reduction can be expressed by the difference between the actual activity of MnO and its activity in the slag at equilibrium conditions. Furthermore, the rate model indicates that the rate of MnO reduction is influenced by two additional factors: the interface area between slag and the carbon

material, and the slag properties affecting the rate constant.

MnO reduction typically occurs in two stages: The first stage in the two-phase area where the slag contains MnO(s)+liquid, and the second stage where the slag is a homogeneous liquid. Figure 2.17 and Figure 2.18 illustrates the reduction during these stages. In the two-phase area of the first stage, the rate of reduction is rapid and almost constant until all the solid MnO is consumed. Later in the second stage, the reduction rate decreases fast with increasing reduction. [4] [20].

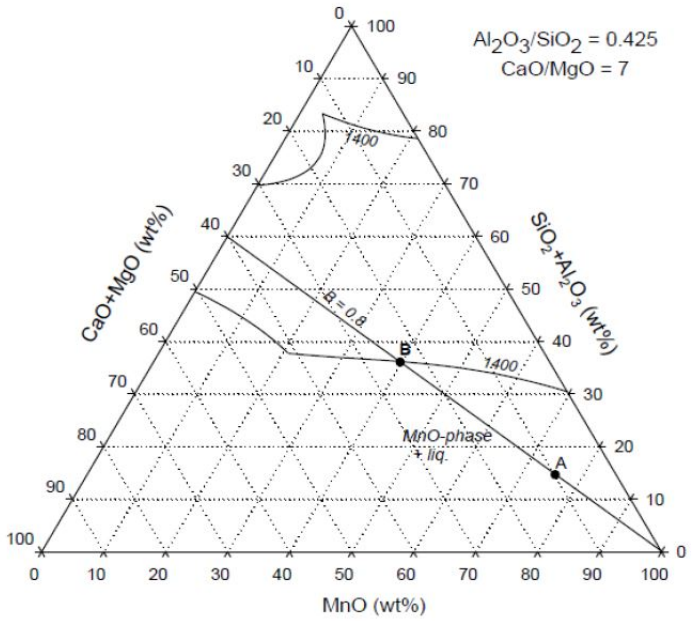

Figure 2.17: Reduction of an initial pre-reduced charge (A) down to completely liquid slag (B). A two-phase reduction from A to B, followed by a liquid phase reduction from B. Typical slag diagram for HC FeMn slags and T = 1400°C
[4].

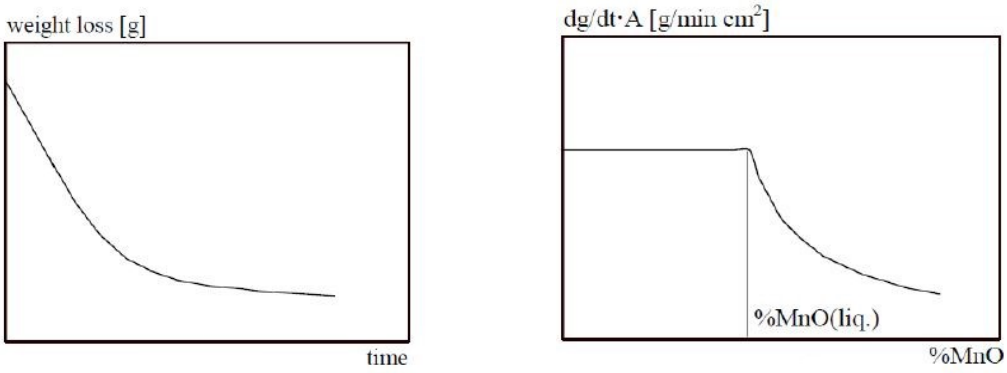

(a) a) Weight loss versus time. **(b)** b) Reduction rate versus %MnO

Figure 2.18: Reduction rate of MnO along basicity line in Figure 2.17, a two stage reduction behavior [4].

2.5.1 Experimental procedures

Various methods and procedures are employed to study different process parameters, including kinetic investigations. In a study conducted by **Safarian and Tangstad** (2010), extensive experimental work was carried out using three different techniques: thermogravimetry, ASEA induction furnace, and sessile drop furnace. The objective of the study was to establish a slag-carbon reactivity test to assess the potential of different carbonaceous materials for reducing slags. Reactivity, in this context, refers to the rate at which a chemical substance undergoes a chemical reaction. The findings indicated that the sessile drop wettability technique had several advantageous characteristics, which corresponds with it being the most commonly used method for studying slag reduction kinetics. The sessile drop technique specifically investigates the wettability between a solid and a liquid sample, providing valuable insights into the interaction between the carbonaceous material and the slag.

Thermogravimetry experiments were conducted in a CO atmosphere at a temperature of 1600°C using a synthetic FeMn slag. Two carbon reductants, coke and charcoal, were utilised in the experiments after being calcined at temperatures of 1200°C and 1600°C. The results revealed that at 1600°C, the reaction rates were similar for both coke and charcoal. However, when the materials were calcined at 1200°C, the coke exhibited a faster weight loss compared to charcoal. This difference can be attributed to the presence of more volatile materials in the coke sample after calcination at 1200°C as compared to the charcoal sample. Results from the sessile drop experiments indicated that the reactivity of slag carbon was higher when using a coke substrate compared to

charcoal [21].

2.5.2 The reduction of FeMn slags

As previously mentioned, the primary difference between SiMn and FeMn lies in the presence of SiO_2 in SiMn, requiring the reduction of both MnO and SiO_2. However, in FeMn production, only MnO reduction takes place. Despite this difference, there are numerous similarities between the production processes of FeMn and SiMn. Factors such as temperature, slag basicity, atmosphere, and other parameters that influence FeMn production also have an impact on SiMn production.

Temperature is one of the most significant process parameters, and the strong dependence of temperature on the reduction reactions is widely recognized. Higher temperatures favor both the kinetic and thermodynamic aspects of the reduction process A study by **Olsø et al.** (1998) illustrated the effect of temperature on the weight loss, serving as an indicator of the reduction rate. The results, seen in Figure 2.19, showed that increased weight loss correlated with higher temperatures, indicating an enhanced rate of reduction [20].

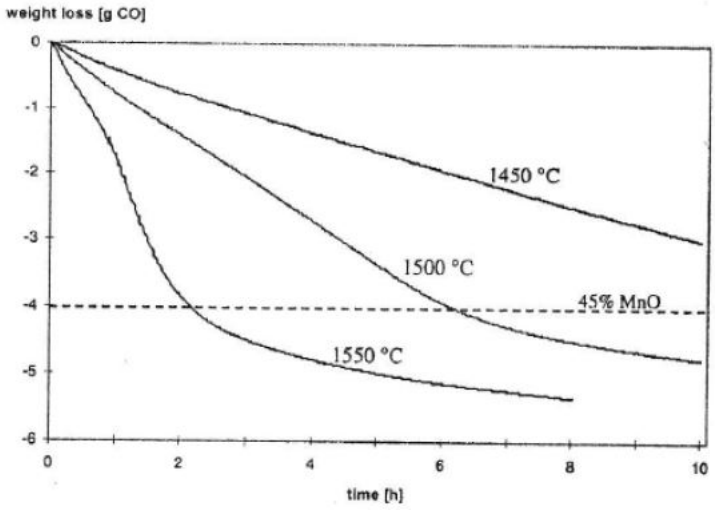

Figure 2.19: The effect of the temperature on the weight loss. (Slag Al_2O_3/SiO_2=0.25, basicity of 2/3) [20].

Figure 2.20, from **Ostrovski et al.** (2002), shows the temperature dependency on the MnO reduction from FeMn slags. The concentration of MnO in the slag decrease with temperature [19].

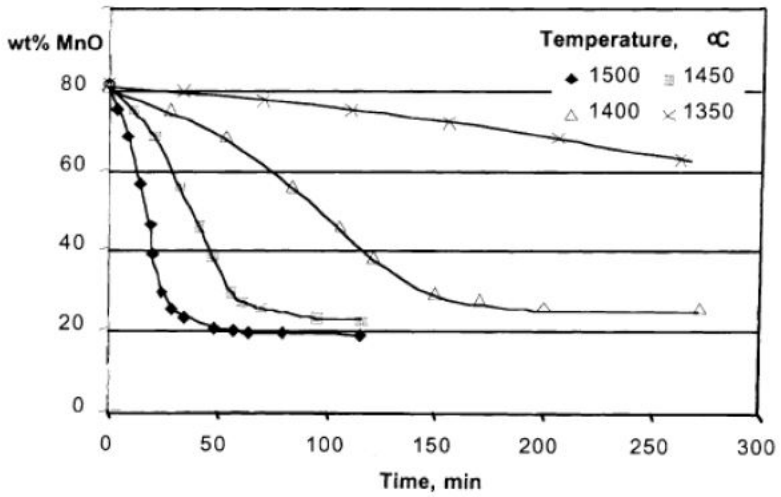

Figure 2.20: Effect of temperature on the MnO reduction rate (calculated results) [19].

The slag basicity refers to the ratio of basic to acidic oxides present in the slag composition. **Ostrovski et al.** examined the effect of slag basicity on MnO reduction. As depicted in Figure 2.21, it was observed that as the slag basicity increases, the concentration of MnO in the slag decreases. This reduction in MnO concentration indicates a higher extent of MnO reduction [19].

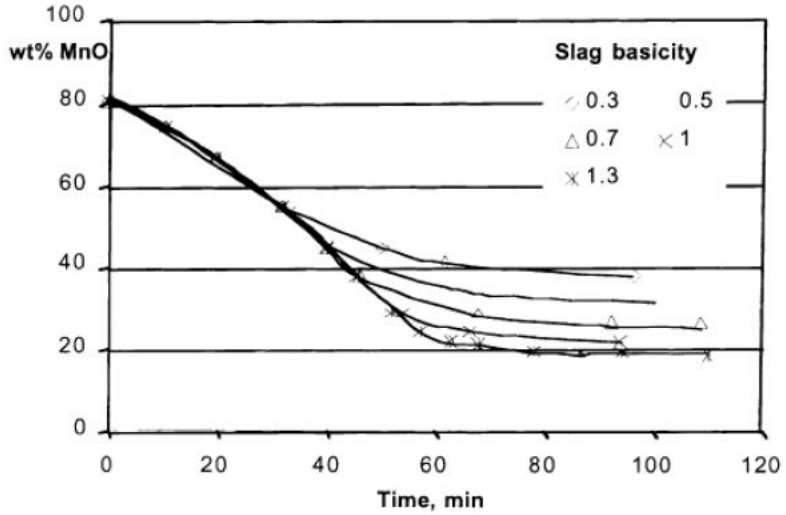

Figure 2.21: Effect of slag basicity in the reduction of MnO from a FeMn slag at 1450°C [19].

2.5.3 The reduction of SiMn slags

In SiMn production, understanding the reduction of both MnO and SiO_2 is essential. The parameters that influence FeMn production also play a role in SiMn production, including temperature, slag basicity, and atmosphere.

SiMn slags exhibit strong similarities to FeMn slags, suggesting that the same rate expression for MnO reduction, as shown in Equation Equation 2.20, can be applied. Assuming that the reduction of SiO_2 in SiMn slags is also controlled by the chemical reaction, a similar rate model can be considered using Equation Equation 2.22 and Equation Equation 2.23 [22].

$$r_{\mathrm{SiO_2}} = \frac{-dm_{\mathrm{SiO_2}}}{dt} = k_{\mathrm{SiO_2}} \cdot A \cdot (a_{\mathrm{SiO_2}} - a_{\mathrm{SiO_2},eq}) = k_{\mathrm{SiO_2}} \cdot A \cdot (a_{\mathrm{SiO_2}} - \frac{aSi \cdot p_{CO}^2}{K_{T,\mathrm{SiO_2}}}) \quad (2.22)$$

$$k_{\mathrm{SiO_2}} = k_{0,\mathrm{SiO_2}} \cdot e^{-\frac{E_{\mathrm{SiO_2}}}{RT}} \quad (2.23)$$

Kim and Tangstad(2018) used the aforementioned equations to study the reduction rates of MnO and SiO_2 in SiMn slags, and to estimate kinetic parameters. The experiments were conducted in a thermogravimetric analysis (TGA) furnace with CO atmosphere. At temperatures below 1500°C, the mass change of MnO and SiO_2 was found to be insignificant, indicating a low reduction rate. However, as the temperature exceeded 1500°C, the reduction rates significantly accelerated. The study involved the use of different raw materials, with coke serving as the reductant in three distinct charges as seen in Figure 2.22.

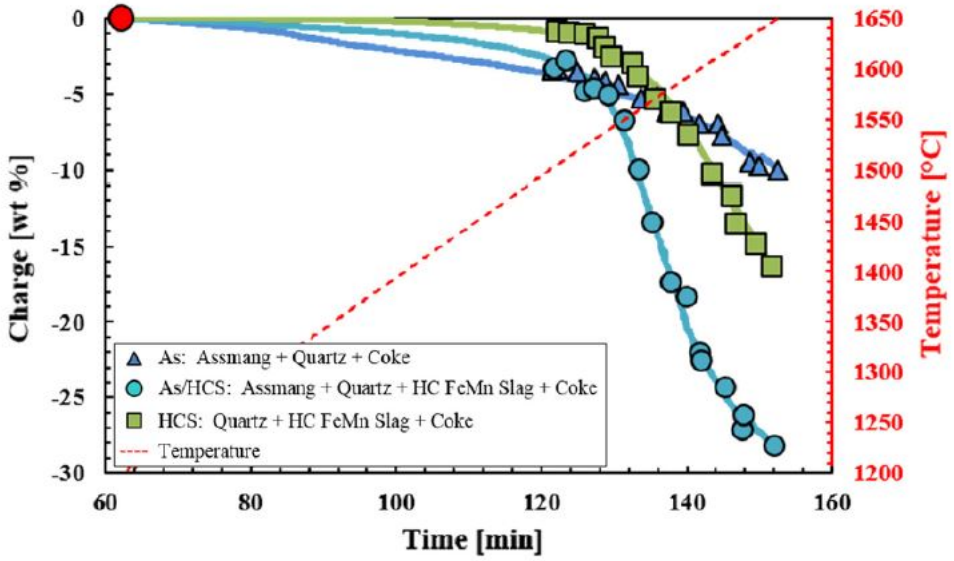

Figure 2.22: Weight loss curves from TGA furnace experiments [22].

The degree of MnO and SiO_2 reduction was calculated using equations Equation 2.24 and Equation 2.25, as shown in Figure 2.23. The figures clearly demonstrate a noticeable difference in the reduction degree among the three different charges, particularly for the reduction of MnO. Moreover, there is a tendency for charges containing HC FeMn slag to exhibit faster reduction. The study's findings indicated that the majority of MnO and SiO_2 reduction occurred at temperatures above 1500°C. The proposed rate models successfully described the reduction of MnO and SiO_2 in various SiMn slags, suggesting that the rate model for MnO reduction in FeMn slags is also applicable to SiMn slags [22].

$$Reduction\ Degree\ MnO = \frac{Produced\ Mn[g]}{Initial\ MnO[g]} \cdot \frac{70.97 \frac{gMnO}{mol}}{54.94 \frac{gMn}{mol}} \tag{2.24}$$

$$Reduction\ Degree\ SiO_2 = \frac{Produced\ Si[g]}{Initial\ SiO_2[g]} \cdot \frac{60.08 \frac{gSiO_2}{mol}}{28.09 \frac{gSiO_2}{mol}} \tag{2.25}$$

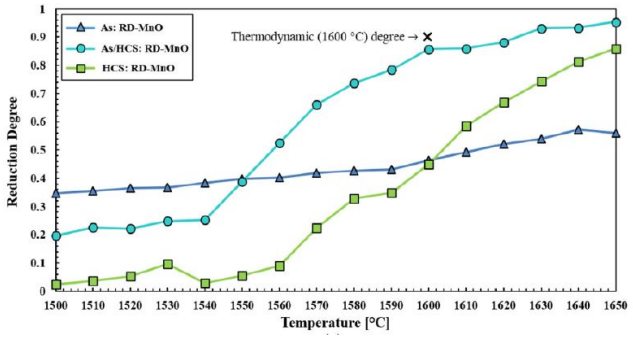

(a) Reduction degree of MnO

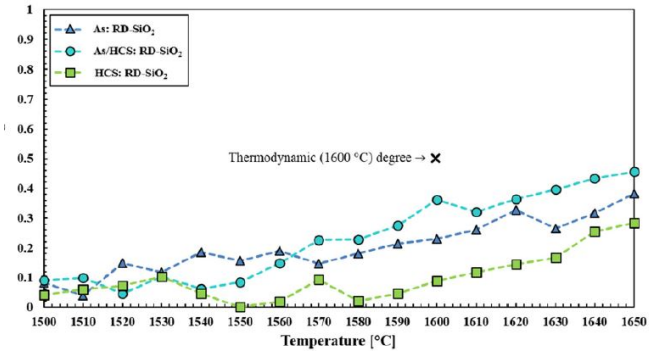

(b) Reduction degree of SiO_2

Figure 2.23: The reduction degrees of a) MnO and b) SiO_2[22].

Another study by **Kim et al.** (2019) further investigated the kinetics of SiMn slags, using a TGA furnace at temperatures ranging from 1500°C to 1650°C and CO atmosphere. The results of this study were consistent with those of **Kim and Tangstad** (2018), indicating that reduction rates were insignificant below 1500°C but increased significantly above this temperature. Additionally, the study found that the reduction rate was higher when the charge contained HC FeMn slag [23] [22].

In a study conducted by **Kim et al.** (2016), the reduction behavior in the SiMn process using Assmang and Comilog manganese ore was investigated. Additionally, different particle sizes, ranging from 0.6-1.6 mm to 4.0-6.3 mm, were employed to examine the impact of particle size on the reduction process. The results demonstrated variations in the influence of particle size for FeMn and SiMn charge samples. Significant differences in mass loss between particle sizes were observed mainly in Assmang or Comilog mixed with only coke, representative of FeMn charge samples. FeMn charge samples with smaller particle sizes (0.6-1.6 mm) exhibited higher mass loss compared to those with larger particle sizes (4.0-6.3 mm). However, when Assmang or Comilog was mixed

with quartz and HC FeMn slag, representative of SiMn charge samples, the mass loss difference between the two particle size groups was insignificant during the reduction process, unlike FeMn charge samples. It was suggested, on the basis of the comparison between FeMn and SiMn charges, that particle size may not be a significant factor influencing the reduction of MnO and SiO_2 in the SiMn process. If manganese ore and quartz particles were to dissolve completely into a slag phase shortly after pre-reduction, particle size would no longer affect the mass loss and the subsequent reduction of MnO and SiO_2 [24].
In a another study by **Canaguier and Tangstad** (2020), a TGA furnace was yet again utilised to investigate three SiMn charges comprising different industrial raw materials. The charges consisted of three distinct manganese ore sources, namely Assmang (Asm), Comilog (Com), and a combination of Assmang with HC FeMn slag (As/HCS), along with quartz and coke as additional components. The experiments were performed with several reduction duration's, and with temperatures ranging between 1510°C and 1610°C.

Figure 2.24 presents the isothermal reduction mass loss curves obtained from the charge experiments. The reduction mass loss was determined by subtracting the mass loss during the pre-reduction stage from the mass loss during the isothermal stage. In the figures, the lines represents a specific experiment, and the markers indicate the end of an experiment. It can be observed that the isothermal reduction occurs through a two-step mechanism, with a rapid increase in the mass loss rate marking the transition between the two steps. This rate change is indicated by the dashed line. Initially, the reduction is stable, with a constant rate until a sudden increase of the rate occurs. Following the rate shift, the rate rapidly peaks and subsequently decreases towards the end of the reduction. While the rate change is clearly visible for Assmang and Comilog, it is less evident for Assmang + HCS and has been a subject of conjecture. The rate change shift occurs earlier at higher temperatures, but it remains relatively constant in relation to the mass loss for a given charge. This suggests that the rate change is influenced by the chemical and/or physical properties of the slag. It is also worth noting that the experiments conducted at equal temperatures displayed remarkable overlap in terms of their results [25]

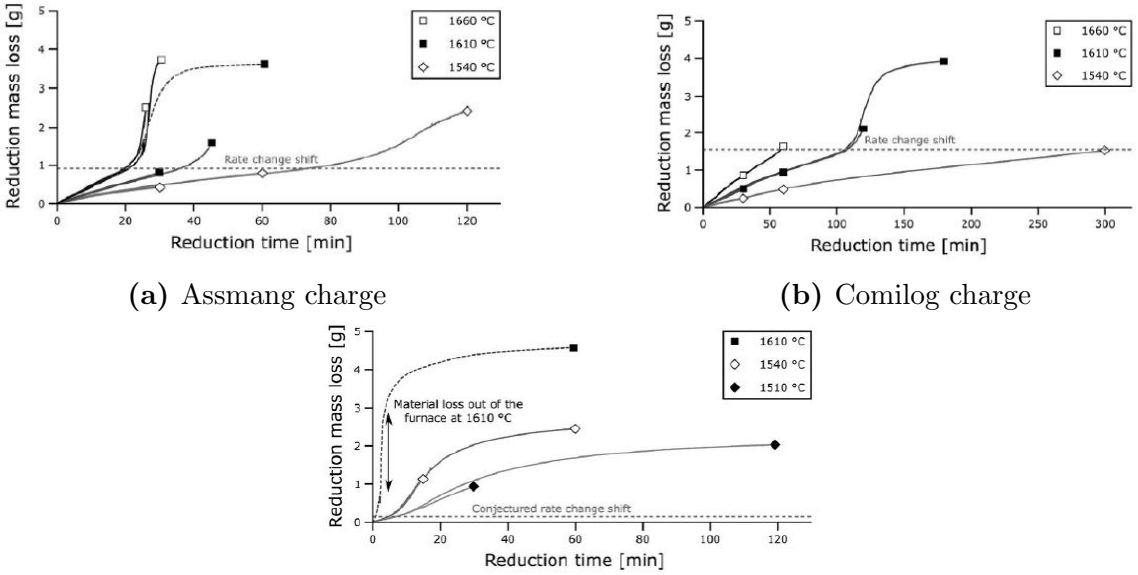

(a) Assmang charge

(b) Comilog charge

(c) Assmang + HCS charge

Figure 2.24: Mass loss curves during reduction for three different charges [25].

Based on the chemical analysis of the slag, calculations were performed to determine the relationship between reduced MnO and SiO_2, as illustrated in Figure 2.25. It can be observed that the reduction paths for the three charges exhibit a strong resemblance. The dashed line represents the calculated equilibrium between the slag and metal, indicating the expected composition if the reactions had reached equilibrium in these experiments [25].

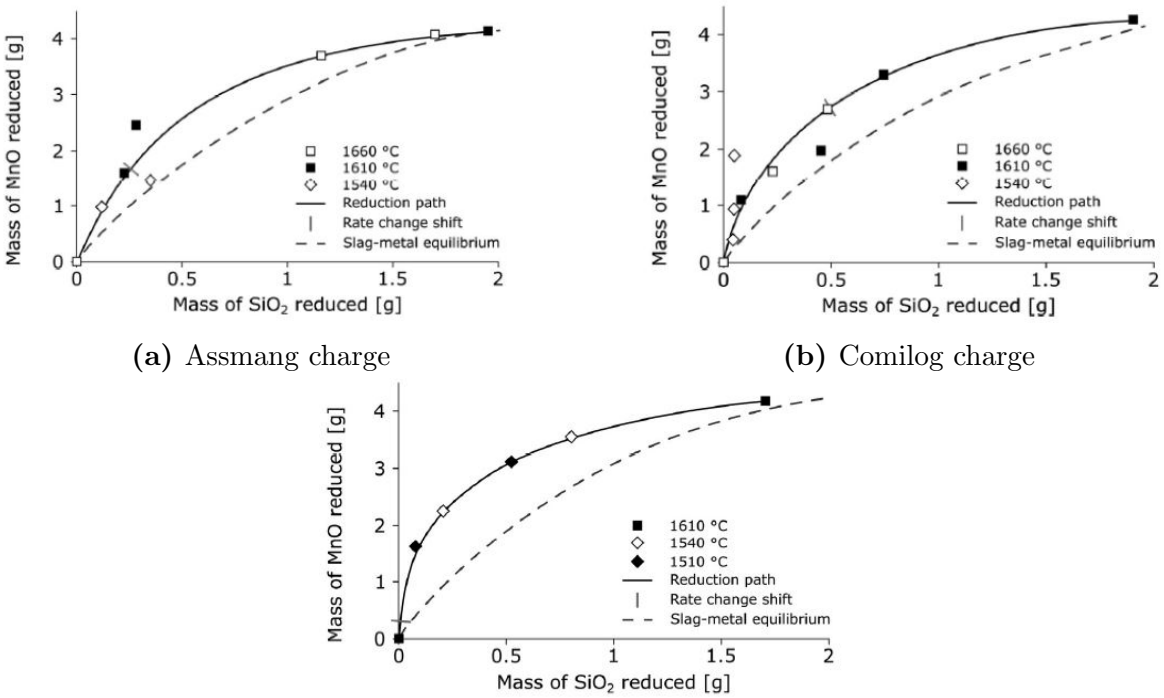

(a) Assmang charge

(b) Comilog charge

(c) Assmang + HCS charge

Figure 2.25: Reduction of MnO and SiO_2 for three different charges [25].

2.5.4 Reactivity between SiMn slags and carbon materials

Haugli (2019) conducted a study on the reactivity of SiMn slags using coke and charcoal derived from hardwood as carbon materials. The experiments were carried out in a sessile drop furnace using two different synthetic slags, each with varying MnO and SiO_2 content but a consistent 0.43 wt% sulfur content.

The results showed that when charcoal was used as the carbon material, it had a significantly lower relative volume compared to coke. This observation indicates that the reduction of MnO and SiO_2 was more pronounced when charcoal was utilised compared to coke. Additionally, the weight loss of the slag drop and carbon pellet was higher in tests conducted with charcoal compared to those with coke as seen in Figure 2.26. This difference was attributed to two factors: the increased presence of volatile substances in charcoal compared to coke and the enhanced reduction of MnO and SiO_2 when charcoal was employed as the reducing agent [26].

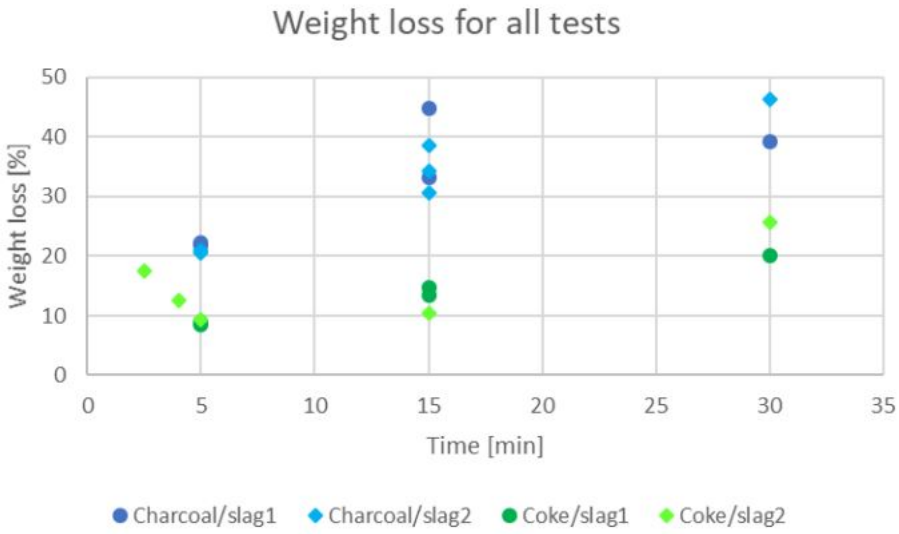

Figure 2.26: Weight loss in wt% [26].

In his master's thesis, **Hosum** (2020) conducted experiments in a sessile drop furnace to investigate the reduction rate of SiMn slags using coke and charcoal as substrates. The findings revealed that charcoal exhibited minimal reduction, whereas coke demonstrated the highest reduction rate. The study also examined the impact of sulfur addition to the slag, and it was observed that sulfur influenced the reduction rate, particularly when charcoal was used as the reductant. Slag with added sulfur and reduced by charcoal exhibited a higher reduction rate compared to coke. However, in the absence of sulfur, coke had a higher reduction rate than charcoal. The changes in MnO concentration from selected experiments are illustrated in Figure 2.27 [27].

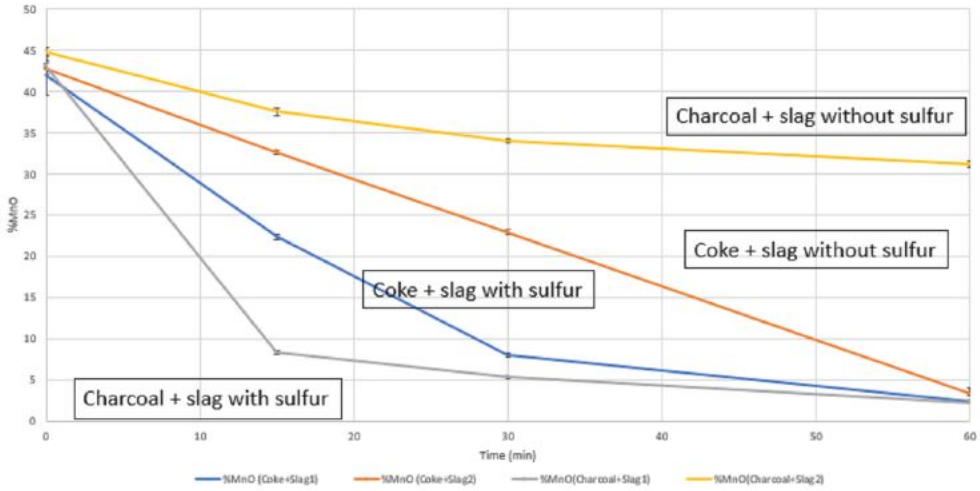

Figure 2.27: Weight fraction of MnO in the slag with both coke and charcoal as substrates, in addition to slags with added sulfur. Experiments were held at 1600°C for 0, 15, 30 and 60 minutes [27].

In a study conducted by **Forberg** (2021), several experiments were conducted using a TGA furnace. The experimental charges consisted of Comilog manganese ore, quartz, and either coke or charcoal. Two different particle sizes were investigated, and the experiments were conducted at temperatures of 1600°C and 1650°C with no holding time. The weight loss resulting from the reduction heating process is depicted in Figure Figure 2.28, showing a slight degree of reduction. The findings indicated that coke exhibited a higher reduction rate compared to charcoal. Additionally, when there was a difference in reduction rate based on particle size, the larger particles demonstrated a higher reduction rate compared to the smaller particles [28].
[28][H]
Expanding on the previous study, **Forberg** (2022) conducted additional experiments in a TGA furnace at a temperature of 1650°C, with the furnace held at this temperature for an extended duration. In these experiments, both coke and charcoal charges were supplemented with flux in the form of limestone. The weight loss curves, depicted in Figure Figure 2.29, clearly demonstrate a significant disparity in the reduction rates between the charges utilizing coke and charcoal as reducing agents. The coke charges exhibited a distinct rate shift at a reduction weight loss of approximately 15 wt%, while the charcoal charge demonstrated a consistently slow and steady reduction rate without any notable shift. [29].

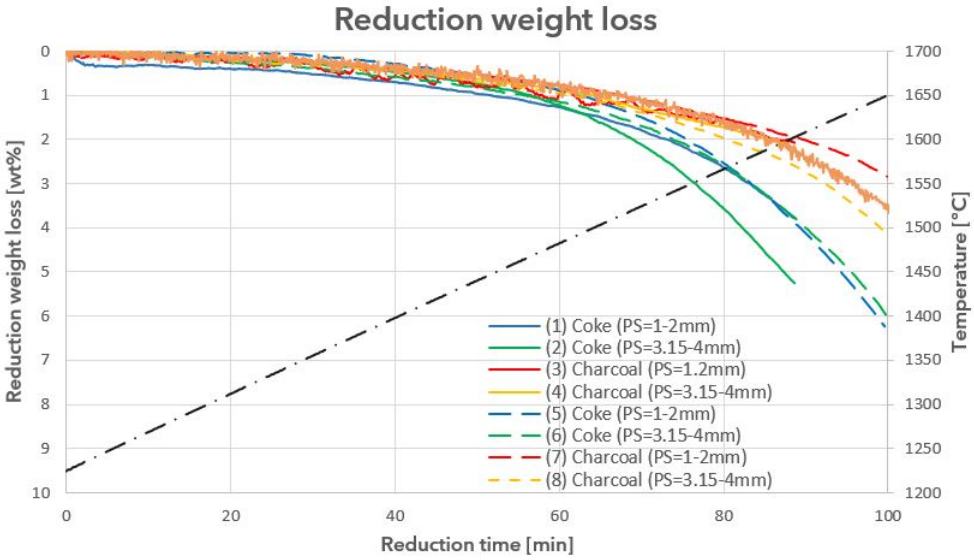

Figure 2.28: Weight loss of SiMn charges with cok and charcoal as reductants. Coke charges depicted in blu and green, charcoal in red and orange [28].

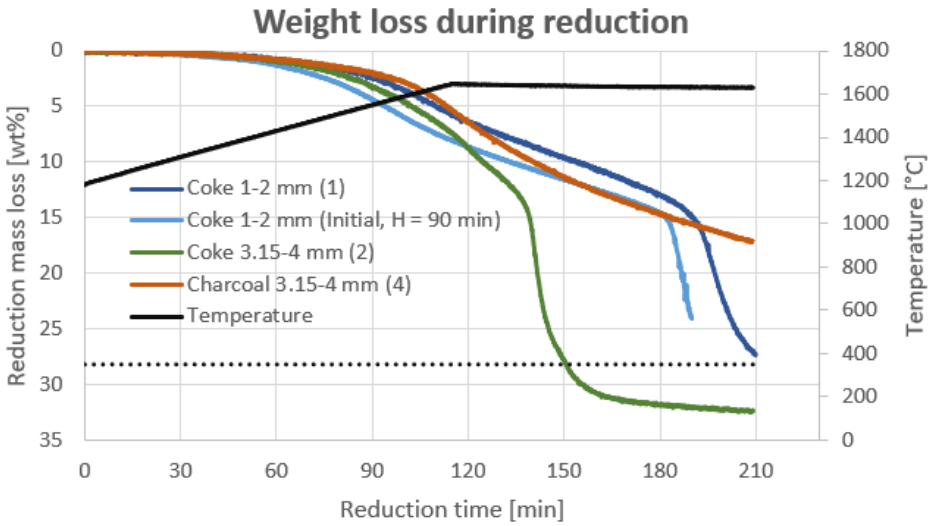

Figure 2.29: Weight loss for coke and charcoal charges [29].

2.5.5 Effect of sulfur on reduction rate

Sulfur is known to be a surface-active element that reduces the surface tension of the slag [15] [30]. Several studies have indicated that sulfur plays an influential role in slag reduction during the SiMn (and FeMn) process.

Skjervheim and Olsen (1995) stated early that sulfur appeared to play an active

role in the reduction reaction mechanism of MnO. They compared the reduction in industrial slags and synthetic slags, finding that industrial slags reduced much faster. Subsequently, they introduced 0.2 wt% sulfur to a three-component slag (MnO-SiO_2-CaO) and observed a significant increase in the rate of reduction, see Figure 2.30. Thus, the presence of sulfur in industrial slags was believed to be a possible reason behind the higher reduction rate of industrial slags [31].

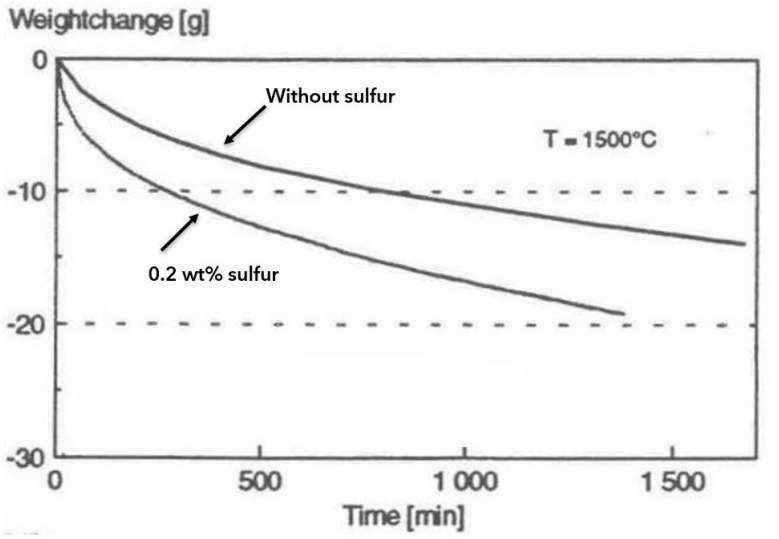

Figure 2.30: Weight change of manganese slag versus time at 1500°C. Effect of a small sulfur addition (0.2 wt% S), showing an increased reduction rate of MnO with sulfur introduced to the slag phase. [31]

In a study by **Kim and Tangstad** (2018), three charges were prepared, each containing a different manganese source and varying initial sulfur content. The results showed that the charge with the lowest sulfur content had the lowest reduction rate. However, as depicted in Figure 2.31, the charge with the highest amount of initial sulfur also showed a low reduction rate. This suggests that there may be an optimal amount of initial sulfur in a charge that affects the reduction rate. It should be noted that the influence of sulfur content alone on the reduction rate is not conclusive, as previous studies have shown that the initial iron content can also impact the kinetics [22].

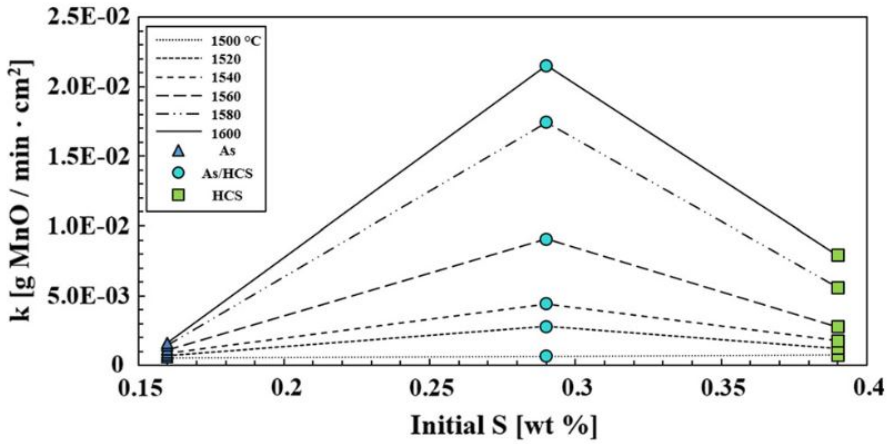

Figure 2.31: Rate constants compared with initial sulfur content of three different charges at six temperatures. Both the charge with the lowest and highest amount initial S had low reduction rate. This The rate constant increased with higher temperatures.[22]

Li and Tangstad (2019) examined the influence of sulfur content on the reduction of SiMn slags. Four synthetic slags were used, with 0, 0.2, 0.44, 1.0 wt% S respectively. Figure 2.32 shows the weight loss curves from a TG furnace [30], with the 0.44 wt% S slag having the highest loss, again implying that there is an optimal sulfur content for reduction rates of SiMn slags, as seen above in Figure 2.31 [22], [30].

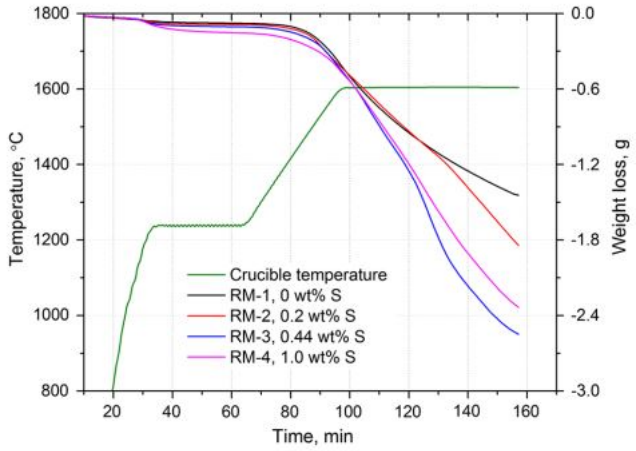

Figure 2.32: Weight loss curves for experiments with three different sulfur contents and one without any sulfur. Temperature profile for the experiments shown as a green graph. [30]

Bublik et al. (2021) investigated interfacial properties between synthetic SiMn and FeMn alloy and their corresponding slags using a sessile drop furnace. The synthetic slags had sulfur content ranging from 0 to 1.00 wt% S. One of the main findings of the experiments was the presence of a maximum extent to which sulfur could alter the interfacial tension between the ferroalloy and slag. The maximum change in interfacial tension was observed 0.25 wt% S in the SiMn alloy. Additionally, it was concluded that sulfur predominantly distributed to the slag after reaching equilibrium [32].

In the aforementioned study by **Hosum** (2020), the reduction rate of SiMn slags towards coke and charcoal as reducing agents was investigated. In some experiments, sulfur was added to the slag. The results showed that sulfur would increase the reduction rate of the slags with both carbon reductants, see Figure 2.27. Interestingly, the effect of sulfur was more pronounced in experiments with charcoal much more compared to coke. When sulfur was added, charcoal exhibited a higher reduction rate than coke. However, in the absence of added sulfur, coke had the higher reduction rate than charcoal.

The thesis proposed a possible explanation for the observation based on the difference in ash content between the two carbon materials. Coke typically contains a much higher ash content, leading to a higher sulfur content than charcoal. Consequently, there is always some sulfur present in the reactions when using coke. On the other hand, charcoal has a minimal sulfur content. Thus, the addition of sulfur to the slags would have a greater effect when using charcoal as the carbon material [[27]].

3 Experimental work

The following chapter presents the procedure and equipment utilized in the experimental work, encompassing the preparation and execution of the TGA furnace experiments, as well as the subsequent sample-analysis. Initially, a concise description of the raw material's composition is provided.

3.1 Raw materials and SiMn charges

The charges used in the experiments consisted of Comilog manganese ore, quartz, limestone, and either Polish coke or charcoal as the carbon material. Additionally, sulfur in the form of K_2SO_4 powder(purity of minimum 99%) were added to some experiments with charcoal. An overview of the chemical composition of the raw materials in weight percentage (wt%) is given in Table 3.1 .

Table 3.1: Composition of raw materials in wt%.

Material	**MnO**	**MnO_2**	**SiO_2**	**Fe_2O_3**	**CaO**	**MgO**	**Al_2O_3**	**C**	**CO_2**	**H_2O**	**Total (wt%)**	
Comilog	3.91	69.40	6.50	6.47	0.29	0.13	6.9	-	0.1	5	98.70	
Quartz	0.14	-	93.85	-	0.09	0.05	1.19	-	-	-	95.32	
Limestone	-	-	1	-	54	1	0.27	-	42.5	1	99.72	56.27*
Coke	0.04	-	5.6	0.86	0.42	0.22	2.79	87.68	-	-	97.61	
Charcoal	0.06	-	0.49	0.02	0.79	0.11	0.05	85.2	-	-	99.42	86.72*

* Total wt% after pre-heating of limestone and charcoal, assuming that all CO_2, H_2O and volatiles goes off.

Both charcoal and limestone raw materials were subjected to separate pre-heating procedures, which are denoted by the "new" total weight percent values marked with an asterisk (*) in Table 3.1. Specifically, charcoal was heated to approximately 1000°C, while limestone was heated to around 1200°C. The weight loss curves resulting from the heating of these materials can be found in subsection B.

The charcoal used in the experiments is a type of Norwegian charcoal with a relatively high fixed carbon content, and used to some extent by silicon producers in Norway. The total wt% mentioned in Table 3.1 includes the amount of fix C, volatile matter, and certain oxides present in the ash of the charcoal. A detailed breakdown of the distribution of the total wt% and an analysis of the ash are presented in Table 3.2.

Table 3.2: Chemical composition of charcoal.

Fix C [wt%]	Volatiles [wt%]	Ash [wt%]	Ash analysis [%]										
			SiO_2	Al_2O_3	CaO	Fe_2O_3	K_2O	MgO	MnO	Na_2O	P_2O_5	SO_3	TiO_2
85.2	12.7	2.1	23.4	2.4	37.4	1.1	5.6	5.4	2.8	2.8	6.4	2.5	0.1

Three charges were prepared for the furnace experiments, one with coke and another with charcoal, and one where sulfur was added to the charcoal charge. Due to the difference in chemical composition between the two carbon materials, charges containing charcoal would have a slight difference in weight compared to charges with coke. Both the charge weights and material contribution are provided in Table 3.3.

Weight calculations were performed with the goal of attaining an end slag composition consisting of 5 wt% MnO and 40 wt% SiO_2, and 18 wt% Si in the alloy. This composition is close to the thermodynamic equilibrium at a temperature of 1600°C [4]. To determine the contributions of charcoal and limestone in the charges, their weight percentages were adjusted after undergoing pre-heating processes.

The addition of limestone aimed to achieve a R-ratio of 1.5. However, since the limestone calculations only considered the contribution of irreducible oxides from the manganese ore and the added limestone, without accounting for the quartz and the two carbon materials, the R-ratio varied. The presence of a higher Al_2O_3 content in coke resulted in a slightly lower R-value in coke charges compared to charcoal charges, ranging from 1.24 to 1.47. Furthermore, the amount of added K_2SO_4 powder was estimated to 0.3 wt% sulfur in the initial slag. Lastly, the carbon material addition was set at 200% of the calculated carbon requirement.

Table 3.3: Overview of the weight of the charge mixtures used in the experiments.

Charge	Comilog [g]	Quartz [g]	Limestone [g]	Coke [g]	Charcoal [g]	K_2SO_4 [g]	R-ratio	Total [g]
Coke (1-4)	7.00	2.23	0.72	3.19	-	-	1.24	13.15
Charcoal (5-8)	7.00	2.23	0.72	-	2.92	-	1.47	12.87
Charcoal + S	7.00	2.23	0.72	-	2.92	0.14	1.47	13.01

The raw materials used, with the exception of the K_2SO_4 powder, were manually crushed and sieved to achieve the target particle sizes of 1-2 mm and 3.15-4 mm. Each charge required separate weighing of the raw materials, which were then layered inside graphite crucibles. The intention of this layering was to facilitate complete melting.

High melting materials were placed at the bottom, while low melting materials were placed at the top. In the crucible, the carbon material (coke or charcoal) was placed first, followed by limestone and quartz. Lastly, the Comilog manganese ore was added as the topmost layer. In the experiments where sulfur powder was introduced to the charcoal charges, it was positioned between the layers of limestone and ore.

The graphite crucibles have the following dimension: 30 mm inner diameter, 36 mm outer diameter, 70 mm height, 61 mm deep. The crucible lid was equipped with three holes to allow for gas exchange. A sketch illustrating the the crucible with its dimensions and the height of the raw materials is shown in Figure 3.1. The height of the carbon materials within the crucibles was 8 mm for coke charges and 13 mm for charcoal charges due to the difference in volume weight. The height of the remaining raw materials was 9 mm for both charges, resulting in a total height of raw materials of 17 mm for coke charges and 22 mm for charcoal charges. There was no significant height difference for each carbon material when varying particle sizes. For a more detailed description of the crucibles, see the subsection A.

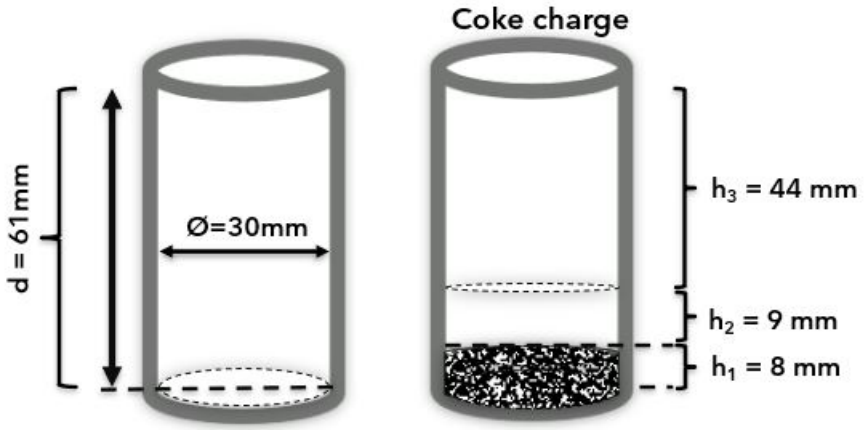

Figure 3.1: Illustration of the graphite crucibles used in the TGA furnace. Inner diameter of 30 mm and depth of 61 mm. The height of the carbon materials (h_1) within the crucibles was 8 mm for coke charges. The height of the rest of raw materials (h_2) was 9 mm for both charges.

3.2 Furnace experiments

Table 3.4 provides a comprehensive parametric overview of the conducted furnace experiments. The primary focus was on investigating the reduction rate of SiMn slags using two different carbon materials: charcoal and coke. Additionally, the effect of

particle size variation within the range of 1-2 mm and 3.15-4 mm was considered as a secondary parameter. Furthermore, the influence of sulfur in charcoal charges was investigated as a specific area of interest.

All experiments were designed with the objective of reaching a temperature of 1650°C and maintaining this temperature for a specific duration to achieve the target weight loss at either reduction time T1 or T2. The reduction times T1 and T2, are illustrated in Figure 3.2 and are based on previous work [29]. These reduction times represents the duration required to achieve specific weight losses. T1 corresponds to the weight loss at which the rate shift for coke was observed, approximately 32 wt% of the charge. T2 corresponds to the weight loss close to the calculated equilibrium weight loss, at approximately 43 wt% of the charge. These holding times were selected to investigate the reduction behavior and kinetics of the samples at specific stages of the process.

Table 3.4: Overview of the planned furnace experiments.

Exp.	**Carbon**	**Particle size [mm]**	***Reduction time [min]**
1	Coke	1-2	T1
2	Coke	1-2	T2
3	Coke	3.15-4	T1
4	Coke	3.15-4	T2
5	Charcoal	1-2	T1
6	Charcoal	1-2	T2
7	Charcoal	3.15-4	T1
8	Charcoal	3.15-4	T2
5 + S	Charcoal	1-2	T1
6 + S	Charcoal	1-2	T2
7 + S	Charcoal	3.15-4	T1
8 +S	Charcoal	3.15-4	T2

*Reduction time to achieve specific weight losses at T1 and T2

The reduction times T1 and T2, mentioned in are illustrated in Figure 3.2 and are based on previous work [29]. These reduction times represents the duration required to achieve specific weight losses. T1 corresponds to the weight loss at which the rate shift for coke was observed, approximately 32 wt% of the charge. T2 corresponds to the weight loss close to the calculated equilibrium weight loss, approximately 43 wt%

of the charge. These holding times were selected to investigate the reduction behavior and kinetics of the samples at specific stages of the process.

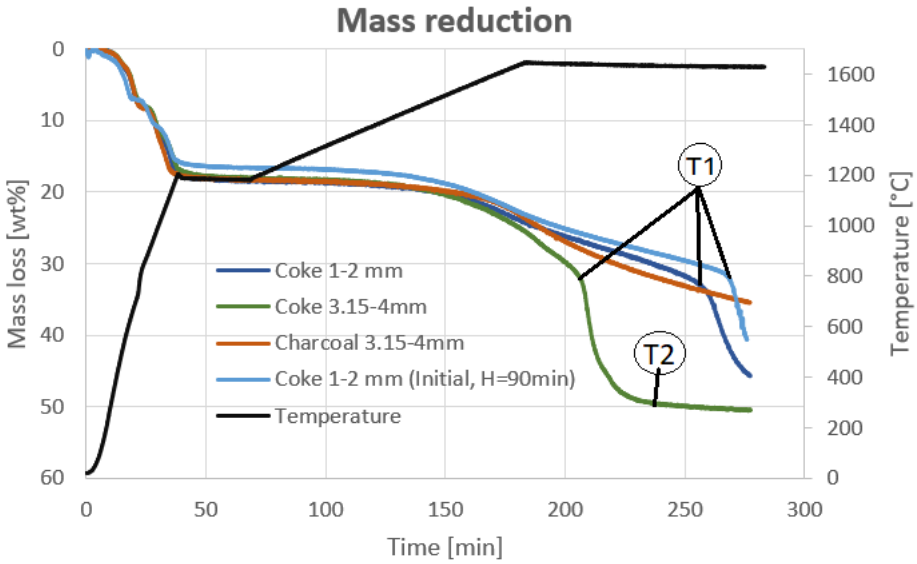

Figure 3.2: Illustration of the target weight loss for the experiments, T1 at the rate shift observed for coke charges and T2 approaching equilibrium state[29].

The experiments were conducted using a thermogravimetric analysis (TGA) graphite tube furnace located at The Department of Material Science and Engineering (DMSE), Norwegian University of Science and Technology (NTNU) [33]. The furnace is equipped with an installed mass balance that continuously measures the weight of the charge as it is heated, allowing for precise determination of the weight loss during the process over a specified time period. A schematic cross-section of the furnace is presented in Figure 3.3 [15].

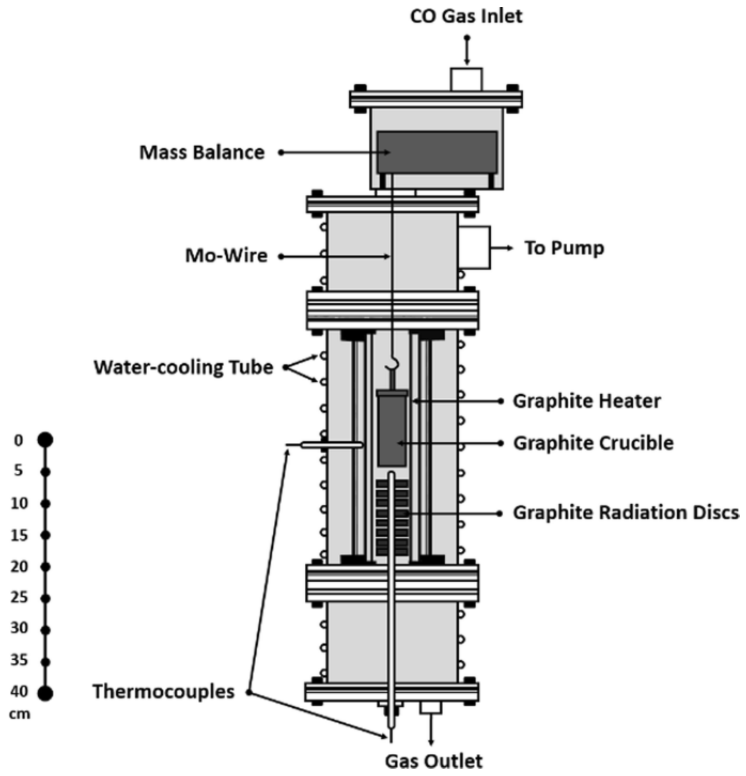

Figure 3.3: Sketch of the furnace setup [15].

The crucibles were suspended inside the furnace chamber using molybdenum (Mo) wires. Initially, one Mo wire was attached to the crucible lid and connected to the mass balance unit at the top of the furnace. However, due to the placement of the thermocouple at the bottom of the furnace and the resulting temperature gradient, an additional Mo wire was required to reach a sufficient depth inside the furnace. This additional wire, approximately 10 cm long, was attached to the crucible lid in one end and hooked to the original Mo wire at the other end, see Figure 3.4. The crucible was positioned in such a way that it hung freely, and did not come into contact with the sidewalls or the bottom of the furnace.

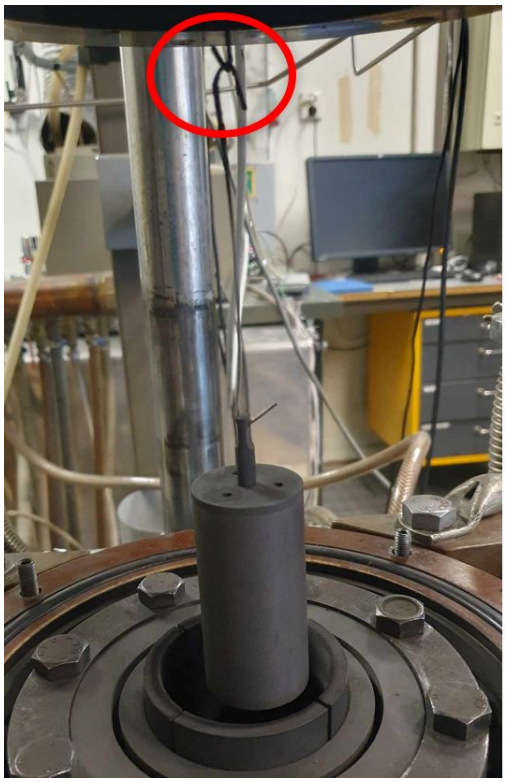

Figure 3.4: Graphite crucible suspended in the TG furnace. The connection between the two Mo wires is marked with red circle.

Two thermocouples were utilized to measure temperatures inside the furnace, taking into account the temperature gradient of the heating elements. The first thermocouple, a C-type thermocouple, was positioned approximately 1 cm from the bottom of the crucible. Since the charge was located in the bottom part of the crucible, this thermocouple was used to measure the temperature of the crucible. The second thermocouple, an S-type thermocouple, was placed along the side wall, adjacent to the crucible. Its purpose was to measure the temperature of the heating element, ensuring accurate control of the furnace heating. This setup allowed for precise monitoring of the temperature during the experimental process.

Figure 3.5 depicts the temperature gradient inside the furnace, along with the position of the C-type thermocouple and the crucible. The measurements of the temperature profile were restricted by the height of the thermocouple, which could only measure the temperature 3 cm above the bottom of the crucible. However, since the height of the raw materials in the charges was below 2.5 cm, this measurement height was deemed sufficient. The temperature in the charge materials, placed in the bottom of

the crucible, was expected to be within 1-2°C of the measured value, considering the proximity of the thermocouple to the charge.

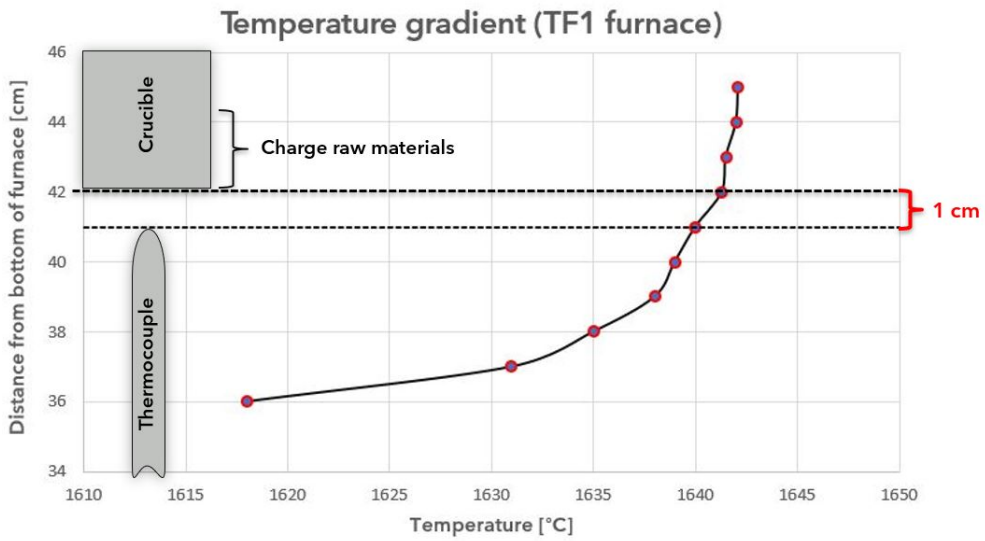

Figure 3.5: Temperature profile inside the furnace. The bottom part of the crucible is positioned 1 cm above the thermocouple.

After the crucible was hooked to the Mo wire and sealing the furnace, the chamber underwent several evacuations to detract any air inside the oven. Following each evacuation, the furnace was filled with argon gas to a pressure around 700 mbar. Following the last evacuation, the furnace was filled with argon gas up to 1050 mbar and set to a constant argon gas flow rate at 0.5 L/min. The heating schedule, as outlined in Table 3.5 Table 3.5, was uploaded to the computer software controlling the power output and temperature logging. Additionally, the initial sample weight was selected before the starting the experiments. Once the temperatures reached 500 °C, the argon gas was replaced by a continuous flow of CO-gas at a rate of 0.5 L/min. This adjustment aimed to simulate the atmosphere found in industrial furnace conditions, where CO-gas is the predominant. Throughout the operation, mass measurements of the crucible were logged every 5 seconds to monitor any changes.

The heating regime of the experiments is described in Table 3.5 and further illustrated in Figure 3.6. Initially, there was a rapid heating phase, where the temperature was quickly increased to 1200°C. Once the temperature reached 1200°C, it was held constant for a duration of 30 minutes. This extended holding period at 1200°C ensured complete pre-reduction of the materials in the crucible. Following the pre-reduction phase, the

temperature was further increased towards the final target temperature of 1650°C. The heating rate during this phase was set at 4.5°C/min, ensuring a controlled and gradual increase in temperature.

To achieve the target weight loss and degrees of reduction at T1 and T2, as referred in Figure 3.2, different holding times at the desired temperature of 1650°C were implemented. These holding times varied from 0 minutes to approximately 100 minutes. By adjusting the duration of the holding time at the final temperature, the experimental conditions were tailored to obtain specific weight loss and degrees of reduction in the samples.

Table 3.5: Heating regimes for furnace experiments.

Step	Temperature [°C]	Heating rate[°C/min]	Holding time [min]
1	1200	25	30
2	1650	4.5	0-100

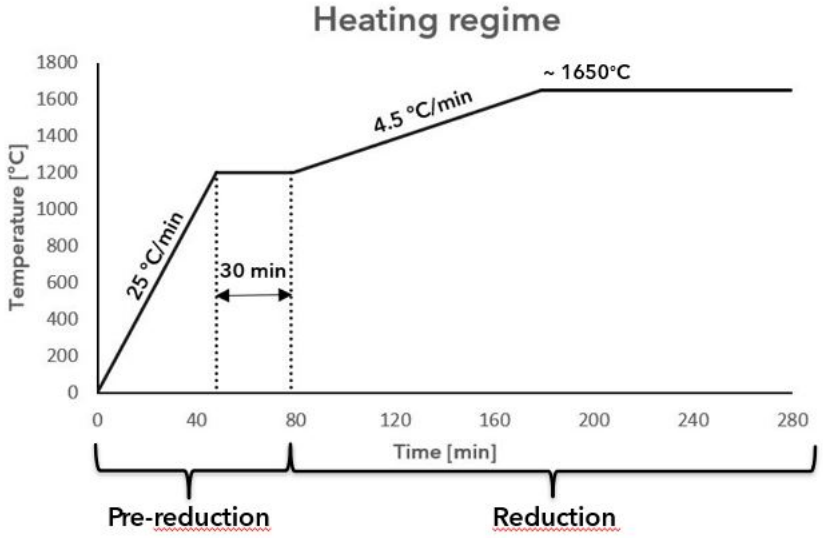

Figure 3.6: Sketch of temperature profile for the furnace experiments. There was a fast heating rate of 25 °C/min up to 1200 °C with a subsequent holding time of 30 minutes. Towards the aimed temperature of 1650 °C, a rate of 4.5°C/min was implemented.

As the experiments approached the end of their holding time at the final temperature, the power supply was disconnected, initiating a rapid cooling process with a significant decrease in temperature. When the temperature reached a range of 800-900 °C, the constant flow of CO-gas was discontinued and replaced with an equal flow of argon

gas. The furnace continued to cool down until it reached room temperature. Once at room temperature, the furnace chamber was evacuated and filled with argon gas twice to ensure the removal of any residual gases. Finally, the crucibles were safely retrieved from the furnace for further analysis.

3.2.1 Furnace stability

Although the target temperature for the experiments was set at 1650°C, the actual temperatures observed during the experiments ranged from approximately 1635°C to 1645°C, as shown in Figure 3.7. However, two experiments exhibited notable deviations from this range. Experiment 7+S reached a maximum temperature of 1661°C, while experiment 2 had the lowest temperature recorded at 1623°C. To address the lower temperature achieved in experiment 2, an additional run was performed, marked as 2.1, in an attempt to reach a higher temperature.

It was observed that maintaining a constant temperature proved to be challenging, as the temperature exhibited a gradual decrease throughout the duration of the holding period. Specifically, during the longest holding times, the temperature dropped by approximately 6°C.

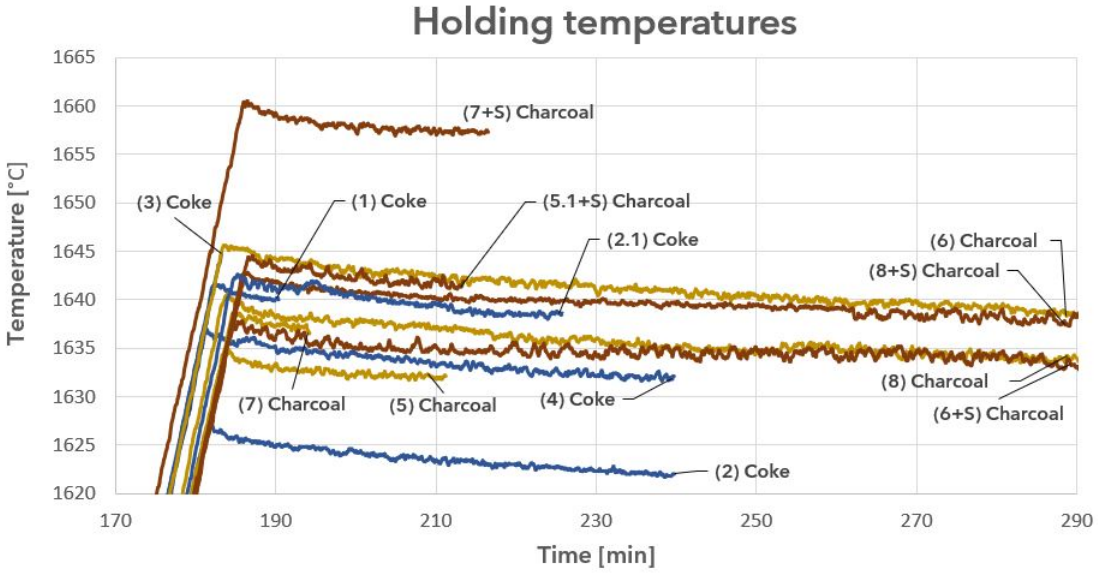

Figure 3.7: Final temperatures for the experiments. The target temperature was 1650°C.

The weight of the crucibles with raw materials was manually measured before and after the furnace experiments, and the resulting weight loss was compared to the weight

loss from the obtained data. Unfortunately, there were significant fluctuations in the data weight readings, leading to significant variations in the differences between the two measuring methods. To mitigate this issue, appropriate averages were taken for the data. The results are presented in Table 3.6, where it can be observed that there are substantial differences in weight loss between the two measurement methods. The experiments with the lowest noise in the weight loss curves generally exhibited the smallest differences, with coke charges typically showing the least noise.

An example of the large fluctuations can be seen in Figure 3.8, where the raw data curve is compared to a curve obtained by applying exponential smoothing with a smoothing factor of 0.9. For some charges, such as the charcoal charge exemplified in the figure, there were fluctuations of approximately 10% around the weight loss readings from the raw data. This level of fluctuation renders the numbers from these particular experiments in Table 3.6 unreliable.

Table 3.6: The discrepancy between the manually weighed crucible weights and the weight loss from the acquired data.

Coke charges: 13.15g
Charcoal charges: 12.87g

Experiment	**Weight in** [g]	**Weight out** [g]	**Weight loss** [g]	**Data weight loss*** [g]	**Differance** [%]
(1) Coke PS=1-2mm, T1	71.12	67.02	4.10	4.10	0.00
(2) Coke PS=1-2mm, T2	71.53	65.60	5.93	6,00	1.75
(3) Coke PS=3.15-4mm, T1	70.38	66.44	3.94	4.02	2.01
(4) Coke PS=3.15-4mm, T2	72.07	66.52	5.52	5.53	0.18
(5) Charcoal PS=1-2mm, T1	70.86	67.71	3.15	3.30	4.65
(6) Charcoal PS=1-2mm, T2	71.58	67.29	4.29	4.55	5.88
(7) Charcoal PS=3.15-4mm, T1	68.53	65.30	3.23	3.23	0.00
(8) Charcoal PS=3.15-4mm, T2	71.37	66.52	4.87	5.13	5.20

*Obtained from appropriate averages

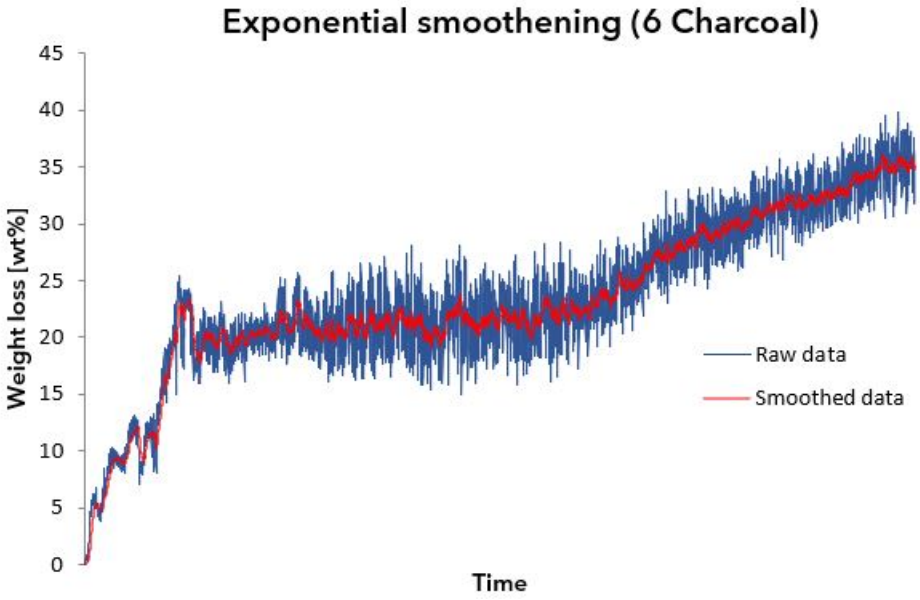

Figure 3.8: Weight loss curves for experiment 6 with charcoal. One curve from obtained raw data and one exponential smoothed curve from the data.

3.3 Microscopy chemical analyses

After the furnace experiments, the slag and alloy samples underwent chemical analysis using an electron probe micro analyser (EPMA) and scanning electron microscopy (SEM). Prior to the microscope analysis, a pre-treatment program was implemented for the samples to ensure optimal sample preparation and analysis.

3.3.1 Sample preparation

The crucibles were retrieved from the furnace and filled with epoxy to provide stability and anchoring for further treatment. Once the epoxy had cured, the crucibles were cut in half to to try to expose a cross section containing both slag and alloy. The cross section of interest was then further trimmed to fit into a circular sample holder, and the empty space around the sample was filled with epoxy. After the epoxy had fully cured, the samples were ready for metallographic preparation.

The metallographic preparation of the samples was carried out using a Struers Tegra-Pol 31 semi-automatic grinding and polishing machine. Initially, grinding was performed using a 220 SiC-paper to remove any surface irregularities and create a flat surface. Following grinding, a three-stage polishing process was conducted, as outlined in Table 3.7. Each polishing step was performed twice to ensure a consistent and high-quality surface

finish. Between each step, the samples were placed in an ultrasound bath to remove any residue and contaminants.

Table 3.7: Overview of the grinding and polishing procedure performed before microscope analysis.

Step	Paper/Plate	Suspension	Lubricant	Time [min]
1	SiC-paper #220	-	Water	1
2	Largo, Allegro/Largo	DiaPro Allegro/Largo	-	5
3	DaC	DiaPro DaC	-	4
4	Nap-R	DiaPro Nap-R	-	2

Before the samples could be analyzed in the microscopes, they underwent a carbon coating process to enhance conductivity. Aluminium foil was wrapped around each sample, and carbon tape was used to ensure good contact with the coated sample surface. The last step involved for the samples to be placed in a heating cabinet for several hours.

3.3.2 Electron Probe Micro Analyser (EPMA)

The EPMA analysis was performed using a Jeol JXA-8500F (Field emission) microscope operated by an own dedicated operator at NTNU. EPMA, a type of electron microscope, was employed to obtain information about the chemical composition of different phases within the slag and metal samples. This technique operates by directing an electron beam onto a solid specimen with sufficient energy to generate X-rays, thereby enabling chemical analysis of the material [34]

In the case of the slag sample analysis, three points on the surface were randomly selected for each phase present. As for the analysed metal droplets, a combination of three-point analyses and defocused averages were conducted.

3.3.3 Scanning Electron Microscopy (SEM)

Additional analyses were conducted using a Zeiss Ultra 55 Field Emission Gun SEM, which involved examining the slag structure using backscatter electrons (BSE) and Energy Dispersive Spectroscopy (EDS) to gather data on the chemical composition of the samples. SEM is a type of microscope that employs accelerated electrons and when the electron beam interacts with the sample, it generates secondary electrons, backscatter electrons, and x-rays. Secondary electrons are used for surface imaging,

while the x-rays are analysed using an electron dispersive spectrometer (EDS) to identify the elements present in the sample.

The same pre-treatment procedure used for the EPMA analyses was also applicable for the SEM EDS analyses. A minimum of three spots or areas were analyzed for each phase present in the slag samples. The slag structure was examined using backscatter electrons (BSE). Some important parameters for the EDS analysis are presented in Table 3.8.

Table 3.8: Overview of EDS parameters.

Parameter	Value
Acceleration voltage	15.0 kV
Aperture diameter	120 µm
High current mode	Yes
Working distance (WD)	10-13 mm
Acquisition time	30 s

3.3.4 Quantitative analysis of the multi-phased slags

ImageJ, an image processing software, was utilised to analyse two-phase slag samples. In cases where the slag was not homogeneous, ImageJ was used to estimate the proportions of the two phases present. It was assumed that the phase distribution was relatively even throughout the slag, but in cases where significant variations were observed, representative sections of the slag were selected for analysis. The relevant slag images obtained from EPMA were adjusted for brightness and contrast to enhance the differentiation between the phases. Dark areas in the images were identified as either pores or carbon, while light and dark grey regions represented the two phases within the crystalline slag structure. The brightest regions corresponded to metal droplets. Precise adjustment of the image was crucial to establish an accurate manually set threshold, thereby reducing measurement uncertainties. The obtained phase fractions were combined with the weight percentages of the chemical components in each phase, allowing for a comprehensive chemical analysis of the overall slag composition.

Figure 3.9 illustrates the threshold setting in ImageJ. Figure 3.9a and Figure 3.9b display the same image obtained from EPMA, with the difference being that the image in Figure 3.9b has undergone processing in ImageJ. The threshold has been adjusted to capture all black and dark grey regions, which are highlighted in red.

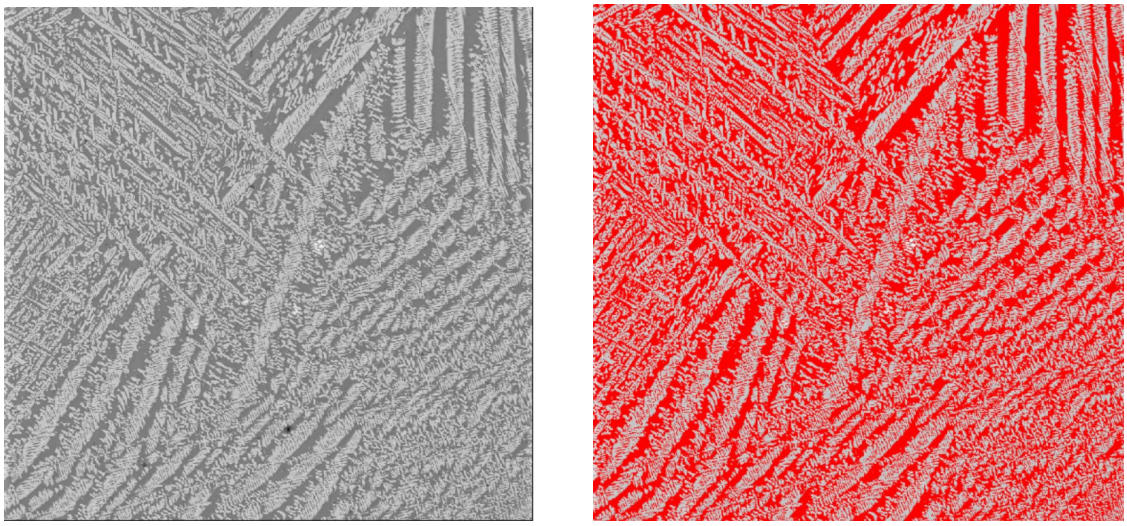

(a) Slag image from EPMA. **(b)** Threshold set in ImageJ.

Figure 3.9: Slag from Test 5 imaged in EPMA, magnitude = 200x. Left: Image from EPMA Right: Threshold set to capture the darker phases.

3.4 Calculations and Assumptions

Based on the chemical composition and the weight of the raw materials used in the coke/charcoal charges, as provided in Table 3.1 and Table 3.3 respectively, the total initial mass of each compound was calculated. The calculation method is exemplified by the calculation of the initial mass of MnO in Equation 3.1.

$$m_{MnO} = m_{ore} \cdot \frac{MnO_{ore}}{ore_{tot}} + m_{carbon} \cdot \frac{MnO_{carbon}}{carbon_{tot}} + m_{quartz} \cdot \frac{MnO_{quartz}}{quartz_{tot}} \tag{3.1}$$

where m_{ore}, m_{carbon} and m_{quartz} represent the total amount of Comilog-ore, carbon source (coke/charcoal) and quartz added to the charge, respectively, measured in grams (g). Similarly, MnO_{ore}, MnO_{carbon} and MnO_{quartz} denote the weight percent (wt%) of MnO in the respective charge component. The values m_{ore}, m_{carbon} and m_{quartz} are the total weight percent (wt%) obtained from the chemical analysis of the corresponding charge component.

The initial quantity calculations of the chemical components serve as the foundation for the subsequent mass transfer analysis. In this analysis, certain assumptions were made regarding the chemical composition after full pre-reduction at approximately 1200°C:

- Complete vaporization of moisture

- All CO_2 has gone off from carbonates
- All MnO_2 and higher Mn-oxides has been reduced in solid-state by CO-gas to MnO
- All iron oxides (ex. Fe_2O_3) has been reduced by CO-gas to metallic iron (Fe)
- All volatiles are evaporated from charcoal

Based on these assumptions, the chemical composition of the primary slag for the charges was calculated, and the results are presented in Table 3.9.

Table 3.9: Calculated chemical composition of the primary slag in wt% for the charges with coke and charcoal as reductants.

Charge	**[wt%]**				
	MnO	**SiO_2**	**Al_2O_3**	**MgO**	**CaO**
Coke	50.42	33.52	7.18	0.36	8.53
Charcoal	51.92	32.50	6.31	0.33	8.94
Charcoal + S	51.06	31.96	6.21	0.32	8.76

The total weight loss from pre-reduction was calculated as shown in Equation 3.2:

$$Weight\,loss_{pre-reduction} = (n_{\mathrm{MnO_2}} \cdot M_{CO}) + (n_{\mathrm{Fe_2O_3}} \cdot 3 \cdot M_{CO}) + m_{\mathrm{CO_2{}^+H_2O^+volatiles}} \quad (3.2)$$

where n represents the moles of the component, M denotes the molar mass of the component in [g/mole], and m represents the mass of the component in [g]. $m_{\mathrm{CO_2{}^+H_2O^+volatiles}}$ represents the total weight of possible carbon dioxide, moisture, and volatiles present in the charge.

Equation 3.3 and Equation 3.4 was used to measure the mass of MnO and SiO_2 in the end slag, both theoretically (with the target 5 wt% MnO and 40 wt% SiO_2 in the end slag) and analysed slag from the experiments.

$$m_{MnO} = \frac{m_{\mathrm{Al_2O_3},MgO,CaO}}{wt\%(\mathrm{Al_2O_3} + MgO + CaO)} \cdot wt\%MnO \quad (3.3)$$

$$m_{\mathrm{SiO_2}} = \frac{m_{\mathrm{Al_2O_3},MgO,CaO}}{wt\%(\mathrm{Al_2O_3} + MgO + CaO)} \cdot wt\%\mathrm{SiO_2} \quad (3.4)$$

The total mass of irreducible oxides is denoted as $m_{Al_2O_3,MgO,CaO}$ [g], where the oxides are calculated individually with the use of Equation 3.1. This is because the mass of these oxides remains constant throughout the process. The weight percentages of MnO and SiO_2 are determined through analysis of the slag samples, along with the total weight percentage of Al_2O_3, MgO, and CaO.

The mass of the metal in the produced alloy is determined by calculating the difference between the compositions of the end slag and the primary slag. The mass of Mn and Si in the alloy can be calculated using 3.5 and 3.6 respectively.

$$Mass_{Mn} = (n_{MnO,primary} - n_{MnO,end}) \cdot M_{Mn} \tag{3.5}$$

$$Mass_{Si} = (n_{SiO_2,primary} - n_{SiO_2,end}) \cdot M_{Mn} \tag{3.6}$$

The weight loss resulting from the reduction process can be determined by considering the mass of CO gas produced during the reactions, as shown in Equation 3.7.

$$Weight\ loss_{reduction} = (n_{Mn} \cdot M_{CO}) + (n_{Si} \cdot 2 \cdot M_{CO}) \tag{3.7}$$

Table 3.10 presents the calculated weight losses in wt% of the charge for the three different charges. These calculations were based on the previously mentioned assumptions and the assumption that the reduction process has reached an equilibrium state.

Table 3.10: Calculated weight loss for the three different charges in wt%

Coke charges: 13.15g Charcoal charges: 12.87g Charcoal + sulfur charges: 13.01g			
	[wt% loss]		
Charge	**Coke**	**Charcoal**	**Charcoal + sulfur**
Pre-reduction	16.76	17.12	16.93
Reduction	25.73	25.52	25.24
Total	42.49	42.64	42.18

4 Results

In this study, the differences between coke and charcoal as reductants in the SiMn production were investigated. Furthermore, the impact of varying the particle size of the raw materials (1-2 mm and 3.15-4 mm) was studied. The influence of sulfur added to charcoal charges on reduction of SiMn slag was also examined. The experiments were conducted in a thermogramivetric (TG) furnace, with continuous recording of weight loss during the experiments. Subsequent analysis of slag and alloy samples was performed using EPMA and SEM.

The following results chapter will present the findings obtained from the conducted experiments. Firstly, weight loss curves from the TG furnace experiments will be presented and the effect of sulfur addition to charcoal charges will be addressed. The chapter will proceed with the results of the slag and alloy analysis conducted using EPMA. Lastly, cross-section pictures from furnace experiments will be provided to enhance the understanding of the slag-carbon interface.

4.1 TGA furnace experiments

The weight loss curves obtained from the TG furnace experiments are presented in relation to the reduction zone, covering a temperature range from full pre-reduction at 1200°C to approximately 1630-1650°C. It should be noted that the zero point of weight loss is reset, excluding the weight loss from pre-reduction and focusing solely on the reduction weight loss. The zero point is set after the 30 minutes of constant heating at 1200°C, marking the end of the pre-reduction phase (see Figure 3.6). The curves have been fitted using exponential smoothing, although some disturbance still persist.

In Figure 4.1, the initial eight furnace experiments are shown. The four experiments with the longest reduction time (T2) are specifically marked in the diagram itself. It may be more challenging to identify the experiments reduced to T1 due to overlapping curves, but subsequent figures will provide clearer indications. It is important to note that no sulfur was added to the depicted charcoal charges. The temperature profile displayed corresponds to experiment (8) Charcoal, PS = 3.15-4 mm, T2, with a maximum temperature of 1640°C. The dotted horizontal line represents the calculated weight loss of about during reduction, approximately 25.73 wt% for coke charges, 25.52 wt% for charcoal charges.

The key observations from the figure includes:

- Charges using coke as the reductant exhibit easier and a faster reduction compared to those using charcoal.
- A distinct two-step reduction mechanism is evident in the coke charges, characterized by a slow and first step and rapid reduction rate in the second step.
- In contrast, the charcoal charges display a slow and steady reduction rate, without the pronounced rapid reduction observed in the coke charges.

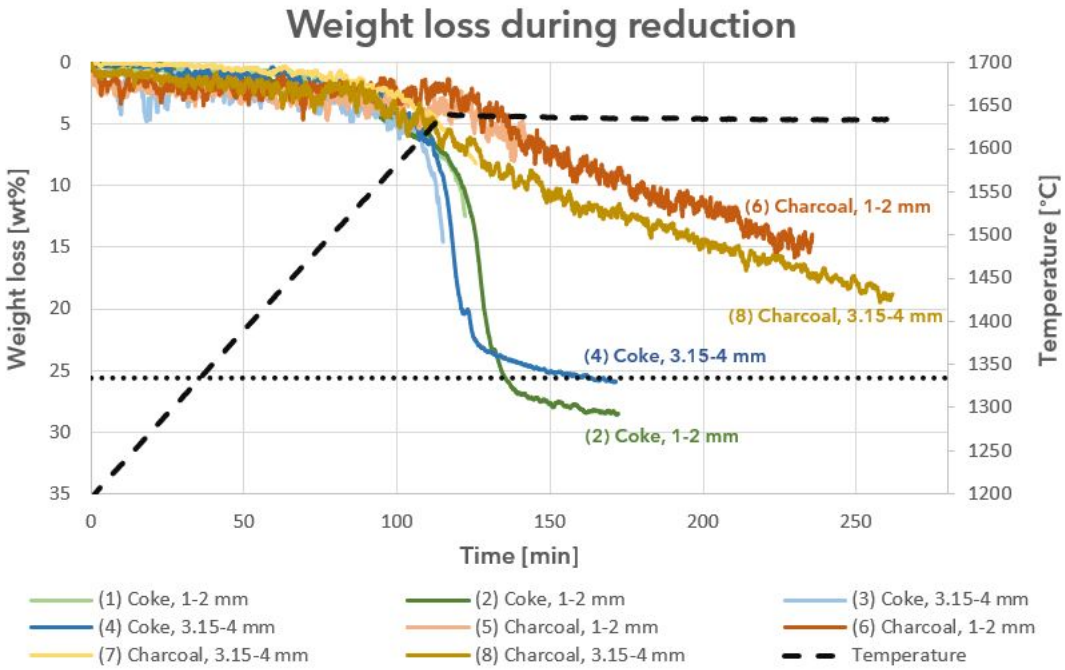

Figure 4.1: Weight loss curves

The following figures, derived from Figure 4.1, provide a more detailed comparison of the reduction behavior in coke and charcoal charges. Figure 4.2 and Figure 4.3 compare the reduction of coke and charcoal charges with the same particle size, allowing for a direct assessment of the two reductants. Moreover, Figure 4.4 and Figure 4.5 focuses on the influence of varying particle sizes in the charges and how it affect the reduction rate.

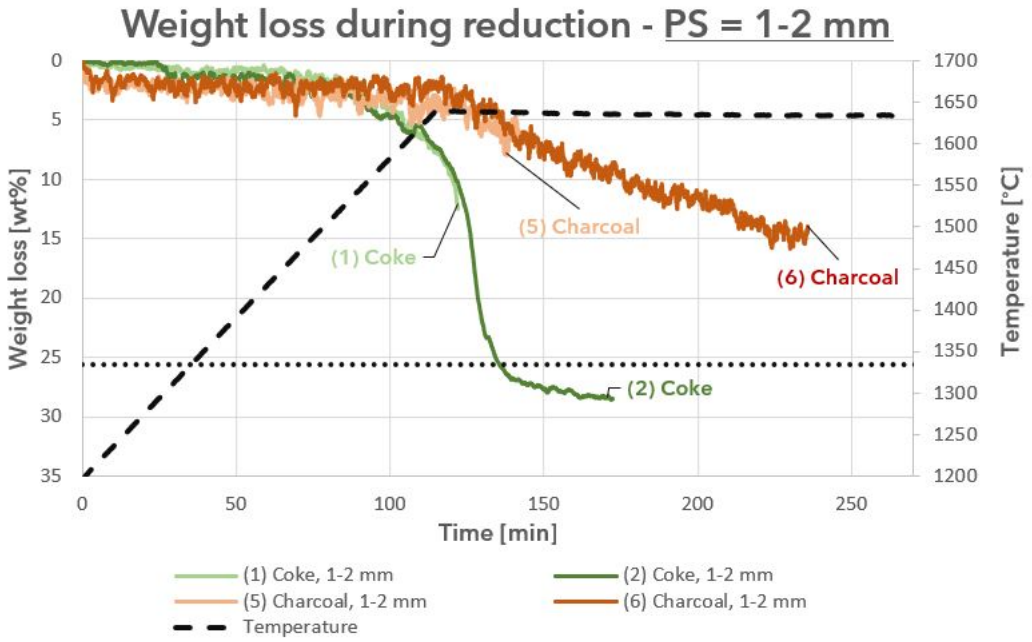

Figure 4.2: Weight loss curves for charges with a particle size of 1-2 mm.

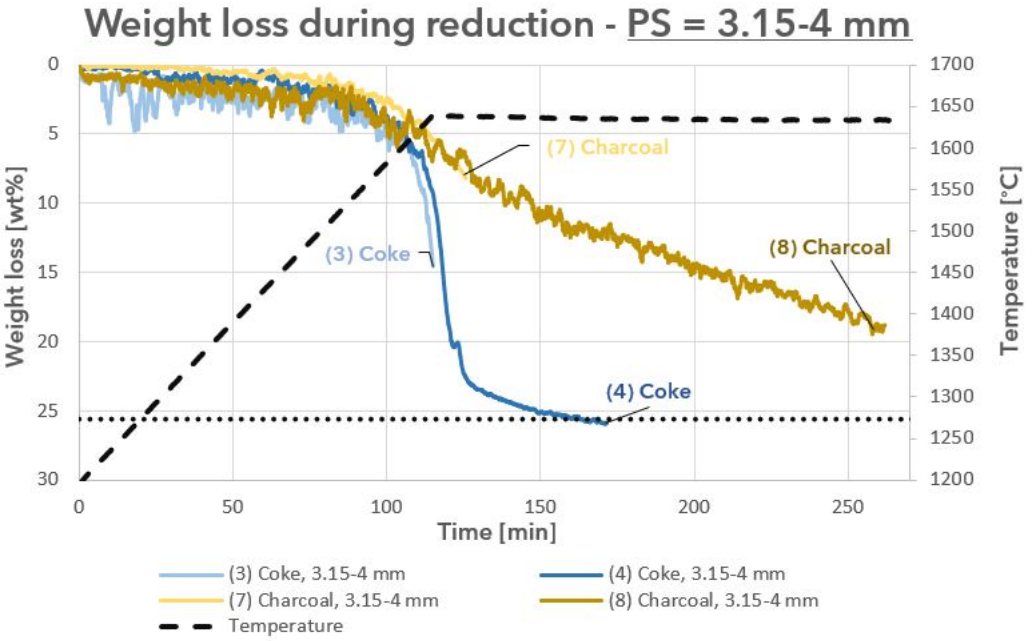

Figure 4.3: Weight loss curves for charges with a particle size of 3.15-4 mm.

Coke charges

From the weight loss curves of coke charges depicted in 4.4, a noticeable trend can be observed. The charges with particle sizes of 3.15-4 mm exhibit a tendency for rapid reduction to occur at slightly lower temperatures compared to the charges with particle sizes of 1-2 mm.

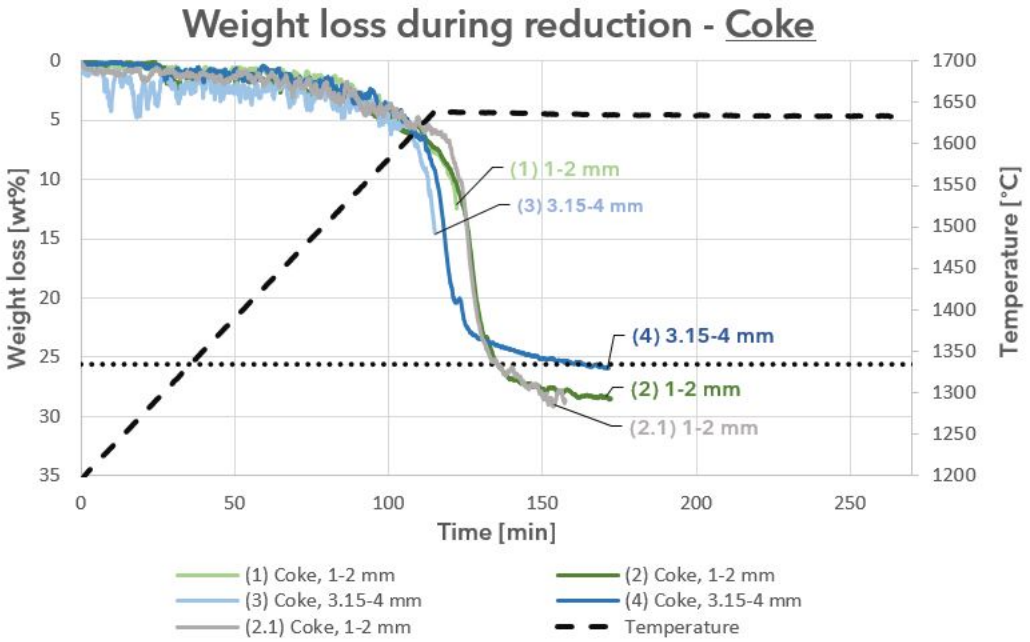

Figure 4.4: Weight loss curves for coke charges.

Charcoal charges

The weight loss curves presented in 4.5 demonstrate a similar trend to that observed in the coke charges. Specifically, charges with particle sizes of 3.15-4 mm display a higher reduction rate at lower temperatures compared to charges with particle sizes of 1-2 mm. However, it is worth noting that the weight loss curves of charcoal charges exhibited a significant degree of unfortunate fluctuations, which may have affected the accuracy and consistency of the results.

Figure 4.5: Weight loss curves for coke charges.

4.1.1 Sulfur addition to charcoal charges

Sulfur was introduced to certain charges with charcoal as the reductant by adding K_2SO_4. However, due to an error in the mass balance unit of the TG furnace, weight loss curves for these experiments could not be obtained. Instead, the weight loss was manually measured, as shown in Table 4.1. As a consequence, the total weight loss from the experiments is provided, not the reduction weight loss.

Table 4.1: Manually measured weight loss for charges with charcoal and added sulfur.

Charcoal + sulfur charge: 13.01g				
Experiment	**Weight in [g]**	**Weight out [g]**	**Weight loss [g]**	**Weight loss* [wt%]**
(5+S) PS=1-2mm, -	71.58	69.14	2.44	18.75
(5.1+S) PS=1-2mm, T1	70.90	65.13	5.77	44.35
(6+S) PS=1-2mm, T2	70.98	64.92	6.06	46.58
(7+S) PS=3.15-4mm, T1	71.81	65.64	6.17	47.43
(8+S) PS=3.15-4mm, T2	70.89	64.70	6.19	47.58
*Total weight loss in wt% of charge weight				

In 4.6, the total weight loss of all experiments conducted with charcoal as the reductant is plotted against time. The charges that had sulfur added to them are denoted with "+S". It is evident that there are significant differences in weight loss when sulfur is present in the charges. The experiments with sulfur addition exhibit a much higher total weight loss, indicating a higher reduction rate compared to the experiments without sulfur.

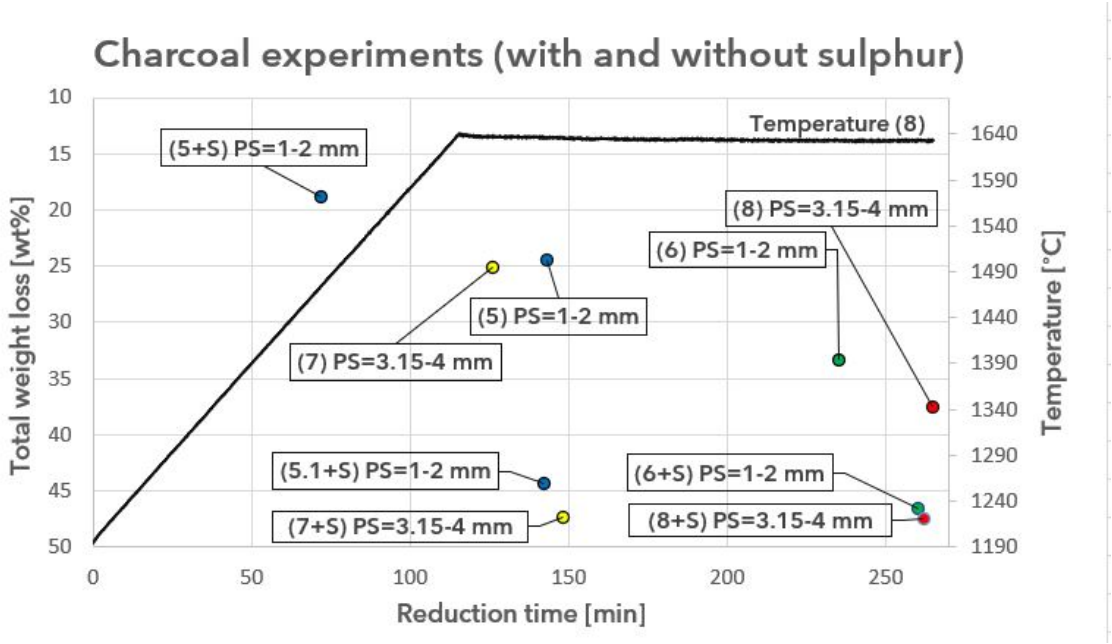

Figure 4.6: Plotted total weight loss for charcoal charges with and without added sulfur.

Figure 4.7 and Figure 4.8 differentiates between the two particle sizes used in the charges. The weight loss curves for the charcoal charges without added sulfur are included to highlight the difference observed when sulfur is added to the slag. It is evident that the addition of sulfur in the charcoal charges enhances the reduction rate and leads to earlier reduction. Moreover, the measured weight loss for charcoal charges with sulfur added to the slag has reached the calculated equilibrium weight loss, not only for charges reduced to T2 but also for those reduced to T1.

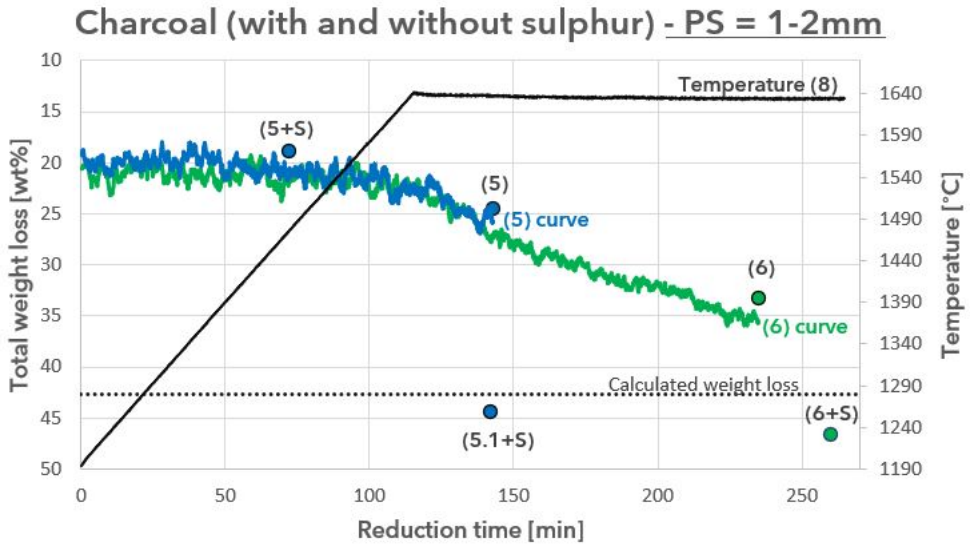

Figure 4.7: Weight loss for charcoal charges with and without sulfur added to the slag. PS = 1-2 mm.

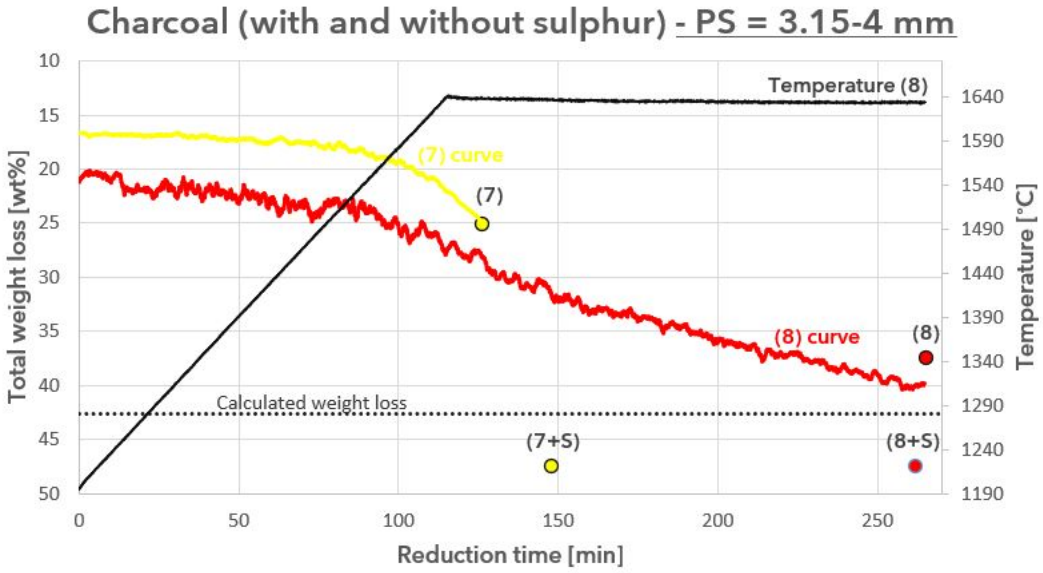

Figure 4.8: Weight loss for charcoal charges with and without sulfur added to the slag. PS = 3.15-4 mm.

4.2 Chemical analysis - slag and alloy

The slag and alloy samples were analysed in EPMA and SEM after the TGA furnace experiments. In this section, only the analysis obtained from the EPMA will be presented. The analysis was performed to determine the chemical composition of the reduced slag

and produced alloy. It is through the examination of the slag composition that the extent of reduction that took place during the process can be assessed.

Table 4.2 shows the average of the three-point analysis from the EPMA for the most prominent oxides, the full analysis can be found in subsection C. It shows that the amount of MnO in slag decrease as the holding time increase. It can be observed that the R-ratio varies somewhat for between the two holding times. To repeat the calculated R-values; R-ratio for coke charges 1.23 and for charcoal charges 1.47.

Experiment 1, which used coke as the reducing agent, was terminated around the observed rate shift, as shown in Figure 4.4. The composition of the resulting slag from this experiment consists of approximately 30 wt% MnO and 45 wt% SiO_2.

Table 4.2: Chemical analysis of the slag samples from EPMA.

Exp.	Parameters	Red. time [min]	Temperature [$^{\circ}C$]	MnO [wt%]	SiO_2 [wt%]	Al_2O_3 [wt%]	CaO [wt%]	Weight loss [wt%]	R-ratio
1	Coke PS=1-2mm	122 (T1)	1641	29.39	45.38	10.76	12.52	31.2	1.2
2	Coke PS=1-2mm	173 (T2)	1626	3.46	39.60	21.94	31.32	45.1	1.5
2.1	Coke PS=1-2mm	158 (T2)	1642	3.17	31.63	30.13	34.89	44.1	1.2
3	Coke PS=3.15-4mm	115 (T1)	1644	21.23	50.04	10.40	17.87	29.9	1.8
4	Coke PS=3.15-4mm	172 (T2)	1636	2.18	38.18	24.02	33.34	42.0	1.4
5	Charcoal PS=1-2mm	143 (T1)	1634	46.16	38.89	5.94	9.26	24.5	1.7*
6	Charcoal PS=1-2mm	235 (T2)	1645	31.13	44.27	9.84	13.72	33.3	1.5
7	Charcoal PS=1-2mm	126 (T1)	1638	44.19	39.27	6.19	11.37	25.1	1.9*
8	Charcoal PS=3.15-4mm	265 (T2)	1639	26.00	44.66	10.48	16.84	37.5	1.7
5+S	Charcoal PS=1-2mm	72 (-)	1473	54.36	31.62	5.85	7.47	18.8	1.3*
5.1+S	Charcoal PS=1-2mm	143 (T1)	1644	6.09	43.08	19.6	27.97	44.4	1.5
6+S	Charcoal PS=1-2mm	260 (T2)	1637	3.37	44.36	21.72	30.05	46.6	1.4
7+S	Charcoal PS=3.15-4mm	148 (T1)	1659	1.72	36.51	23.67	36.74	47.4	1.6
8+S	Charcoal PS=3.15-4mm	262 (T2)	1643	1.81	37.36	25.04	33.90	47.5	1.4

*two-phase slag

Table 4.2 has been condensed and presented as Table 4.3.The amount of reduced MnO and SiO_2 have been calculated as a percentage of the amount of MnO and SiO_2 reduced

from the calculated initial slag. It is important to note that when calculating the reduced amount of MnO and SiO_2, it was assumed that the remaining oxides (CaO, MgO and Al2O3) are not reducible and therefore remain unchanged throughout the reduction process. The presence of negative values for reduced SiO2 and MnO in the two-phase slags indicates little reduction, along with uncertainties associated with measurements related to the two phases.

It is evident that there is a noticeable difference in the reduction of MnO and SiO_2 compared to charges without sulfur addition. Experiments 5.1+S and 7+S indicate that the addition of sulfur to the slags in charcoal charges leads to an earlier onset of reduction. However, without the addition of sulfur, the reduction of both MnO and SiO_2 is relatively low for charcoal charges, particularly for SiO_2.

Table 4.3: Chemical analysis of the slag samples from EPMA.

Exp.	Parameters	Red. time [min]	Temp. [$°C$]	MnO [wt%]	SiO_2 [wt%]	$CaO^+MgO^+Al_2O_3$ [wt%]	Reduced MnO[%]	Reduced SiO_2[%]	R-ratio
1	Coke PS=1-2mm	122 (T1)	1641	29.39	45.38	23.89	60.81	8.96	1.2
2	Coke PS=1-2mm	173 (T2)	1626	3.46	39.60	54.76	97.98	65.35	1.5
2.1	Coke PS=1-2mm	158 (T2)	1642	3.17	31.63	65.56	98.55	78.23	1.2
3	Coke PS=3.15-4mm	115 (T1)	1644	21.23	50.04	29.05	76.72	17.47	1.8
4	Coke PS=3.15-4mm	172 (T2)	1636	2.18	38.18	58.55	98.81	68.75	1.4
5	Charcoal PS=1-2mm	143 (T1)	1634	46.16	38.89	15.75	12.05	-18.38	1.7*
6	Charcoal PS=1-2mm	235 (T2)	1645	31.13	44.27	24.18	61.37	12.23	1.5
7	Charcoal PS=1-2mm	126 (T1)	1638	44.19	39.27	18.15	26.94	-3.71	1.9*
8	Charcoal PS=3.15-4mm	265 (T2)	1639	26.00	44.66	28.16	72.30	23.98	1.7
5+S	Charcoal PS=1-2mm	72 (-)	1473	54.36	31.62	13.67	-19.29	-10.85	1.3*
5.1+S	Charcoal PS=1-2mm	143 (T1)	1644	6.09	43.08	48.91	96.97	57.78	1.5
6+S	Charcoal PS=1-2mm	260 (T2)	1637	3.37	44.36	52.96	98.09	59.85	1.4
7+S	Charcoal PS=3.15-4mm	148 (T1)	1659	1.72	36.51	61.81	99.17	71.69	1.6
8+S	Charcoal PS=3.15-4mm	262 (T2)	1643	1.81	37.36	60.51	99.10	70.40	1.4

*two-phase slag

The slags from the three samples marked with asterisks (*) in the above tables were found to be non-homogeneous. These samples were as follows:

- 5 Charcoal. Heated to 1634°C and held until a reduction weight loss approxi-

mately 7-8 wt%.

- 7 Charcoal. Heated to 1638°C and held until a reduction weight loss approximate 8 wt%.
- 5+S Charcoal with sulfur slag. This experiment was terminated prematurely at 1473°C due to the snapping of the Mo-wire.

The two-phase slags from these samples were analysed using ImageJ to determine the relative amounts of each phase in the slag. The results, shown in Table 4.4, were normalised by excluding the contributions of pores/carbon and metal. The process of differentiating the phases using ImageJ is described in Figure 3.9.

Table 4.4: Overview of the approximate amount [%] of the two slag phases in the slag structure, analysed in ImageJ.

Slag sample	**Pores/C**	**Alloy**	**Slag phase**		**Tot.**	**Slag norm.**		**Tot.n.**
			Grey (d)	Grey (l)		Grey (d)	Grey (l)	
5	0.08	0.02	45.14	55.60	100.84	44.81	55.19	100
7	0.29	0.00	48.67	51.34	100.30	48.67	51.33	100
5+S	0.39	0.02	24.94	74.97	100.29	24.94	75.06	100

Similar to the homogeneous slags, the two phases of the slags were subjected to a three-spot analysis using EPMA. Table 4.5, displays the average weight percentages of the analysed spots for compounds present in the respective phase. The analysis reveals that the light phase exhibits a higher content of MnO and lower content of SiO2 compared to the dark phase.

Table 4.5: Analysed composition of the two slag phases given in average wt% of a three point analysis EPMA

		[wt%]				
	Slag phase	**MnO**	**SiO_2**	**Al_2O_3**	**MgO**	**CaO**
5	Dark grey	25.61	46.48	12.99	0.15	15.50
	Light grey	62.84	32.73	0.22	0.87	4.18
7	Dark	25.25	45.93	12.52	0.21	17.58
	Light	62.15	32.95	0.19	0.95	5.48
5+S	Dark	30.86	29.91	22.57	0.03	12.21
	Light	62.18	32.19	0.30	0.45	5.90

Figure 4.9 displays the two-phase slags obtained from experiments 5 and 7, using charcoal as the reducing agent. The images reveal a significant variation in the coarseness of the slag structure, leading to increased uncertainty in the measurements.

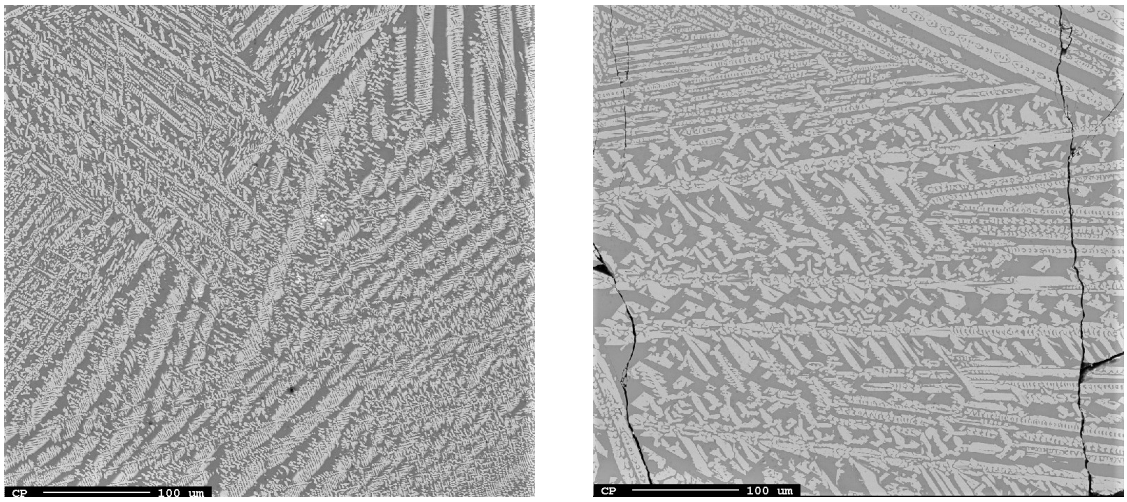

(a) 5 Charcoal **(b)** 7 Charcoal

Figure 4.9: Slag micrographs from EPMA, experiments 5 and 7 with charcoal. Heated to 1634-1638°C.

An example of a more homogeneous slag is provided in Figure 4.10.

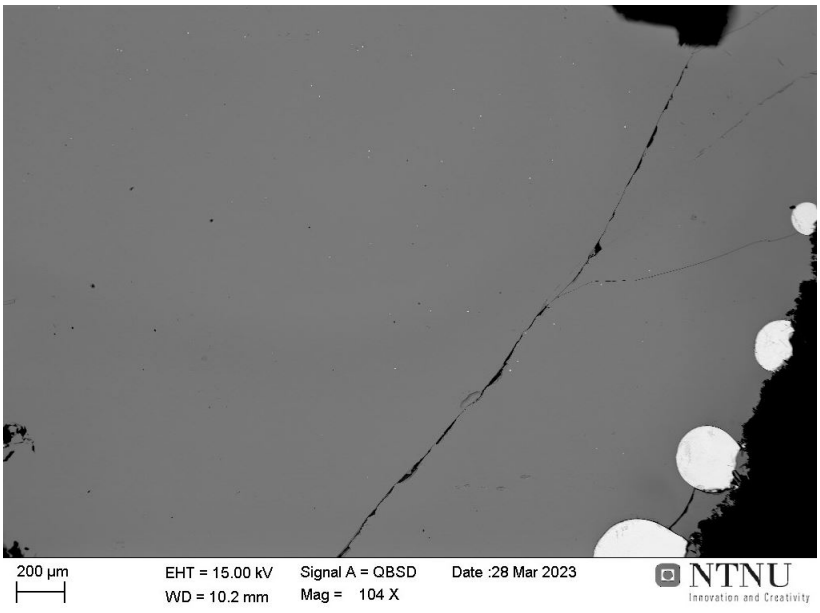

Figure 4.10: Image from BSE in SEM of homogeneous slag from experiment 1 coke heated to 1641°C. Small metal droplets can be observed at the edge of the slag.

In experiments with added sulfur, the slags exhibited white areas, as shown in the overview image of the slag from experiment 8+S in Figure 4.11. A closer look at these areas is provided in Figure 4.12. These white areas are believed to be metal prills with a precipitated layer of MnS on the outer surface of the metal [27].

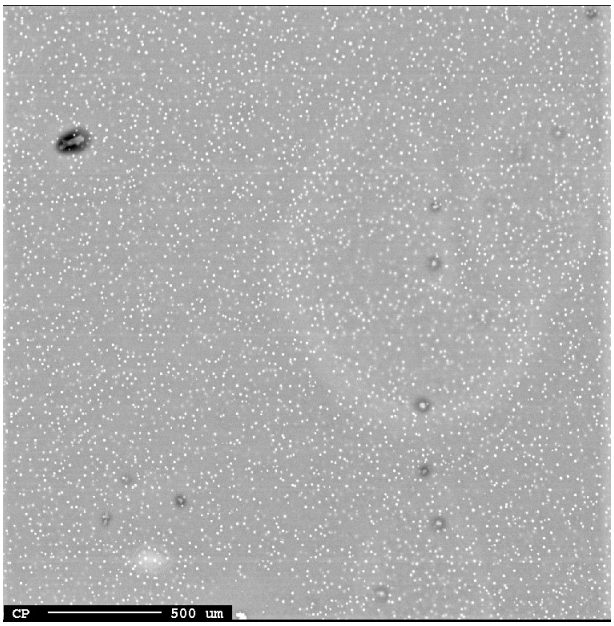

Figure 4.11: Overview EPMA image of slag from experiment 8+S.

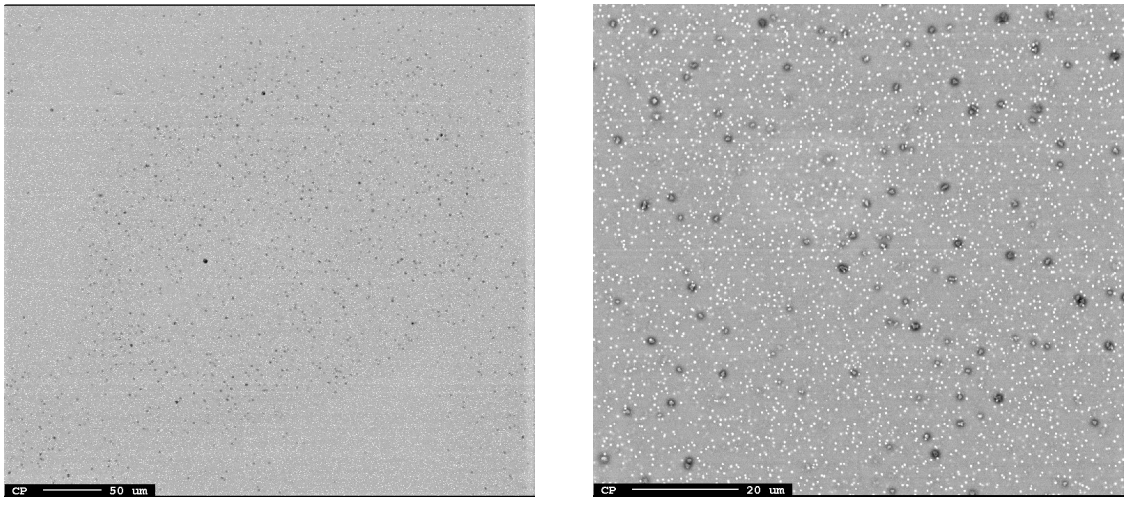

(a) **(b)**

Figure 4.12: EPMA images of experiments 8+S with charcoal. Heated to 1643°C.

The metal was also subjected to analysis using EPMA, employing a three-point/defocused

area average analysis. The average composition of these points is presented in Table C2, with a detailed analysis provided in the subsection C and complementing images in Table C. It should be noted that the chemical analysis of the metal is often less reliable compared to the slag analysis. The metal particles may exhibit different compositions, with smaller particles inside the slag having a higher iron content, while larger particles on the surface of the slag may have a higher manganese content.

Table 4.6: EPMA analysis of the metal alloy produced from the slag.

Exp.	Parameters	Red. time [min]	Temperature [$^{\circ}C$]	Mn [wt%]	Si [wt%]	Fe [wt%]	Tot. weight loss [wt%]
1	Coke PS=1-2mm	122 (T1)	1641	86.14	8.86	4.31	31.2
2	Coke PS=1-2mm	173 (T2)	1626	83.76	16.29	0.98	45.1
2.1	Coke PS=1-2mm	158 (T2)	1642	87.91	10.34	1.58	44.1
3	Coke PS=3.15-4mm	115 (T1)	1644	85.12	13.96	0.76	29.9
4	Coke PS=3.15-4mm	172 (T2)	1636	82.10	11.63	5.55	42.0
5	Charcoal PS=1-2mm	143 (T1)	1634	71.57	1.54	22.63	24.5
6	Charcoal PS=1-2mm	235 (T2)	1645	84.71	5.01	8.65	33.3
7 Light	Charcoal PS=1-2mm	126 (T1)	1638	61.59	3.15	33.60	25.1
7 Grey				69.65	0.00	27.62	
7 Dark				72.25	0.00	22.97	
8	Charcoal PS=3.15-4mm	265 (T2)	1639	81.52	7.21	9.83	37.5
5+S	Charcoal PS=1-2mm	72 (-)	1473	38.68	0.00	53.86	18.8
5.1+S	Charcoal PS=1-2mm	143 (T1)	1644	72.08	12.96	13.59	44.4
6+S	Charcoal PS=1-2mm	260 (T2)	1637	81.11	18.33	0.56	46.6
7+S	Charcoal PS=3.15-4mm	148 (T1)	1659	78.02	15.76	4.88	47.4
8+S	Charcoal PS=3.15-4mm	262 (T2)	1643	73.33	18.57	9.12	47.5

From the table above, it is evident that experiment 7 with charcoal exhibited three distinct metal phases within its droplet, as depicted in Figure 4.13. The dark phase was found to have a higher manganese content, while the light grey phase displayed the highest iron content and also contained a small amount of silicon. Additionally,

phosphorus was observed in the light grey phase.

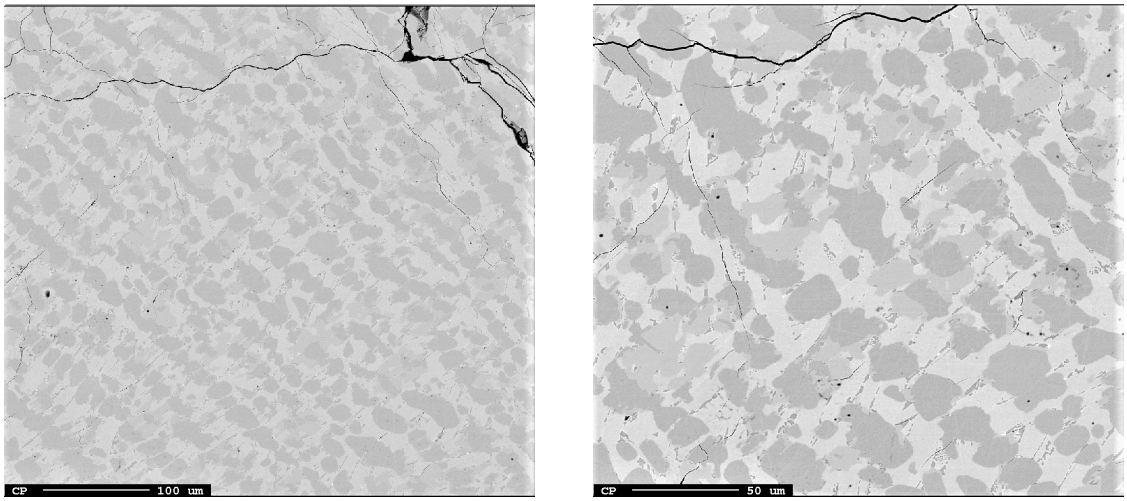

(a) **(b)**

Figure 4.13: EPMA images of metal sample from experiment 7 with charcoal at different magnitudes. Heated to 1638°C. Three phases present as three different tones of grey.

4.3 Slag-carbon interface from crucible cross-sections

The interface between the carbon material and the slag were investigated with varying particle sizes of 1-2 mm and 3.15-4mm.

Figure 4.14 depicts some crucible cross-sections of experiment 1 and 3 with coke with different particle sizes. Polished samples of the same experiments are shown in Figure 4.15. The figures depict a glassy transparent brown-red slag and some metal droplets.

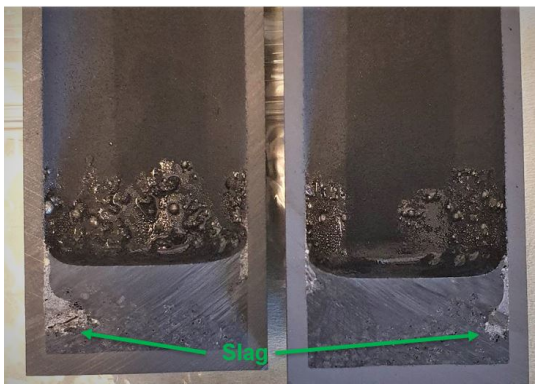

(a) (1) Coke, PS = 1-2 mm

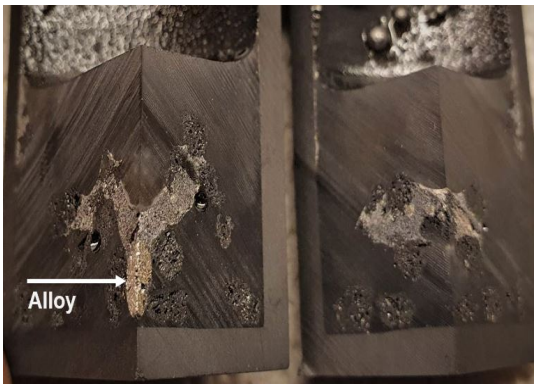

(b) (3) Coke, PS = 3.15-4mm

Figure 4.14: Cross-sections for coke experiments with a) PS = 1-2mm and b) PS = 3.15-4mm.

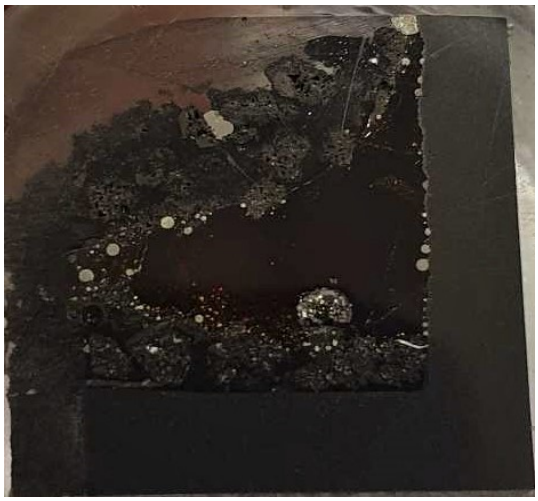

(a) (1) Coke, PS = 1-2 mm

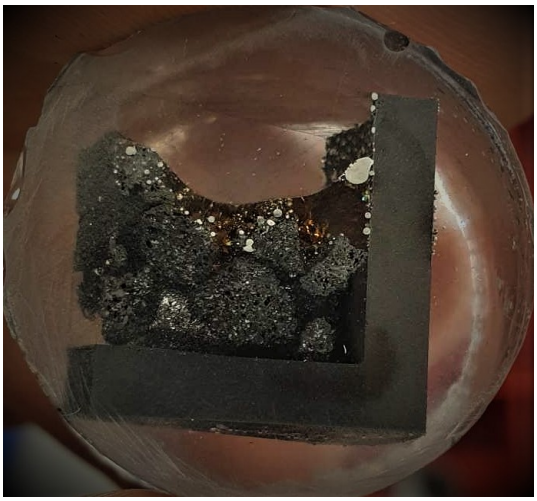

(b) (3) Coke, PS = 3.15-4mm

Figure 4.15: Polished cross-sections of slag samples from Figure 4.14.

Figure 4.16 depicts two charcoal charges with varying particle sizes placed on a bed of charcoal.

(a) (5) Charcoal, PS = 1-2 mm **(b)** (7) Charcoal, PS = 3.15-4mm

Figure 4.16: Charcoal charges with varying particle sizes. Slag on a bed of charcoal.

The figures presented above suggest a tendency that slag tends to cover the larger particles to a greater extent compared to charges with smaller particles. This results in an increased interface area for reduction. In the figures depicting charges with carbon particles of 1-2 mm, a more compact carbon bed can be observed, indicating less penetration of slag into the carbon bed.

5 Discussion

This chapter delves into the discussion of the findings obtained from the SiMn production in the TGA furnace and the subsequent chemical analysis. Firstly, the focus is on the furnace experiments, specifically the weight loss curves, the impact of sulfur addition to charcoal charges, and the observations of the slag-carbon interface. The chemical analysis conducted using EPMA is also examined, providing insights into the composition and the reduction of MnO and SiO_2. Finally, the reliability, and any limitations or uncertainties associated with the furnace experiments are addressed.

5.1 TGA furnace experiments

Figure 4.1 shows the experiments using coke and charcoal without added sulfur. It clearly depicts the difference in reduction rate with the two carbon materials.

The charges reduced by coke followed a two-stage reduction mechanism, as previously described by **Canaguier** (2019). This reduction involves an initial slow and stable stage, followed by a rapid rate increase during the second stage. This behavior has also been observed in other studies [25] [28].

Figure 5.1 specifically focuses on the two coke charges reduced to T1. The objective was to analyse the composition when the coke charges initiated the rate shift. However, due to significant fluctuations in the weight loss readings, obtaining precise data by ending the experiment at the exact time was challenging. Nevertheless, from the figure, it can be observed that experiment 3 reached the rate shift at a reduction weight loss of approximately 6 wt%, while experiment 1 exhibited the rate shift at a loss of around 10 wt%. It must be noted that these readings have a high uncertainty due to the degree of fluctuation.

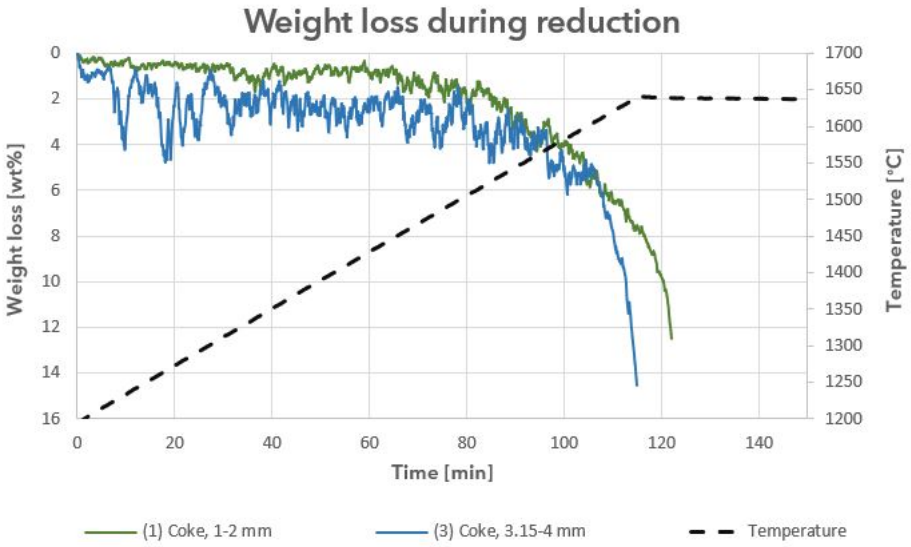

Figure 5.1: Weight loss of charcoal experiments aimed towards high degree of reduction. Equilibrium was not reached

Figure 5.2 provides a closer look at the slow reduction observed in the charcoal experiments, specifically experiments 6 and 8. These experiments were conducted with the intention of reaching an equilibrium state. However, the holding times for the experiments were too limited. A consistent and gradual reduction rate was observed, not anything like the rate shift which coke charges experienced.

Additionally, it can be noted that there was minimal reduction occurring before reaching temperatures of approximately 1550°C for experiment 8 and above 1600°C for experiment 6. However, it is important to acknowledge that the large degree of fluctuation in the weight loss readings makes it challenging to accurately determine these temperature readings.

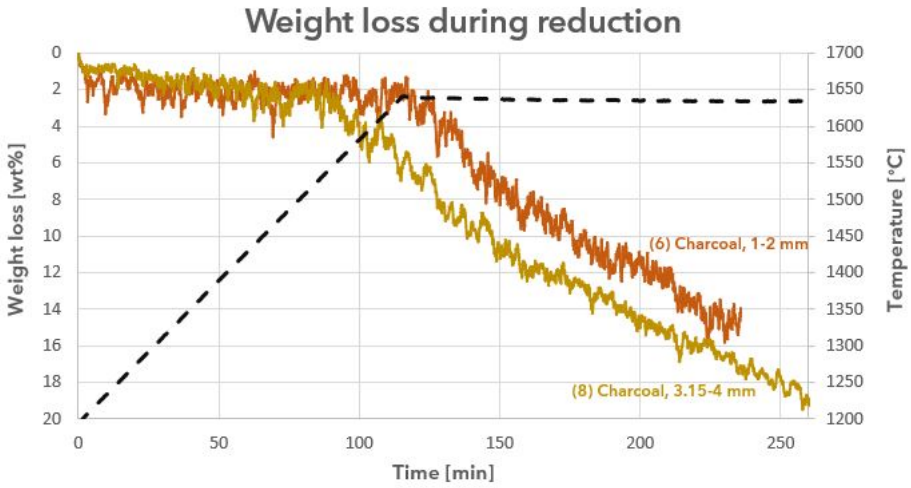

Figure 5.2: Weight loss for charcoal charges without added sulfur.

5.1.1 Slag-carbon interface with varying particle size

From Figure 4.4 and Figure 4.5, particle size variations were observed to have little impact on the reduction rates in the furnace experiments. However, in those cases where differences were observed, charges with larger particle sizes tended to initiate reduction earlier compared to charges with smaller particle sizes. This trend aligns with the findings of two earlier studies conducted by **Forberg** (2021, 2022) [28] [29].

However, the rate of reduction is generally expected to increase as the particle size of the reducing agent decreases. This expectation is based on the larger surface area available for reaction and improved inter-particle contact, which facilitate more efficient reduction processes [12]. In their study, **Kim et al.** (2016) concluded that there was no significant difference in the reduction rate of SiMn production when varying the selected particle sizes used [24].

In contrast to the particle size observations in this study, the findings of **Jayakumari and Tangstad** (2019) in their work using an induction furnace revealed a trend that aligns with expectations. They observed that larger carbon particles had slower reduction rates compared to smaller particles, resulting in higher reduction temperatures. This phenomenon was attributed to the higher flow of slag into the coke bed facilitated by smaller coke particles, which in turn promoted a higher reduction rate.[10].

From the figures shown in section 4.3 and later in Figure 5.8, it is possible to suggest

that carbon particles of size 1-2 mm create a compact carbon bed under the burden of the slag. It appears that the carbon bed is so compact that it limits the flow of slag into the bed, thus restricting the slag-carbon interface and the area available for reduction.

In contrast, when examining charges with carbon particles of 3.15-4 mm, it seems that the slag has a little more room to move and to a greater extent encompasses the carbon particles. This increased interaction between slag and carbon particles potentially leads to a larger reduction area.

It is important to emphasize that these suggestions are specific to the particle size range and slag properties studied in this research.

5.1.2 Foaming in coke charges

Foaming was observed in all of the conducted coke charges. However, there was a noticeable difference in the extent of foaming based on the amount of reduction. Charges that were reduced towards equilibrium (T2) exhibited a higher degree of foaming compared to those reduced towards the coke reduction rate shift (T1). For example, experiments 2.1 and 4 reached T2 and experienced foaming throughout the process, with the foam rising up to the lid and solidifying on the bottom, as shown in Figure 5.3 and Figure 5.4. In contrast, no foaming was observed in any of the charcoal charges without sulfur addition.

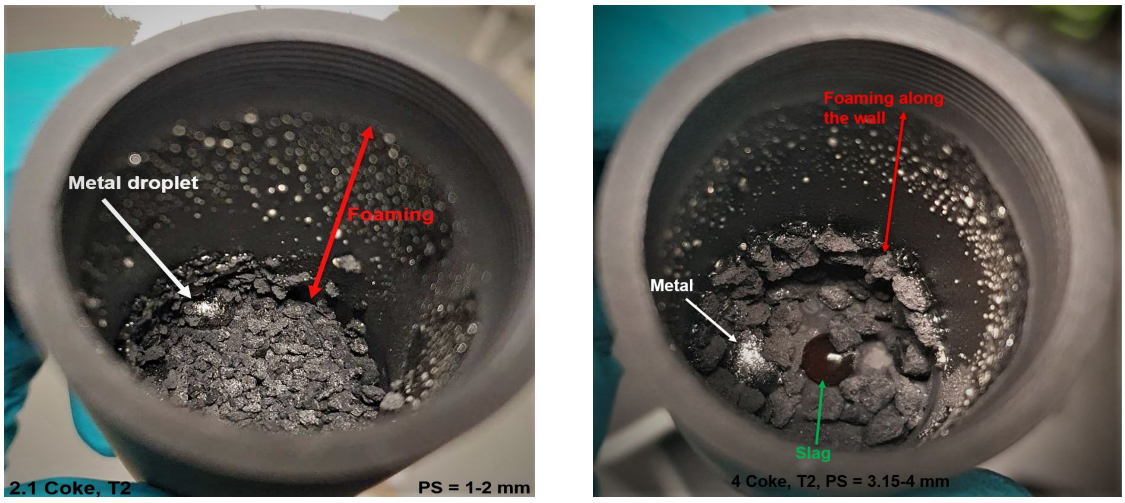

(a) (2.1) Coke, PS = 1-2 mm **(b)** (4) Coke, PS = 3.15-4 mm

Figure 5.3: Pictures of the crucible from above. Slag/metal is marked and red arrows indicate height of foaming.

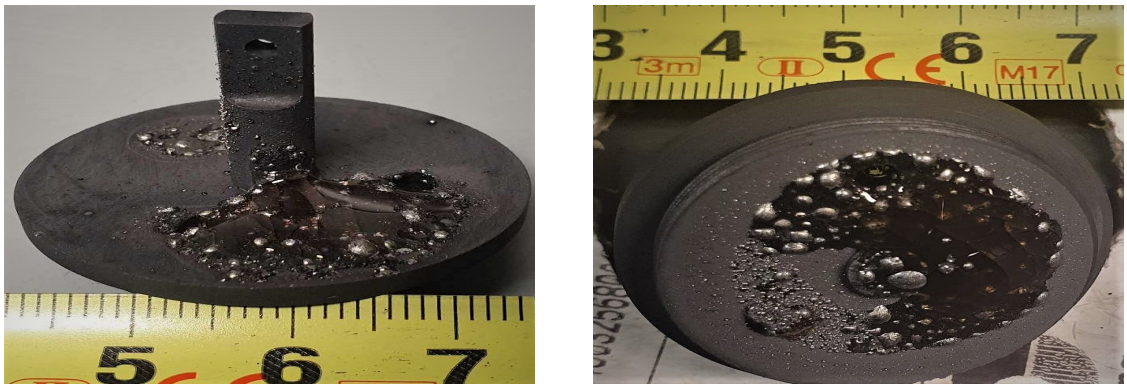

(a) (2.1) Coke, PS = 1-2 mm **(b)** (4) Coke, PS = 3.15-4 mm.

Figure 5.4: Foaming up the length of crucibles and solidifying above and under the lids for coke charges reduced towards equilibrium (T2).

Table 5.1 provides the chemical composition for coke charges 1 and 4. Slag retrieved from the crucible wall for charge 1, and slag obtained from the bottom of the crucible lid for charge 4 have been investigated in EPMA.

Table 5.1: Composition of slag for coke charges 1 and 4. Retrieved from EPMA.

		[wt%]				
	Charge	**MnO**	**SiO_2**	**Al_2O_3**	**MgO**	**CaO**
1	Slag	29.39	45.38	10.76	0.61	12.52
	Wall-foam	28.53	47.76	10.66	0.60	12.32
4	Slag	2.18	38.18	25.02	1.19	33.34
	Lid	7.97	52.11	15.49	1.22	22.10

5.1.3 Influence of sulfur in charcoal charges

In addition to the coke and charcoal charges, sulfur in the form of K_2SO_4 powder was added to four additional charcoal charges with the aim of achieving 0.3wt% S in the initial slag.

However, the charcoal+sulfur experiments faced some challenges. Firstly, the mass balance unit broke down before these experiments, resulting in the absence of weight curves. Only the total weight loss was measured by comparing the weight before and after the experiments, see Table 4.1. Consequently, the reduction times, which was dependent on the weight loss, had to be be adjusted for the charcoal+sulfur charges, and were set to match the reduction times of the charcoal charges without sulfur. Specifically, the reduction time of experiment 5 was used for T1 and experiment 8

for T2. Additionally, during experiment 5+S, the bottom Mo-wire broke at a low temperature (1473°C). As a result, an additional experiment, 5.1+S, was conducted. The temperature regimes for the other sulfur addition experiments were later corrected based on the temperature offset observed in experiment 7+S, as shown in Figure 3.7.

Several studies have investigated the effect of sulfur on the reduction, as mentioned in subsection 2.5.5. These studies have indicated that sulfur has an impact on the reduction of slag in both FeMn and SiMn production processes. [31] [22] [30] [27]. The weight loss differences shown in Figure 4.6 correlates with findings from the mentioned studies. Charges with charcoal as reductant and added sulfur are seen to have significant higher reduction rate than charcoal charges without sulfur.

As the charcoal samples were pre-heated, the calculated weight loss from pre-reduction and reduction stages were found to be very similar. Consequently, the total weight loss for both charcoal charges and coke charges, as shown in Table 3.10, is also comparable. This similarity enables a certain degree of comparison between the charges in terms of their total weight loss.

To compare the effect of sulfur in charcoal charges with the two coke charges reduced at T2 (close to equilibrium), the weight loss curves of these coke experiments are included in Figure 4.7 and Figure 4.8, shown as Figure 5.5 and Figure 5.6 respectively. Based on the limited information due the lack of weight loss curves, these experiments provide less conclusive results as to whether charcoal charges with sulfur are reduced earlier or at a higher rate compared to the coke charges. Further analysis and additional data may be necessary to make such determinations. With that said, upon comparing the weight loss point of the 5.1+S charge with the curve of coke experiment 2.1 in Figure 4.7, it can be concluded that the charcoal charge with added sulfur does not undergo reduction later than the coke experiment.

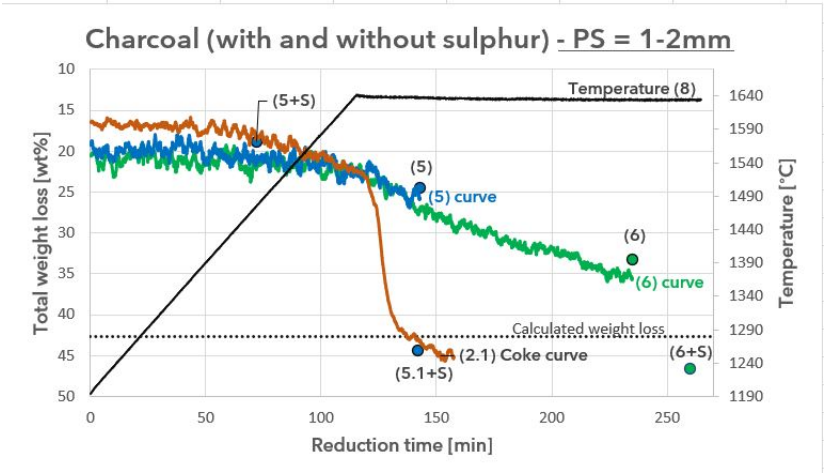

Figure 5.5: with coke experiment 4

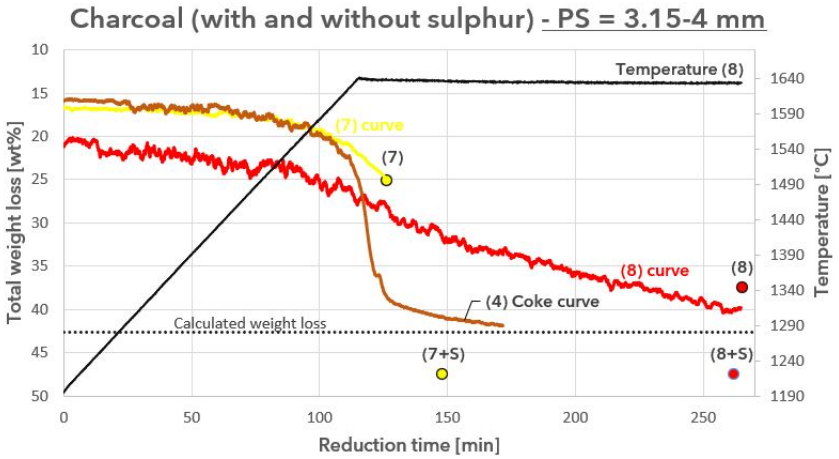

Figure 5.6: coke experiment 2.1

The weight loss difference between the two sulfur charges, 5+S and 5.1+S, as illustrated in Figure 5.5, highlights a notable increase in the reduction rate with the inclusion of sulfur compared to charcoal charges without sulfur addition. This observation suggests that the presence of sulfur accelerates the reduction process in the charcoal charges. Furthermore, to emphasize the earlier reduction with sulfur added, charge 7 and 7+S depicted in Figure 5.6 demonstrate the accelerated reduction due to their close proximity in time and significant difference in weight loss.

As previously mentioned, foaming of the slag was observed in the coke charges, particularly those reduced towards equilibrium (T2). Foaming was also observed in the

charcoal charges with sulfur, although to a significantly lesser extent than in the coke experiments, as depicted in Figure 5.7. Despite both depicted experiments, 2.1 Coke and 5.1+S Charcoal with sulfur, exhibiting similar weight loss, as shown in Figure 5.5, the degree of foaming varied significantly. This observation suggests that the introduction of sulfur in the charcoal charges may contribute to a slower and more controlled reduction process compared to the rapid reduction seen with T2 coke charges, as indicated by the limited foaming.

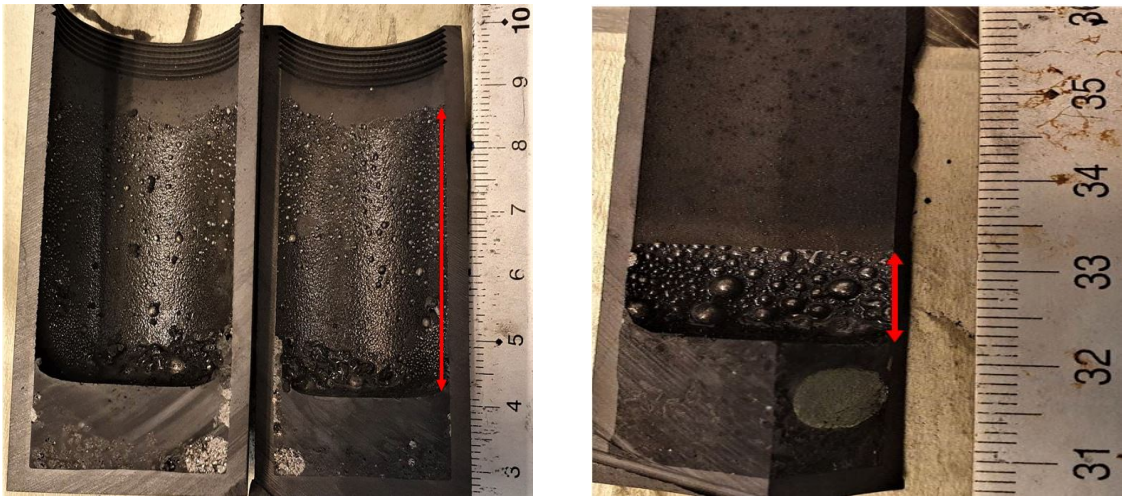

(a) (2.1) Coke, PS = 1-2 mm **(b)** (5.1+S) Charcoal, PS = 1-2 mm.

Figure 5.7: Cross section for a) coke experiment and b) charcoal + sulfur experiment. Red arrows indicate height of foaming.

Another notable observation from this comparison is the distinct differences in the positioning of the slag/alloy and coke bed, despite both charges having the same weight loss. In the coke experiment in Figure 5.7a, the produced alloy is located in the corner of the crucible and the minimal visible slag appears to "pushed" up along the wall, with no significant presence of a carbon bed. On the other hand, Figure 5.7b demonstrates a distinct coke bed with a substantial slag formation on top. This observation, combined with the limited foaming observed, further indicates a more controlled and less "turbulent" reduction compared to what the coke charges experienced.

The produced slag from charcoal with sulfur charges exhibited green tints and a glassy appearance, as presented in Figure 5.8. In the samples of charges with 1-2 mm particles, the slag rests on a compact carbon bed. Notably, Figure 5.8a shows a large metal droplet within the slag, while Figure 5.8b displays numerous small droplets at the slag-carbon interface. In comparison, charges with 3.15-4 mm particles show a relatively smaller

carbon bed. Figure 5.8c depicts experiment 7+S with a large metal droplet at the bottom of the crucible (which has been cut off during the preparation process). It is worth mentioning that this experiment reached the highest temperature of 1660°C. Additionally, Figure 5.8d illustrates the lower carbon bed compared to that observed for charges with 1-2 mm particle charges, and the presence of numerous small metal droplets at the slag-carbon interface.

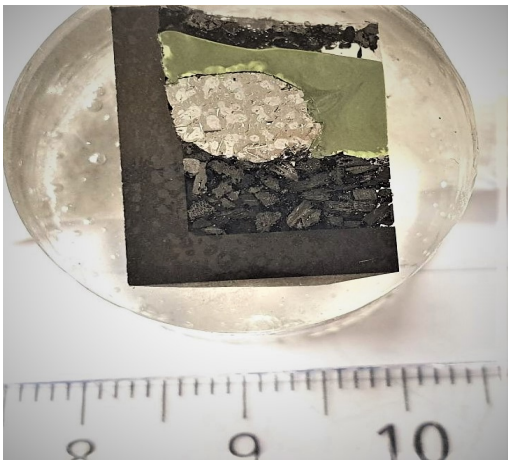

(a) 5.1+S Charcoal, PS = 1-2 mm

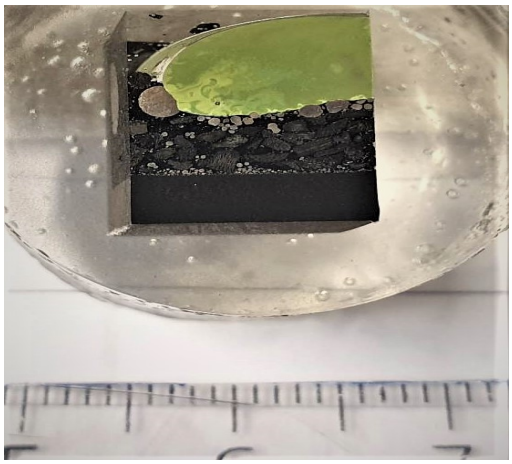

(b) 6+S Charcoal, PS = 1-2 mm

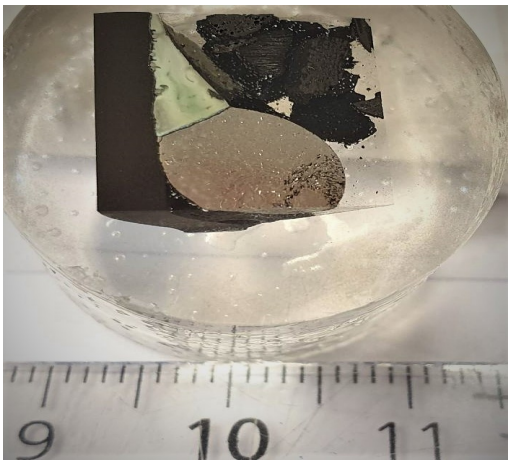

(c) 7+S Charcoal, PS = 3.15-4 mm

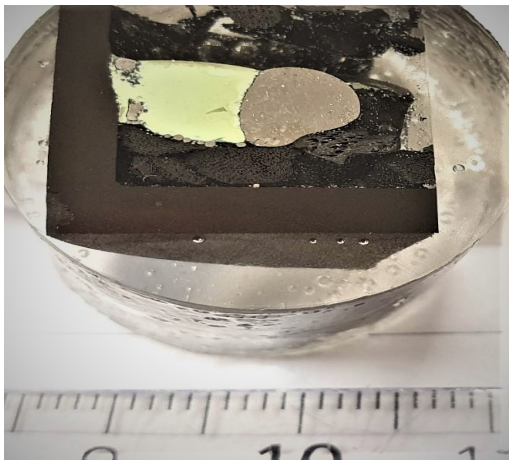

(d) 8+S Charcoal, PS = 3.15-4mm mm

Figure 5.8: Cross-section images of slag and alloy produced from charcoal charges with added sulfur.

The chemical composition of the charcoal charges with sulfur addition was shown in Table 3.1 and will be addressed section 5.2.

5.2 Chemical analysis

To validate the correlation between the observed weight loss of SiMn slags in the TG furnace and the reduction of MnO and SiO_2, it is necessary to conduct chemical analysis of the slag samples. While the weight indicates occurring reactions, primarily the generation of gas (CO) in the high temperature reduction zone, these results alone are inconclusive. Chemical analysis is essential to provide a comprehensive understanding of the reduction process and confirm the extent of MnO and SiO_2 reduction.

The chemical analysis of slag and alloy samples were performed with EPMA and SEM EDS, but only the results from the EPMA analysis was further used in this thesis. For the slag samples a three point analysis were performed, where the operator chooses three random point in the glassy and homogeneous slag. If the slag was heterogeneous, three points were selected for each of the phases. Two-phase slags have an increased margin for error than the one-phase slags. Additional error comes along with the determining the fraction of each phase, in this study performed with ImageJ, see Table 4.4. There is additional error in choosing a representative part of the slag in addition to the error due to overlapping thresholds in ImageJ. However, metal analysis are the most difficult to achieve accurately results from.

Chemical analysis with the three-point approach brings along certain errors. Analysis seen in Table C1 shows the three selected points for each sample and it shows certain deviations among the numbers. Additionally, the total percentage is seldom 100.00%, and Figure 5.9 and Figure 5.10 shows the difference from 100% from all the phases in the slag and alloy samples respectively. The difference in slag samples are seen to be not that large even if there are three samples with two-phase slag. Looking at the difference for metal samples, a larger variance is observed. The three metal samples that had the biggest difference were metal where the slag was two-phase.

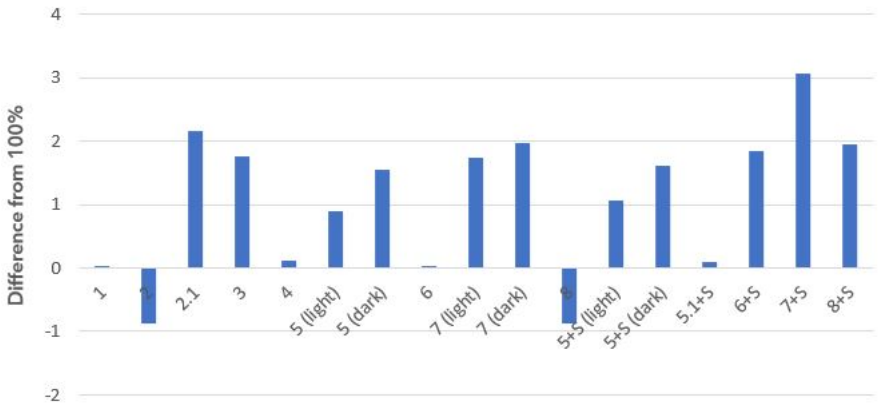

Figure 5.9: Difference from 100% from EPMA analysis for slag samples.

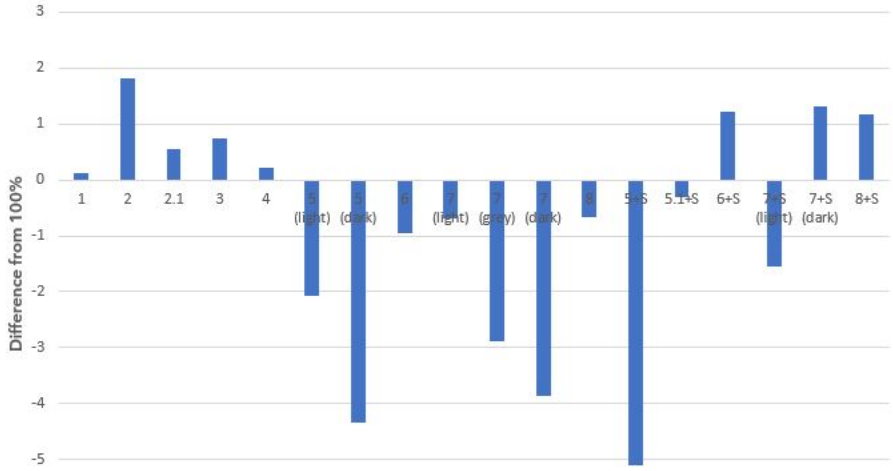

Figure 5.10: Difference from 100% from EPMA analysis for alloy samples.

As seen in the result chapter, Table 4.6 shows the chemical analysis for the slag samples from the TGA furnace experiments. MnO content in the slag are seen as expecting decreasing with longer reduction time. It can be seen from the table that the three two-phase slag samples had negative values for reduced SiO_2(%), thus it can be assumed that the image used to decide phase fractions was far from ideal, especially for 5+S.

Experiment 1, as depicted in Figure 4.4, appears to be the closest experiment to the rate shift in terms of composition. The slag composition in this experiment consisted of approximately 30% MnO and 45% SiO_2, translating to 60% reduced MnO and 9% reduced SiO_2.

The addition of sulfur to the charcoal-reduced slag resulted in a significant difference in the reduction of both MnO and SiO2. The reduction rate was notably higher when sulfur was added to the slag compared to experiments without sulfur. Due to the malfunction of the mass balance unit in the TGA furnace, it was challenging to determine the exact point at which reduction started in the sulfur-added experiments. However, it was observed that reduction began earlier when sulfur was present.

4.7 and 4.8 shows the earlier and more substantial reduction in the presence of sulfur in the slag. For instance, when comparing experiments 5 and 5.1+S, both conducted for a total reduction time of 143 minutes towards T1, the addition of sulfur led to a significant increase in MnO reduction. In experiment 5, without sulfur, the MnO reduction was only 12%, whereas in experiment 5.1+S, with added sulfur, the MnO reduction reached 97%. This exemplifies the enhanced reduction rate achieved through the incorporation of sulfur.

As discussed by **Jayakumari and Tangstad** (2019), a slower reduction rate or slower slag flow into the coke bed can result in increased temperature in the slag. This, in turn, leads to higher silicon content in the metal and lower MnO content in the slag [10]. The limited foaming observed in the sulfur-added slags suggests a potentially slower reduction rate compared to the corresponding coke charges.

Analyzing the silicon content in 4.6, it can be observed that the sulfur-added charges (6+S and 8+S) exhibit higher Si content compared to the coke charges (2 and 4) that were reduced towards equilibrium. This further supports the notion of a slower reduction rate in the sulfur-added slags, leading to increased silicon content in the metal.

5.3 Furnace Operation

The stability of furnace operation must be addressed. Figure 3.7 and Table 3.6 address the temperature stability and weight measurement, respectively.

To address the temperature first, Figure 3.7 clearly illustrates a decrease in temperature during the holding time. Despite targeting a temperature of 1650°C, the actual temperatures observed during the experiments ranged from approximately 1635°C to 1645°C. It is evident that maintaining a constant temperature throughout the holding period was challenging, as the temperature gradually decreased over time. Notably,

during the longest holding times, the temperature dropped by approximately 6°C. This fluctuation is unfortunate and poses relevance concerns for the experiments. It is possible that the thermocouple encountered issues, leading to these temperature variations.

It is worth mentioning that experiments conducted with the same temperature schedule did not consistently reach the desired temperature. Furthermore, two experiments exhibited notable deviations from the expected temperature range. Experiment 7+S reached a maximum temperature of 1661°C, while experiment 2 recorded the lowest temperature at 1623°C. Interestingly, experiment 7+S was conducted after the Mo-wire had broken, suggesting a potential influence on the observed temperature variation.

To ensure the reliability and accuracy of the experimental results, it is essential to address the challenges related to furnace temperature stability. Further investigations should be conducted to identify the causes of temperature fluctuations and develop strategies to maintain a more consistent temperature throughout the holding period. Additionally, a thorough examination and potential calibration of the thermocouple are recommended to ensure precise temperature readings. By addressing these concerns, the experiments can produce more reliable and relevant results, enhancing the overall quality of the findings.

Two experiments exhibited notable deviations from the mentioned temperature range. Experiment 7+S reached a maximum temperature of 1661°C, while experiment 2 had the lowest temperature recorded at 1623°C. Experiment 7+S was performed after the Mo-wire had broken.

To address the lower temperature achieved in experiment 2, an additional run was performed, labeled as experiment 2.1, in an attempt to reach a higher temperature. This was done to rectify the temperature discrepancy observed in the initial experiment 2.

In order to assess the reproducibility, Figure 5.11 displays the weight loss curves for both experiments. It demonstrates a positive indication of reproducibility. Additionally, Table 5.2 provides an abridged version of Table 4.3 and highlights the differences in chemical composition between the two experiments, where the only variation was the end temperature. Since the experiments were conducted near an equilibrium state, it is observed that the MnO content remains relatively consistent at around 3wt%, but

there are slight variations in the SiO_2 content and R-ratio. As anticipated, the experiment that reached the highest temperature exhibited the highest silicon yield and SiO_2 content. This observation aligns with Figure 2.12, which demonstrates an increase in SiO_2 concentration in the slag with an increase in R-ratio, as reported by Olsen et al. [4].

These findings provide valuable insights into the impact of temperature variations on the chemical composition of the slag. Further analysis and exploration of these relationships will contribute to a deeper understanding of the process dynamics and aid in optimizing the experimental conditions for desired outcomes.

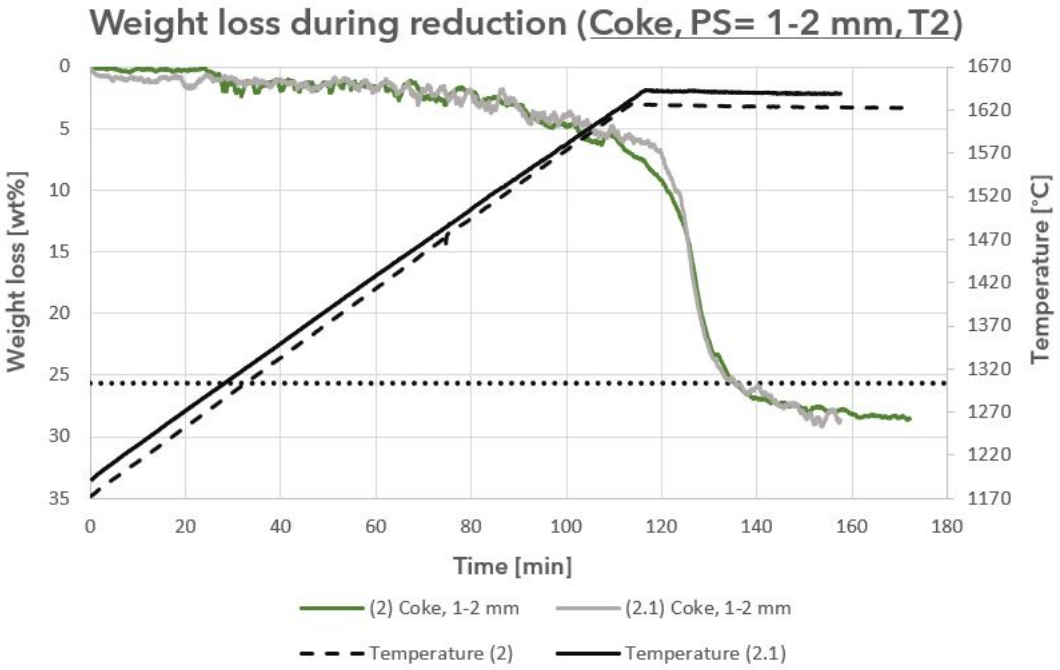

Figure 5.11: Weight loss curves for experiment 2 and 2.1 with coke as reductant.

Table 5.2: Chemical analysis of the slag samples of experiment 2 from EPMA.

Exp.	Red. time [min]	Temp. [$^{\circ}C$]	MnO [wt%]	SiO_2 [wt%]	$CaO^{+}MgO^{+}Al_2O_3$ [wt%]	Reduced MnO[%]	Reduced SiO_2[%]	R-ratio
2	173 (T2)	1626	3.46	39.60	54.76	97.98	65.35	1.5
2.1	158 (T2)	1642	3.17	31.63	65.56	98.55	78.23	1.2

6 Conclusion

In this study, the reduction rate of silicomanganese slag using two carbon materials, coke and charcoal, was investigated through experiments conducted in a thermogravimetric (TGA) furnace. Additionally, the effect of sulfur addition to charcoal-reduced slags was examined. The experiments were performed with two different particle sizes, namely 1-2 mm and 3.15-4 mm.

The weight loss curves obtained from the experiments demonstrated a higher reduction rate for charges utilising coke compared to charcoal. The reduction pathway of coke charges exhibited two distinct stages: an initial slow and stable stage, followed by a rapid rate increase during the second stage. A coke experiment, stopped right after the observed rate shift, showed a slag composition of 30 wt% MnO and 45 wt% SiO_2.

On the other hand, charges with charcoal exhibited a slow and consistent reduction rate throughout the isothermal heating process. However, the introduction of sulfur in the charcoal charges significantly enhanced the reduction rate. The EPMA analysis further emphasized the increased reduction of charcoal charges when sulfur was added to the slag. At a total reduction time of 143 minutes, the charcoal-reduced slag experienced an increased MnO reduction, from 12% to 97%. Chemical analysis using EPMA confirmed the expected decrease in MnO content in the slag wich increasing holding time.

Particle size variations had minimal impact on the reduction process, but in cases where differences were observed, charges with larger particle sizes tended to initiate reduction earlier compared to charges with smaller particle sizes. It was suggested that the smaller particles created a compact carbon bed which decreased the flow of slag into the carbon bed, thus limiting slag-carbon interface the area of reduction.

7 Further work

Suggestions to further work put emphasize on exploring various charge compositions to gain a better understanding of the process. The following investigations could be implemented:

- Incorporation of HC FeMn slag: Including HC FeMn slag in the charge would provide a more realistic representation of an industrial charge composition. This addition could be a source of som sulfur to the slag.
- Evaluation of particle sizes: Investigating different particle sizes for both the carbon materials and other charge materials would offer insights into their influence on the reaction kinetics and overall performance. This analysis could reveal optimal size combinations that promote efficient operation.
- Comparative analysis of pre-heated and non-pre-heated charcoal: Conducting further tests comparing pre-heated charcoal and non-pre-heated charcoal will shed light on the significance of pre-heating in the process. This investigation can provide valuable information regarding the potential benefits or drawbacks of pre-heating the carbon material, especially with regards of volatile matter.
- Evaluate different amounts of carbon in the charges.
- Further investigations regarding sulfur in slag, with both coke and charcoal as reductants. The reduction behavior and pathway should be of interest.

Furthermore, it is of importance to enhance the stability of furnace operation to ensure consistent temperatures during the holding period and minimize fluctuations in weight readings. Achieving a stable furnace operation will contribute to improved reproducibility and reliability of the experimental results.

Bibliography

[1] *The Paris Agreement — UNFCCC*, https://unfccc.int/process-and-meetings/the-paris-agreement, 2023-05-31.

[2] *Miljømål 5.2*, https://miljostatus.miljodirektoratet.no/miljomal/klima/miljomal-5.2, 2023-05-31, 2023.

[3] M. Sommerfeld and B. Friedrich, "Replacing Fossil Carbon in the Production of Ferroalloys with a Focus on Bio-Based Carbon: A Review," *Minerals*, vol. 11, no. 11, p. 1286, 2021.

[4] S. E. Olsen, M. Tangstad, and T. Lindstad, *Production of Manganese Ferroalloys*. Tapir Academic Press, 2007.

[5] Tangstad, Merete, *Metal Production in Norway*. Akademika Publishing, 2013.

[6] M. Tangstad, "Chapter 7 - Manganese Ferroalloys Technology," in *Handbook of Ferroalloys*, M. Gasik, Ed., Oxford: Butterworth-Heinemann, 2013, pp. 221–266.

[7] M. Tangstad, S. Bublik, S. Haghdani, K. E. Einarsrud, and K. Tang, "Slag Properties in the Primary Production Process of Mn-Ferroalloys," *Metallurgical and Materials Transactions B*, vol. 52, no. 6, pp. 3688–3707, 2021.

[8] B. Monsen, M. Tangstad, and H. Midtgaard, "Use of charcoal in silicomanganese production," *Proceedings of the INFACON X, Cape Town, South Africa*, pp. 392–404, 2004.

[9] M. Subramanian and ̇*Harman*, "Problems and Prospects of carbonaceous reducing agents in ferro alloys production," *Proceedings of the Seminar on Problems and Prospects of Ferro-Alloy Industry in India 1983*, 1983.

[10] S. Jayakumari and M. Tangstad, "Carbon materials for silicomanganese reduction," *Proceedings of the INFACON XIV, Kiev, Ukraine*, vol. 1, p. 374, 2015.

[11] B. Monsen, M. Tangstad, I. Solheim, M. Syvertsen, R. Ishak, and H. Midtgaard, "Charcoal for manganese alloy production," *Proceedings of the INFACON XI, New Delhi, India*, pp. 18–21, 2007.

[12] D. Dijs HM* & Smith, "Factors affecting the resistivity and reactivity of carbonaceous reducing agents for the electric-smelting industry," *Journal of the Southern African Institute of Mining and Metallurgy*, vol. 80, no. 8, pp. 286–296, 1980.

[13] E. Ringdalen, S. Gaal, M. Tangstad, and O. Ostrovski, "Ore Melting and Reduction in Silicomanganese Production," *Metallurgical and Materials Transactions B*, vol. 41, no. 6, pp. 1220–1229, 2010.

[14] G. R. Surup, A. Trubetskaya, and M. Tangstad, "Charcoal as an Alternative Reductant in Ferroalloy Production: A Review," *Processes*, vol. 8, no. 11, p. 1432, 2020.

[15] P. P. Kim, "Reduction Rates of SiMn Slags from Various Raw Materials," Doctoral Thesis, NTNU, 2018.

[16] K. Tang and *Olsen*, "Computer simulation of the equilibrium relations associated with the production of manganese ferroalloys," *Proceedings of the INFACON X, Cape Town, South Africa*, 2004.

[17] Ding, Weizhong and Olsen, Sverre E., "Manganese and silicon distribution between slag and metal in silicomanganese production," *ISIJ international*, vol. 40, no. 9, pp. 850–856, 2000.

[18] S. E. Olsen and M. Tangstad, "Silicomanganese Production – Process Understanding," *Proceedings of the INFACON X, Cape Town, South Africa*, p. 8, 2004.

[19] O. Ostrovski, S. Olsen, M. Tangstad, and M. Yastreboff, "Kinetic Modelling of MnO Reduction from Manganese Ore," *Canadian Metallurgical Quarterly*, vol. 41, no. 3, pp. 309–318, 2002.

[20] V. Olsø, Tangstad, Merete, and Olsen, Sverre E., "Reduction Kinetics of MnO-Saturated Slags," *Proceedings of the INFACON VIII, Beijing, China*, p. 5, 1998.

[21] J. Safarian and M. Tangstad, "SLAG-CARBON REACTIVITY," *The Twelfth International Ferroalloys Congress*, p. 12, 2010.

[22] P. P. Kim and M. Tangstad, "Kinetic Investigations of SiMn Slags From Different Mn Sources," *Metallurgical and Materials Transactions B*, vol. 49, no. 3, pp. 1185–1196, 2018.

[23] P. P. Kim, T. A. Larssen, and M. Tangstad, "Reduction rates of MnO and SiO2 in SiMn slags between 1500 and 1650°C," *Journal of the Southern African Institute of Mining and Metallurgy*, vol. 119, no. 5, pp. 494–501, 2019.

[24] P. Kim, J. Holtan, and M. Tangstad, "Reduction Behavior of Assmang and Comilog Ore in the SiMn Process: Proceedings of the 10 th International Conference on Molten Slags, Fluxes and Salts," in 2016, pp. 1285–1292.

[25] V. Canaguier and M. Tangstad, "Kinetics of Slag Reduction in Silicomanganese Production," *Metallurgical and Materials Transactions B*, vol. 51, no. 3, pp. 953–962, 2020.

[26] I. M. F. Haugli, "Reactivity of silicomanganese slag towards carbon materials - A comparison of coke and charcoal as reducing agents," M.S. thesis, NTNU, 2019.

[27] B. D. Hosum, "Reduction Rate of SiMn Slags With Different Carbon Materials," M.S. thesis, NTNU, 2020.

[28] Forberg, Sigmund, "A Comparative Study of Coke and Charcoal as Reductants in the SiMn Production," Intern Rapport, NTNU, Department of Material Science and Engineerings, 2021.

[29] Forberg, Sigmund, "Slag Reactivity in the Silicomanganese Process - a Comparative Study of Coke and Charcoal as Reductants," Intern Rapport, NTNU, Department of Material Science and Engineerings, 2022.

[30] X. Li and M. Tangstad, "The Influence of Sulfur Content on the Carbothermal Reduction of SiMn Slag," *Metallurgical and Materials Transactions B*, vol. 50, no. 1, pp. 136–149, 2019.

[31] T.-A. Skjervheim and Olsen, Sverre E., "THE RATE AND MECHANISM FOR REDUCTION OF MANGANESE OXIDE FROM SILICATE SLAGS," *Proceedings of the INFACON VII, Trondheim, Norway*, pp. 631–640, 1995.

[32] S. Bublik, S. Bao, M. Tangstad, and K. E. Einarsrud, "Interfacial Behaviour in Ferroalloys: The Influence of Sulfur in FeMn and SiMn Systems," *Metallurgical and Materials Transactions B*, vol. 52, no. 6, pp. 3624–3645, 2021.

[33] *Graphite tube furnace - TF1 thermoweight - Department of materials science and engineering - Laboratory equipment - NTNU Wiki*, https://www.ntnu.no/wiki/display/imtlab/Graphite+tube+furnace+-+TF1+thermoweight.

[34] *Electron probe micro-analyzer (EPMA)*, https://serc.carleton.edu/msu_nanotech/methods/EPMA.html.

Appendix

A Crucible dimensions

Figure A1 shows a detailed sketch of the graphite crucibles used in the TGA furnace.

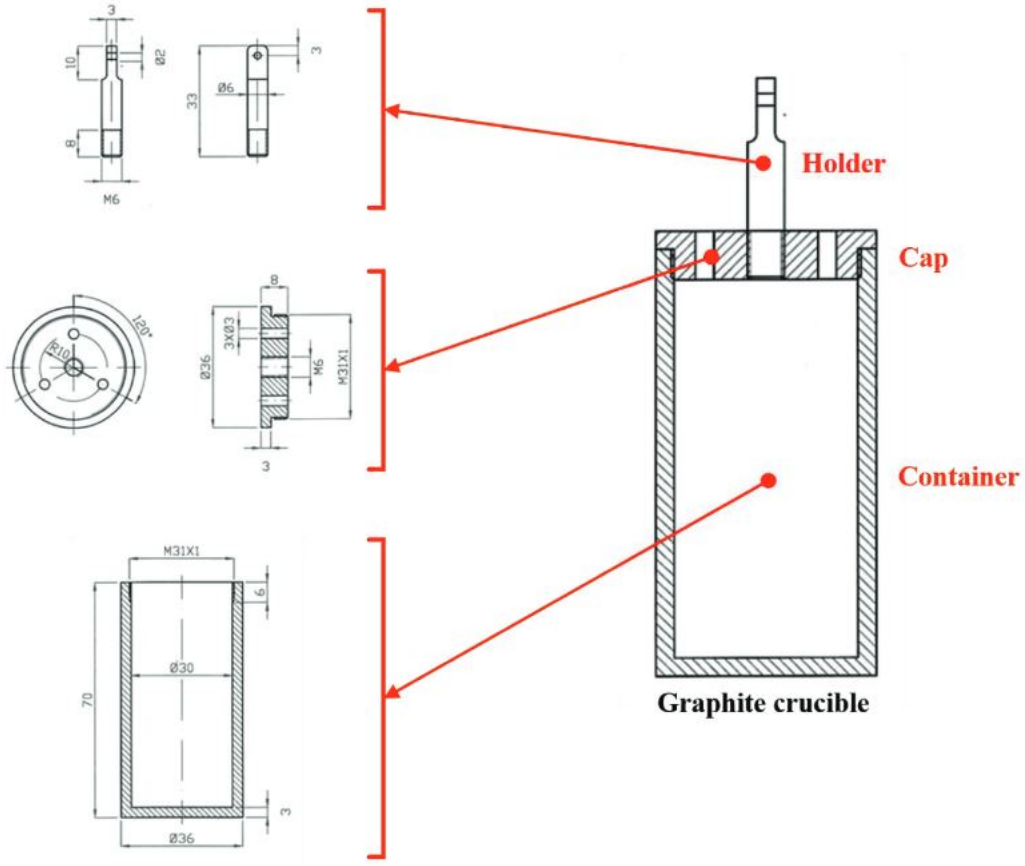

Figure A1: Sketch of graphite crucibles[15].

B Preheating of charcoal and limestone

Figure B1 shows the weight loss curves from pre-heating of charcoal heated to 1000°C.

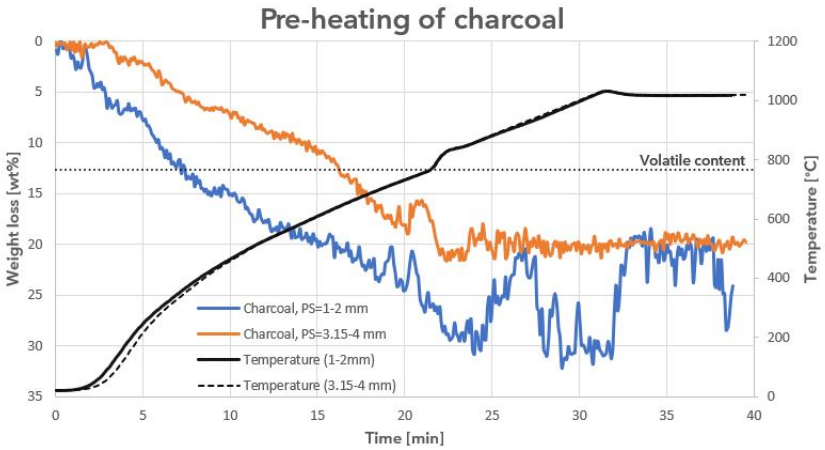

Figure B1: Preheating of charcoal.

Figure B2 shows the weight loss curves from preheating of limestone.

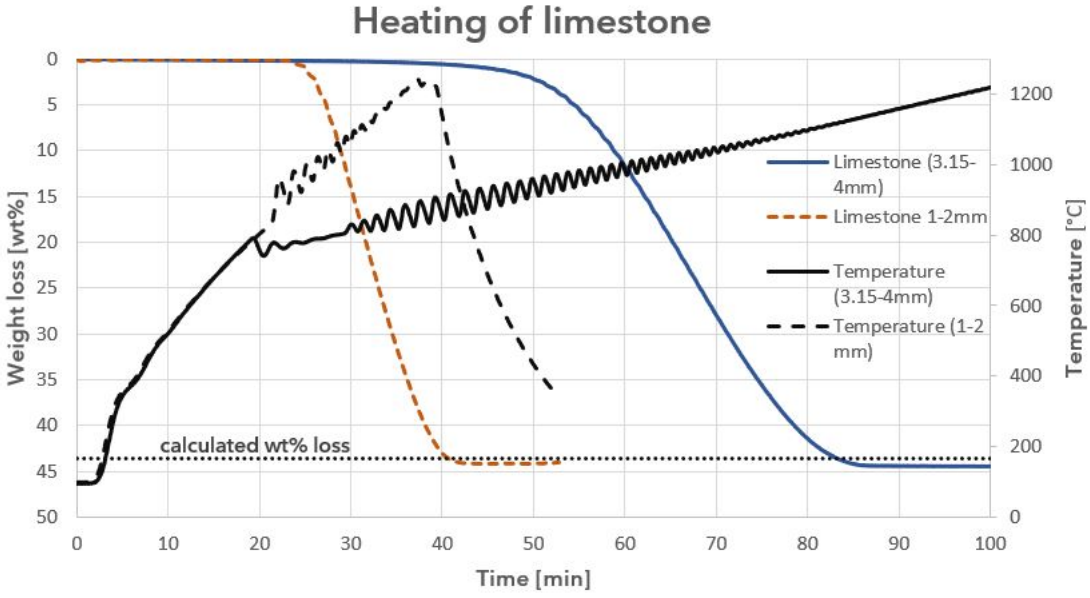

Figure B2: Preheating of limestone, performed in previous study [29].

C Full analysis EPMA

The following tables presents the full slag- and metal analysis performed in EPMA. Three randomly selected points at phases of interest were used in the analysis.

Table C1: Three point chemical analysis of the slag phases with EPMA

Exp	No.	{wt%}							
		Al2O3	MgO	K2O	MnO	SiO2	CaO	SO3	Total
1 Coke	1	10,432	0,598	0,868	29,755	44,751	12,345	0,436	99,185
	2	10,728	0,596	0,894	29,393	45,921	12,408	0,543	100,483
	3	11,108	0,633	0,899	29,009	45,48	12,808	0,504	100,441
	1avg	10,76	0,61	0,89	29,39	45,38	12,52	0,49	100,04
2 Coke	4	22,187	1,48	0,214	3,357	40,046	31,502	1,147	99,933
	5	21,873	1,521	0,159	3,474	39,38	31,05	1,104	98,561
	6	21,761	1,491	0,153	3,563	39,371	31,417	1,094	98,85
	2avg	21,94	1,50	0,18	3,46	39,60	31,32	1,12	99,11
2.1 Coke	37	29,795	0,508	0,002	3,043	31,999	34,912	1,632	101,891
	38	29,589	0,523	0,029	3,3	31,925	34,927	1,858	102,151
	39	30,999	0,582	0	3,172	30,97	34,832	1,887	102,442
	2.1avg	30,128	0,538	0,010	3,172	31,631	34,890	1,792	102,161
3 Coke	7	10,266	0,744	0,868	21,878	49,589	17,433	0,532	101,31
	8	10,151	0,763	0,796	22,437	50,283	17,595	0,62	102,645
	9	10,787	0,84	0,829	19,379	50,255	18,581	0,666	101,337
	3avg	10,40	0,78	0,83	21,23	50,04	17,87	0,61	101,76
4 Coke	10	23,772	1,267	0,059	2,268	37,1	33,771	1,084	99,321
	11	23,957	1,225	0,038	2,324	38,259	33,565	1,008	100,376
	12	24,332	1,087	0,039	1,947	39,188	32,679	1,375	100,647
	4avg	24,02	1,19	0,05	2,18	38,18	33,34	1,16	100,11
	25	0,126	0,838	0,045	62,971	32,665	4,188	0	100,833

Table C1 continued from previous page

	26	0,242	0,855	0,027	62,89	32,606	4,282	0,028	100,93
	27	0,282	0,918	0,025	62,673	32,926	4,082	0,042	100,948
	5avg-light	0,217	0,870	0,032	62,845	32,732	4,184	0,023	100,904
	28	13,115	0,169	0,663	25,665	46,428	15,476	0,08	101,596
5 Charcoal	29	13,037	0,147	0,755	25,535	46,611	15,563	0,106	101,754
	30	12,831	0,148	0,643	25,625	46,389	15,473	0,16	101,269
	5avg-dark	12,994	0,155	0,687	25,608	46,476	15,504	0,115	101,540
	5avg*	5,850	1,837	17,677	28,118	27,659	8,437	56,212	145,789
	13	9,781	0,608	0,354	31,616	44,439	13,623	0,09	100,511
	14	9,852	0,658	0,355	30,343	44,422	13,587	0,061	99,278
6 Charcoal	15	9,898	0,604	0,334	31,425	43,963	13,935	0,158	100,317
	6avg	9,84	0,62	0,35	31,13	44,27	13,72	0,10	100,04
	31	0,193	0,934	0,013	61,941	32,828	5,704	0	101,613
	32	0,178	0,981	0,01	62,183	32,986	5,381	0,01	101,729
	33	0,206	0,934	0,015	62,321	33,04	5,357	0	101,873
	7avg-light	0,192	0,950	0,013	62,148	32,951	5,481	0,003	101,738
	34	12,716	0,219	0,388	24,923	45,879	17,633	0,163	101,921
7 Charcoal	35	12,853	0,194	0,391	24,926	46,042	17,548	0,123	102,077
	36	11,982	0,222	0,342	25,906	45,86	17,559	0,022	101,893
	7avg-dark	12,517	0,212	0,374	25,252	45,927	17,580	0,103	101,964
	7avg*	6,190	0,591	0,188	44,193	39,266	11,369	0,052	101,848
	16	10,601	0,852	0,2	25,989	45,208	17,017	0,064	99,931
	17	10,524	0,845	0,214	26,085	45,099	16,819	0,084	99,67
8 Charcoal	18	10,322	0,837	0,251	25,924	43,676	16,677	0,087	97,774
	8avg	10,48	0,84	0,22	26,00	44,66	16,84	0,08	99,13
	40	0,249	0,514	0,01	63,432	32,594	5,724	0	102,523

Table C1 continued from previous page

5 Charcoal + S	41	0,23	0,342	0,011	61,012	31,924	6,052	0,01	99,581
	42	0,418	0,504	0,043	62,081	32,05	5,918	0,063	101,077
	5+S avg-light	0,299	0,453	0,021	62,175	32,189	5,898	0,024	101,060
	43	22,809	0	3,278	30,608	29,731	12,153	2,681	101,26
	44	21,797	0,05	3,202	31,47	30,155	12,382	2,699	101,755
	45	23,09	0,054	3,433	30,5	29,83	12,099	2,786	101,792
	5+S avg-dark	22,565	0,035	3,304	30,859	29,905	12,211	2,722	101,602
	5+S*	5,85	0,35	0,84	54,36	31,62	7,47	0,70	101,20
5.1 Charcoal + S	46	20,188	1,338	1,008	6	43,073	27,7	1,037	100,344
	47	19,008	1,302	0,935	6,228	42,854	28,149	1,148	99,624
	48	19,598	1,395	0,954	6,034	43,326	28,063	0,975	100,345
	5.1+S avg	19,598	1,345	0,966	6,087	43,084	27,971	1,053	100,104
8 Charcoal + S	55	25,082	1,517	0,031	1,769	37,474	33,894	1,921	101,688
	56	24,911	1,566	0	1,789	37,62	34,094	2,442	102,422
	57	25,136	1,609	0,052	1,862	36,999	33,713	2,381	101,752
	8+S avg	25,043	1,564	0,028	1,807	37,364	33,900	2,248	101,954
1. wallfoam Coke	19	10,641	0,61	0,952	28,418	47,85	12,496	0,44	101,407
	20	10,687	0,594	0,892	28,617	47,715	12,209	0,492	101,206
	21	10,656	0,594	0,901	28,566	47,723	12,242	0,508	101,190
	1.wall avg	10,661	0,599	0,915	28,534	47,763	12,316	0,480	101,268
4. lid Coke	22	15,329	1,238	0,751	7,976	51,342	22,148	0,646	99,43
	23	15,611	1,258	0,684	8,231	52,598	22,211	0,548	101,141
	24	15,54	1,156	0,697	7,696	52,398	21,931	0,653	100,071
	4.lid avg	15,493	1,217	0,711	7,968	52,113	22,097	0,616	100,214

Table C1 continued from previous page

*consists of both liquid and solid phases

Table C2: Three point chemical analysis of the metal

Exp	No.	{wt%}					
		Si	**C**	**Mn**	**Fe**	**P**	**Total**
1 Coke	1	9,107	0,826	86,462	3,828	-	100,223
	2	9,153	0,811	89,402	1,248	-	100,614
	3	8,317	0,768	82,552	7,842	-	99,479
	1avg	8,86	0,80	86,14	4,31	-	100,11
2 Coke	4	14,825	0,697	85,318	1,404	-	102,244
	5	13,315	0,758	86,337	1,196	-	101,606
	6	20,744	0,838	79,63	0,345	-	101,557
	2avg	16,29	0,76	83,76	0,98	-	101,80
2.1 Coke	40	10,121	0,693	87,997	1,518	0,008	100,337
	41	10,779	0,734	87,447	1,687	-	100,647
	42	10,13	0,695	88,281	1,52	-	100,626
	2.1avg	10,34	0,71	87,91	1,58	0,01	100,54
3 Coke	7	16,053	0,943	81,918	0,629	-	99,543
	8	12,473	0,811	88,232	1,028	-	102,544
	9	13,359	0,896	85,222	0,633	-	100,11
	3avg	13,96	0,88	85,12	0,76	-	100,73
4 Coke	10	15,336	1,054	83,174	0,624	-	100,188
	11	10,994	0,848	86,936	1,311	-	100,089
	12	8,562	0,869	76,19	14,718	-	100,339
	4avg	11,63	0,92	82,10	5,55	-	100,21
	25	3,417	0,649	63,937	27,782	0,341	96,126

Table C2 continued from previous page

5 Charcoal	26	3,279	0,639	66,926	27,737	0,249	98,83
	27	3,381	0,63	66,512	27,968	0,305	98,796
	5avg-light	3,36	0,64	65,79	27,83	0,30	97,92
	28	0,038	0,93	76,219	18,416	-	95,603
	29	0,028	0,938	76,151	18,257	-	95,374
	30	0,067	0,934	76,72	18,282	-	96,003
	5avg-dark	0,04	0,93	76,36	18,32	-	95,66
	5avg*	1,55	0,80	71,57	22,63	-	96,54
6 Charcoal	13	3,558	0,604	81,123	14,244	-	99,529
	14	3,916	0,775	83,056	10,716	-	98,463
	15	7,553	0,707	89,959	0,951	-	99,17
	6avg	5,01	0,70	84,71	8,64	-	99,05
7 Charcoal	31	3,223	0,618	61,063	33,714	0,286	98,904
	32	3,164	0,623	61,447	33,835	0,289	99,358
	33	3,056	0,634	62,25	33,254	0,449	99,643
	7avg-light	3,148	0,625	61,587	33,601	0,341	99,302
	34	0	0,842	68,438	27,687	-	96,967
	35	0	0,835	68,41	27,834	-	97,079
	36	0,01	0,839	69,101	27,333	0,015	97,298
	7avg-grey	0,003	0,839	68,650	27,618	0,015	97,125
	37	0	0,926	72,65	23,045	-	96,621
	38	0	0,929	71,933	22,973	-	95,835
	39	0	0,93	72,18	22,893	-	96,003
	7avg-dark	0,000	0,928	72,254	22,970	-	96,153
	16	8,389	0,742	80,638	9,805	-	99,574
	17	6,829	0,809	82,013	9,541	-	99,192

Table C2 continued from previous page

8 Charcoal	18	6,425	0,757	81,91	10,13	-	99,222
	8avg	7,21	0,77	81,52	9,83	-	99,33
5 Charcoal + S	43	0	1,246	40,315	52,535	0,866	94,962
	44	0,006	1,169	38,054	54,36	1,418	95,007
	45	0,005	1,238	37,682	54,689	1,109	94,723
	5+S avg	0,00	1,22	38,68	53,86	1,13	94,90
5.1 Charcoal	46	16,43	0,675	69,208	13,557	0,088	99,958
	47	12,44	0,678	72,771	13,806	0,527	100,222
	48	9,995	0,719	74,253	13,394	0,511	98,872
	5.1+S avg	12,96	0,69	72,08	13,59	0,38	99,68
6 Charcoal + S	49	18,848	1,236	81,564	0,565	-	102,213
	50	17,327	1,216	81,574	0,525	-	100,642
	51	18,816	1,206	80,198	0,577	-	100,797
	6+S avg large droplet	18,33	1,22	81,11	0,56	-	101,22
	52	18,218	1,217	81,831	0,135	-	101,401
	53	18,019	1,357	81,007	0,155	-	100,538
	54	18,415	1,402	81,789	0,116	-	101,722
	6+S avg small droplets	18,217	1,325	81,542	0,135	-	101,220
	55	9,463	1,238	83,665	4,705	-	99,071
	56	9,195	1,275	82,617	4,716	0,007	97,81
	57	9,464	1,318	82,901	4,794	-	98,477
	7+S avg-light	9,37	1,28	83,06	4,74	0,01	98,46
	58	22,314	1,133	72,91	5,164	0,011	101,532

Table C2 continued from previous page

7 Charcoal + S	59	22,232	1,174	72,885	4,855	-	101,146
	60	21,912	1,142	73,117	5,057	0,005	101,233
	7+S avg-dark	22,15	1,15	72,97	5,03	0,01	101,31
	7+S avg**	15,76	1,21	78,02	4,88	0,00	99,87
8 Charcoal + S	61	19,956	0,678	73,325	9,228	0,071	103,258
	62	16,915	1,237	73,6	9,183	0,041	100,976
	63	18,851	1,249	73,062	8,939	0,002	102,103
	8+S avg large droplet	18,57	1,05	73,33	9,12	0,04	102,11
	64	16,569	1,23	82,494	0,52	-	100,813
	65	16,291	1,201	83,344	0,542	-	101,378
	66	16,644	1,226	82,849	0,562	-	101,281
	8+S avg small droplets	16,501	1,219	82,896	0,541	-	101,157
1. wallfoam Coke	19	8,079	0,767	90,648	0,491	-	99,985
	20	8,856	0,759	91,012	0,499	-	101,126
	21	8,28	0,768	90,666	0,444	-	100,158
	1. wall avg	8,405	0,765	90,775	0,478	-	100,423
4. lid Coke	22	11,512	0,829	89,114	0,189	-	101,644
	23	15,009	0,918	85,638	0,153	-	101,718
	24	13,976	0,894	85,796	0,2	-	100,866
	4. lid avg	13,499	0,880	86,849	0,181	-	101,409

* 5 Coke - phase fraction light = 0.45 and dark = 0.55, obtained from imageJ

** 7+S Charcoal phase fraction light = 0.5 and dark = 0.5, visually estimated

EPMA - Images

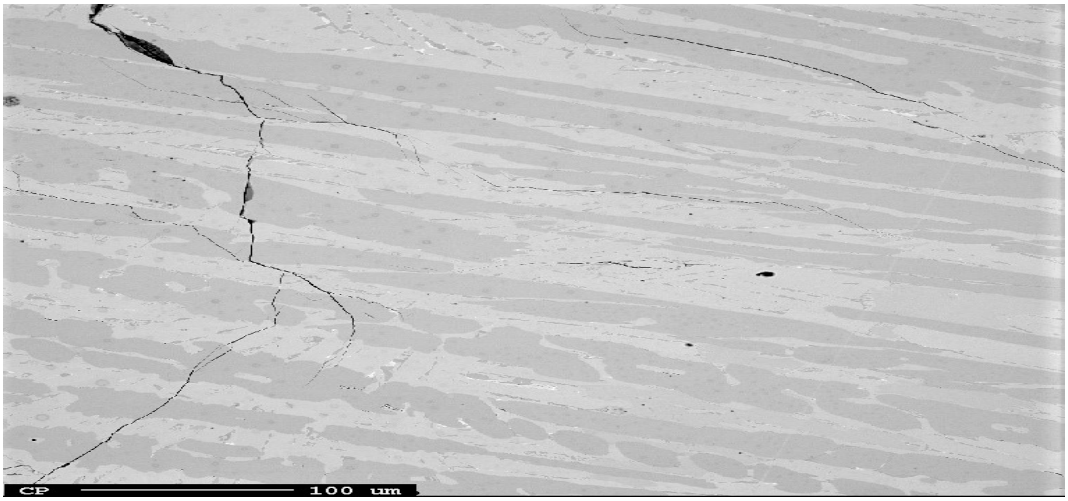

Figure C1: Metal phases in experiment 5 with charcoal depicted in EPMA.

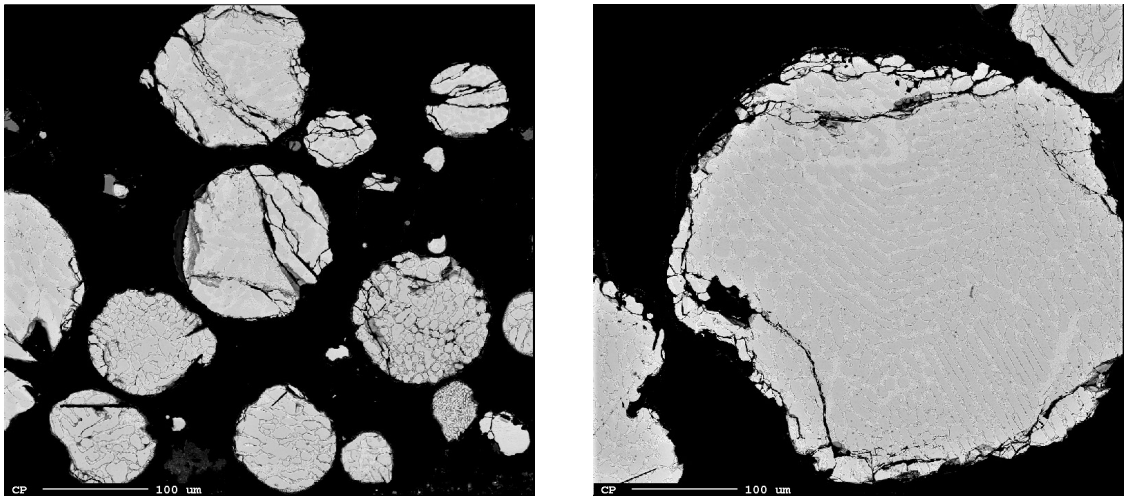

(a) Small metal droplets **(b)** Big metal droplet

Figure C2: Metal droplets from experiment 6+S, charcoal with sulfur slag, depicted with EPMA.

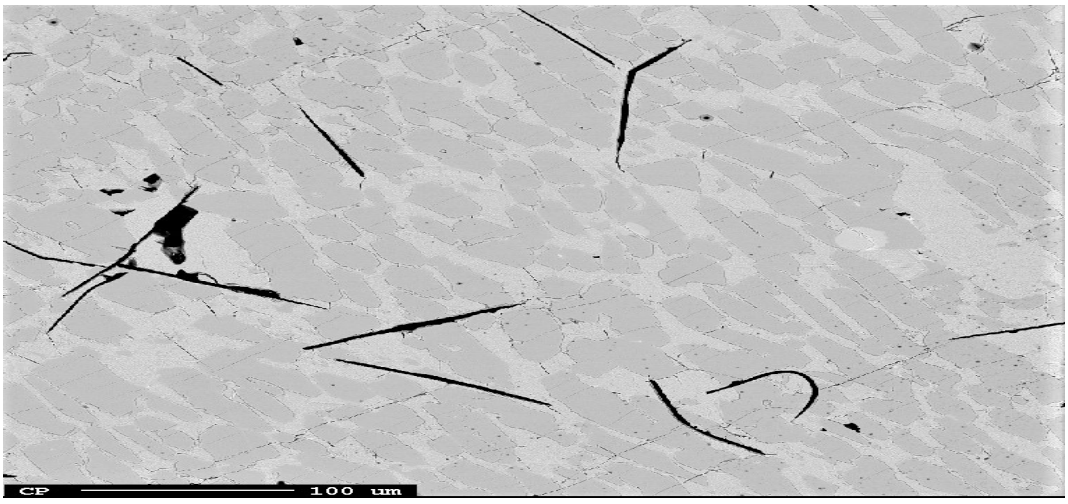

Figure C3: Metal phases from experiment 7+S, charcoal with sulfur slag, depicted with EPMA.

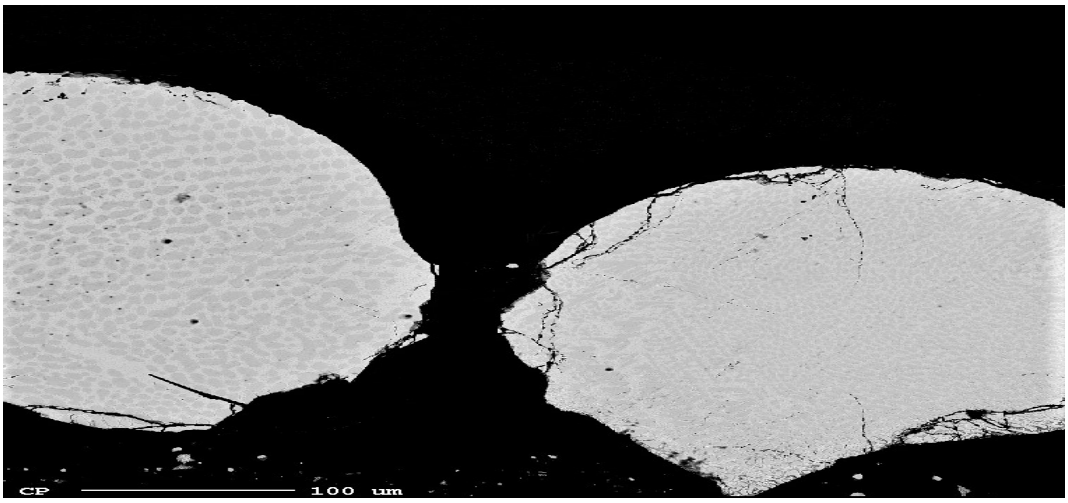

Figure C4: Metal droplets from experiment 8+S, charcoal with sulfur slag, depicted with EPMA.

D Chemical analysis - SEM EDS

Table D1: Chemical analysis for slag samples from SEM EDS - Not normalized results

	Parameters	***MnO***	***SiO2***	***Al2O3***	***CaO***	***MgO***	***K2O***	***TOT***	***R-ratio***
1.Coke	T1, 1-2mm	25.3	33.8	17.3	10.9	0.9	1.4	89.7	0.7
2	**T2, 1-2mm**	3.7	32.0	36.4	28.0	1.1	-	101.2	0.8
3	T1, 3-4mm	15.2	35.2	18.3	16.0	0.6	1.5	86.7	0.9
4	**T2, 3-4mm**	3.4	29.7	40.4	30.4	0.9		104.8	0.8
5.Charcoal	T1, 1-2mm	-	-	-	-	-	-	-	-
6	**T2, 1-2mm**	25.6	31.6	14.6	10.6	0.3	-	82.7	0.7
7	T1, 3-4mm	37.2	26.5	9.1	8.6	0.2	-	81.6	1.0
8	**T2, 3-4mm**	22.3	34	16.6	13.9	0.5	-	87.3	0.9
1.droplet	-	22.8	33.9	15.9	9.6	0.3	1.4	83.9	0.6
4.lid	-	7.4	41.8	26.2	20.3	0.9	1.7	98.3	0.8

Table D2: Chemical analysis for slag samples from SEM EDS - Normalized results

	Parameters	***MnO***	***SiO2***	***Al2O3***	***CaO***	***MgO***	***K2O***	***R-ratio***
1.Coke	T1, 1-2mm	28.2	37.7	19.3	12.2	0.9	1.6	0.7
2	**T2, 1-2mm**	3.6	31.6	36.0	27.7	1.1	-	0.8
3	T1, 3-4mm	17.5	40.6	21.1	18.4	0.6	1.7	0.8
4	**T2, 3-4mm**	3.2	28.4	38.5	29.0	0.9	-	0.8
5.Charcoal	T1, 1-2mm	-	-	-	-	-	-	-
6	**T2, 1-2mm**	30.9	38.2	17.7	12.9	0.3	-	0.7
7	T1, 3-4mm	46.6	32.3	10.6	10.3	0.3	-	1.0
8	**T2, 3-4mm**	25.5	39.0	19.0	15.9	0.5	-	0.9
1.droplet	-	27.2	40.5	19.0	11.4	0.4	1.6	0.6

Table D2 continued from previous page

4.lid	-	7.5	42.5	26.7	20.7	0.9	1.7	0.8

RISIKOANALYSE (alternativ til bruk av RiskManager)

Enhet/institutt:	IMA	**Dato opprettet:**	18.06.2021
Ansvarlig linjeleder (navn):	Einar Magne Hjorthol	**Sist revidert:**	26.09.2023
Ansvarlig for aktiviteten som risikovurderes (navn):	Merete Tangstad (ansv. veileder), Sigmund Forberg (student)		
Deltakere (navn):	Sigmund Forberg		

Beskrivelse av den aktuelle aktiviteten, området mv.:

Prosjektoppgave: Reduskjon av Mn-malm i høytemeratursovn i CO(g)-atomsfære. Bruk av høytemperatursovn TF1, rom E-214.

Aktivitet/arbeidsoppgave	Mulig uønsket hendelse	Eksisterende risikoreduserende tiltak	Vurdering av sannsynlighet (S)	Vurdering av konsekvens (K) *Vurder en konsevenskategori om gangen. Menneske skal alltid vurderes.*				Risikoverdi (S x K)	Forslag til forebyggende og/eller korrigendene tiltak *Prioriter tiltak som kan forhindre at hendelsen inntreffer (sannsynlighetsreduserende tiltak) foran skjerpet beredskap (konsekvensreduserende tiltak)*	Restrisiko etter tiltak (S x K)
			(1-5)	Menneske (1-5)	Øk/materiell (1-5)	Ytre miljø (1-5)	Omdømme (1-5)			
Sette på CO(g)	Gasslekkasje	Gassdetektor (CO-detektor)	1	4				4	Kontakte romansvarlig hvis detektor går av, gå ut av rom	
Ta ut prøve etter forsøk	Klemfare,brannskade	Vente til prøve blir kald, hanske.	1	2				2	Vente god tid, se på temperatur på skjerm	
Jobbe med gasstrykk	Over-/undertrykk ved åpning	Grundig brukermanual, instrument	1	1				2	Følge brukermanual nøye, ha atm. trykk ved åpning av ovn	
		Vernebriller								

RISIKOANALYSE (alternativ til bruk av RiskManager)

Enhet/institutt:	IMA	**Dato opprettet:**	18.06.2021
Ansvarlig linjeleder (navn):	Einar Magne Hjorthol	**Sist revidert:**	26.09.2023
Ansvarlig for aktiviteten som risikovurderes (navn):	Merete Tangstad (ansv. veileder), Sigmund Forberg (student)		
Deltakere (navn):	Sigmund Forberg		

Beskrivelse av den aktuelle aktiviteten, området mv.:

Prosjektoppgave: Prøvepreparering, knuse og sikte råmaterialer, Bergbygget M-115

Aktivitet/arbeidsoppgave	Mulig uønsket hendelse	Eksisterende risikoreduserende tiltak	Vurdering av sannsynlighet (S)	Vurdering av konsekvens (K) *Vurder en konsevenskategori om gangen. Menneske skal alltid vurderes.*				Risikoverdi (S x K)	Forslag til forebyggende og/eller korrigendene tiltak *Prioriter tiltak som kan forhindre at hendelsen inntreffer (sannsynlighetsreduserende tiltak) foran skjerpet beredskap (konsekvensreduserende tiltak)*	Restrisiko etter tiltak (S x K)
			(1-5)	Menneske (1-5)	Øk/materiell (1-5)	Ytre miljø (1-5)	Omdømme (1-5)			
Knuse og sikte råmaterialer	Hørselskade	Hørselvern	2	2				4	Bruk sikkerhetsutstyr tilpasset arbeidet	
	Sprut av råmateriale ved knusing	Vernebriller	3	3				9		
	Støv fra knusing	Støvmaske og hansker	5	2				10		

Sigmund A. K. Forberg
Student

Merete Tangstad
Ans. veileder

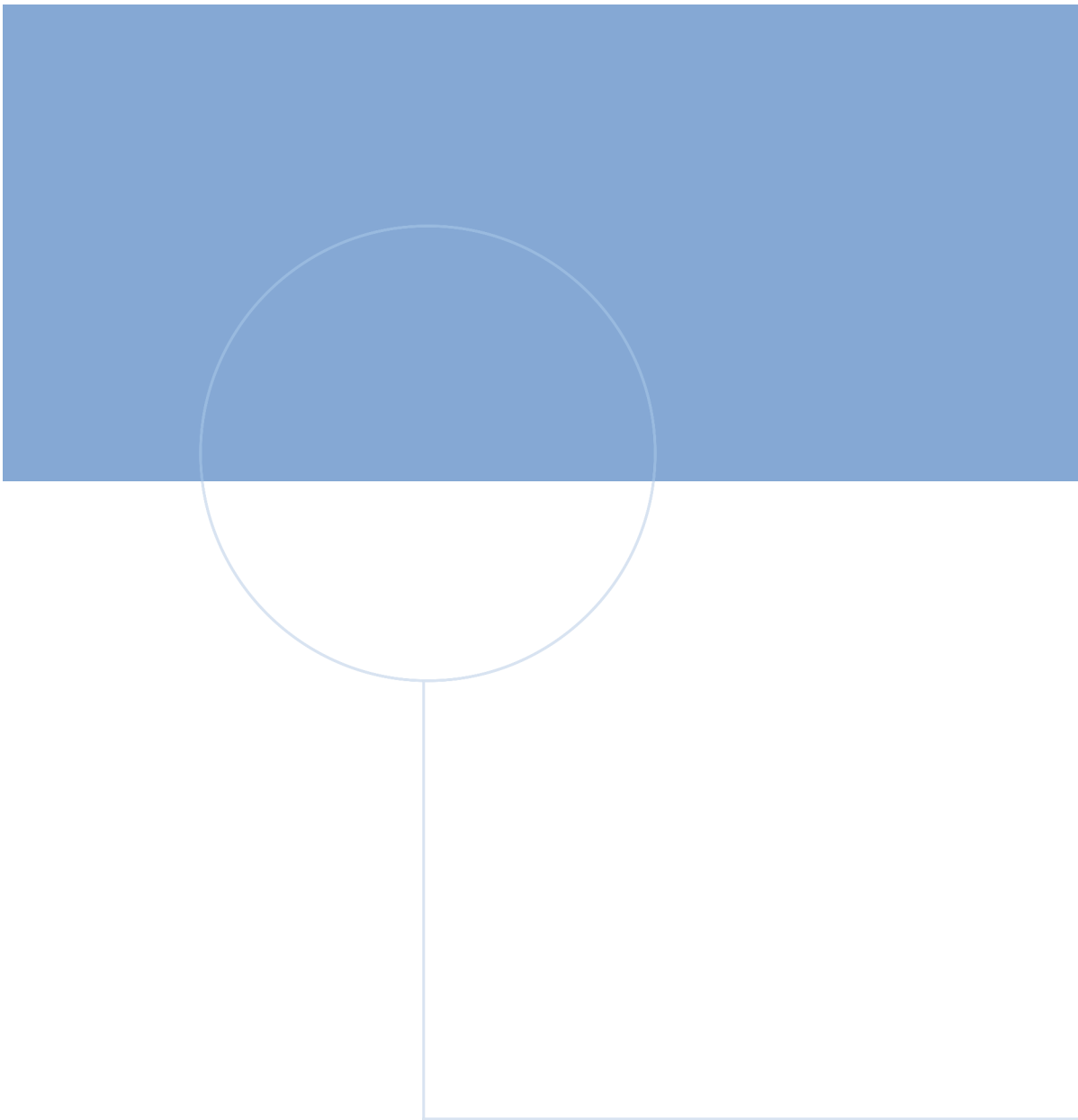

NTNU

Norwegian University of
Science and Technology